

MTP-AERO-63-38
May 20, 1963



A SURVEY OF THE INFLUENCE OF VARIATIONS
IN STAGE CHARACTERISTICS ON OPTIMIZED TRAJECTORY SHAPING

PART II: TRANSFER FROM CIRCULAR ORBITS
INTO A SPACE FIXED ELLIPSE

By

Gary McDaniel

OTS PRICE

XEROX

\$

MICROFILM

\$



FOR INTERNAL USE ONLY

GEORGE C. MARSHALL SPACE FLIGHT CENTER

MTP-AERO-63-38

A SURVEY OF THE INFLUENCE OF VARIATIONS
IN STAGE CHARACTERISTICS ON OPTIMIZED TRAJECTORY SHAPING

PART II: TRANSFER FROM CIRCULAR ORBITS
INTO A SPACE FIXED ELLIPSE

By

Gary McDaniel

ABSTRACT

Trajectories have been investigated for upper stage vehicles, characterized by thrust to weight ratio and specific impulse, departing from a circular orbit and injecting into an elliptical orbit. The orbits are coplanar and both cases where the initial orbit intersects or does not intersect the terminal orbit have been considered.

Two families of solutions have been found for a given thrust to weight ratio and specific impulse. Emphasis has been directed toward weight into orbit, trajectory shapes, tilt angle histories, and angle of attack histories for both families.

GEORGE C. MARSHALL SPACE FLIGHT CENTER

MTP-AERO-63-38

May 20, 1963

A SURVEY OF THE INFLUENCE OF VARIATIONS
IN STAGE CHARACTERISTICS ON OPTIMIZED TRAJECTORY SHAPING

PART II: TRANSFER FROM CIRCULAR ORBITS
INTO A SPACE FIXED ELLIPSE

By

Gary McDaniel

FUTURE PROJECTS BRANCH
AEROBALLISTICS DIVISION

TABLE OF CONTENTS

<u>Title</u>	<u>Page</u>
SECTION I. PROBLEM DESCRIPTION AND APPROACH	1
SECTION II. DISCUSSION	4
SECTION III. RESULTS	5
APPROVAL	77
DISTRIBUTION	78

GEORGE C. MARSHALL SPACE FLIGHT CENTER

MTP-AERO-63-38

A SURVEY OF THE INFLUENCE OF VARIATIONS
IN STAGE CHARACTERISTICS ON OPTIMIZED TRAJECTORY SHAPING

PART II: TRANSFER FROM CIRCULAR ORBITS
INTO A SPACE FIXED ELLIPSE

By Gary McDaniel

SUMMARY

Trajectories have been investigated for upper stage vehicles, characterized by thrust to weight ratio and specific impulse, departing from a circular orbit and injecting into an elliptical orbit. The orbits are coplanar and both cases where the initial orbit intersects or does not intersect the terminal orbit have been considered.

Two families of solutions have been found for a given thrust to weight ratio and specific impulse. Emphasis has been directed toward weight into orbit, trajectory shapes, tilt angle histories, and angle of attack histories for both families.

SECTION I. PROBLEM DESCRIPTION AND APPROACH

This study is concerned with trajectory shapes, weight into orbit, and control histories of an upper stage vehicle departing from circular orbits and injecting into a space-fixed elliptical orbit. Different types of vehicles are considered and are characterized by their thrust to weight ratio at ignition, F/W_0 , and specific impulse, I_{sp} . These two parameters have been restricted to $.5 \leq F/W_0 \leq 2$ and $400 \leq I_{sp} \leq 1500$.

The initial circular orbits considered are coplanar with the terminal elliptical orbit. Three initial circular orbits have been considered with altitudes, y_0 , of 100, 200 and 300 km. The elliptical orbit has an altitude at perigee of 150 km. Hence, the 200 and 300 km orbits intersect the terminal orbit.

The two quantities, energy and angular momentum, which define the shape of the ellipse were taken from a trajectory which circumnavigates the moon and re-enters into the gravitational field of the earth. This particular ellipse has energy and angular momentum values per unit mass of -1.495811×10^6 (m^2/sec^2) and 7.1158378×10^{10} (m^2/sec), respectively. These values yield a total flight time of approximately 122 hours. This particular elliptical orbit was chosen in order that the results in this study may be of significance in future lunar studies.

The motion is assumed to take place in two dimensions in the gravitational field of a spherical earth free of atmosphere. When the initial conditions have been specified along with a F/W_0 and I_{sp} value the vehicle's trajectory is numerically integrated in a (r, v, ϕ) coordinate system. The burning time of the trajectory is extremized by the calculus of variations technique. Since this is a problem of optimum orbital transfer between a circular orbit and an elliptical orbit which is space-fixed, a ϕ -independent program was used, where ϕ is the angle between the launch vertical and the local vertical on the trajectory. This implies that ignition can occur at any time on the initial orbit and the line of apsides of the terminal orbit is fixed.

In order that the end conditions are achieved the initial angle of attack and its time derivative, α_0 and $\dot{\alpha}_0$, have to be determined. This is a numerical procedure that determines α_0 and $\dot{\alpha}_0$ by an interpolation or extrapolation on several cases which approach the desired end conditions.

α_0 and $\dot{\alpha}_0$ have been chosen as the isolation parameters rather than the Lagrangian multipliers, λ_1 's. This transformation is easily seen. Consider the differential equations of constraint

$$\dot{r} - v \cos \phi = G_1$$

$$\dot{v} - \frac{F}{m} \cos \alpha + g \cos \phi = G_2 \quad (1)$$

$$\dot{\phi} - \frac{F}{mv} \sin \alpha - \left(\frac{g}{v} - \frac{v}{r} \right) \sin \phi = G_3$$

along with the function to be extremized

$$f = 1 + \sum_{i=1}^n \lambda_i G_i, \quad i = 1, \dots, n. \quad (2)$$

The Euler-Lagrange equation where α is the independent variable is

$$\frac{\partial f}{\partial \alpha} - \frac{d}{dt} \left(\frac{\partial f}{\partial \dot{\alpha}} \right) = 0. \quad (3)$$

By applying (3) to (1) and (2) one obtains

$$\lambda_2 \frac{F}{m} \sin \alpha - \lambda_3 \frac{F}{mV} \cos \alpha = 0 \quad \text{or}$$

$$\lambda_2 v \sin \alpha = \lambda_3 \cos \alpha. \quad (4)$$

Using the trigonometric identity $\sin^2 \alpha + \cos^2 \alpha = 1$ (4) becomes

$$\cos \alpha = \frac{\lambda_2 v}{\sqrt{\lambda_3^2 + \lambda_2^2 v^2}} \quad (5)$$

$$\sin \alpha = \frac{\lambda_3}{\sqrt{\lambda_3^2 + \lambda_2^2 v^2}}$$

By differentiating (5) with respect to time the equation for $\dot{\alpha}$ is determined.

SECTION II. DISCUSSION

When F/W_0 , I_{sp} , and y_0 are specified along with α_0 and $\dot{\alpha}_0$, a trajectory is determined. In this study α_0 has been parameterized in order that all permissible trajectories can be investigated.

For a given F/W_0 , I_{sp} , y_0 , and α_0 a trajectory is computed until the energy condition has been attained. $\dot{\alpha}_0$ is then varied until the angular momentum condition has been satisfied along with the energy condition.

It has been found that for some interval on α_0 , $\alpha_{0L} < \alpha_0 < \alpha_{0R}$, there is a pair of $\dot{\alpha}_0$'s for each α_0 in this interval which satisfies the end conditions. This can be seen in Figures (1 - 6) where trajectories have been computed for different $\dot{\alpha}_0$'s when only the energy condition has been achieved. These figures were obtained using a $F/W_0 = .5$ and one with an $I_{sp} = 700$ sec for $y_0 = 100, 200$, and 300 km. Other diagrams similar to Figures (1 - 6) will not be shown since different parameters produce a similar effect.

The angular momentum taken from these trajectories has been plotted as a function of $\dot{\alpha}_0$ for parameters of α_0 . In this interval on $\dot{\alpha}_0$ the angular momentum attains a maximum, or the change of angular momentum with respect to $\dot{\alpha}_0$, $\frac{\Delta M}{\Delta \dot{\alpha}_0}$, goes to zero.

For convenience this maximum value for the angular momentum will be expressed as M_{max} and the angular momentum of the desired ellipse will be expressed as M^* . If $M_{max} > M^*$ for some α_0 then $\alpha_{0L} < \alpha_0 < \alpha_{0R}$ and there are two solutions corresponding to

$$\frac{\Delta M}{\Delta \dot{\alpha}_0} > 0 \text{ or } \frac{\Delta M}{\Delta \dot{\alpha}_0} < 0$$

evaluated at M^* . If $M_{max} = M^*$ then there is only one solution. This defines the lower and upper limits on α_0 , α_{0L} and α_{0R} . If $M_{max} < M^*$ then $\alpha_0 < \alpha_{0L}$ or $\alpha_{0R} < \alpha_0$ and the desired end conditions can not be satisfied.

This result has been consistent with all parameters F/W_0 , I_{sp} , and y_0 . This, of course, is not inconsistent with the calculus of variations formulation since it guarantees only a relative maximum (minimum) in the two point boundary value problem with variable end points.

SECTION III. RESULTS

Trajectories were computed for parameters of α_0 where $\alpha_{0L} < \alpha_0 < \alpha_{0R}$ for both solutions corresponding to

$$\frac{\Delta M}{\Delta \dot{\alpha}_0} > 0 \quad \text{and} \quad \frac{\Delta M}{\Delta \dot{\alpha}_0} < 0.$$

Hereafter, a T_1 solution will refer to the $\frac{\Delta M}{\Delta \dot{\alpha}_0} > 0$ solution

and a T_2 solution will refer to the $\frac{\Delta M}{\Delta \dot{\alpha}_0} < 0$ solution.

From these trajectories we have investigated weight into orbit, trajectory shapes, and control histories.

Figures (7 - 12) illustrate the ratio of the weight into orbit to the initial weight for different parameters of F/W_0 , I_{sp} , and y_0 as a function of α_0 . This ratio is designated as $\frac{W_c}{W_0}$. Subscripts of L and R on this ratio will refer to the T_1 and T_2 solution, respectively.

When α_0 was chosen near α_{0L} and was allowed to increase in the positive direction the T_1 solutions yielded

$\frac{W_c}{W_0}$ values greater than the T_2 solutions. However, as α_0 increased the difference between $\frac{W_c}{W_0}$ for the two solutions decreased until for some α_0^*

$$\left(\frac{W_c}{W_0}\right)_L - \left(\frac{W_c}{W_0}\right)_R = 0. \quad \text{In the interval } \alpha_{0L} < \alpha_0 < \alpha_0^*, \left(\frac{W_c}{W_0}\right)_L$$

attained a maximum value. This was consistent for all values of F/W_0 , I_{sp} , and y_0 considered. These maximum values of

$$\left(\frac{W_c}{W_0}\right)_L$$

have been plotted as a function of y_0 in Figures (13 - 15).

$(\frac{W_c}{W_o})_R$ did not always yield a maximum as a function of α_o . Certain restrictions were found on F/W_o , I_{sp} and y_o . These restrictions were:

1. For $y_o = 100$ km $(\frac{W_c}{W_o})_R$ did not maximize for any F/W_o and I_{sp} considered. Here, α_{oR} appears to be equivalent to α_o^* .
2. For $y_o = 200$ and 300 km $(\frac{W_c}{W_o})_R$ did maximize for $F/W_o = 1$ and $F/W_o = 2$. This maximum occurs in the interval $\alpha_o^* < \alpha_o < \alpha_{oR}$.
3. For $F/W_o = .5$ $(\frac{W_c}{W_o})_R$ did maximize for $y_o = 300$ km with $I_{sp} = 400$ and 500 sec. This maximum occurs in the interval $\alpha_o^* < \alpha_o < \alpha_{oR}$.

Since $(\frac{W_c}{W_o})_R$ did not maximize for $y_o = 100$ km for the different F/W_o and I_{sp} values, graphs similar to Figures (13 - 15) can not be shown for the T_2 solutions.

For launch window considerations the angle ω is defined as the angle between the launch vertical and perigee of the terminal orbit. ω is negative when measured clockwise from perigee and positive when measured counter-clockwise. ω is determined once the end conditions have been satisfied. Remembering that the end conditions are determined by α_o and $\dot{\alpha}_o$ it is obvious that a non-optimum α_o yields a non-optimum ω , whereas, an optimum α_o yields an optimum ω . In this study an optimum α_o is defined as the α_o which maximizes

$$(\frac{W_c}{W_o}).$$

Thus, a launch window representation can be given with $\frac{W_c}{W_o}$ as a function of $\Delta\omega$, where $\Delta\omega$ is defined as the deviation between non-optimum ω 's and the optimum ω , i.e., $\Delta\omega = \omega_{n-opt} - \omega_{opt}$. If $\Delta\omega$ is negative this will imply

departure is prior to the optimum ω and if $\Delta\omega$ is positive this will imply departure is after the optimum ω .

$\frac{W_c}{W_0}$ has been plotted as a function of $\Delta\omega$ in Figures (16 - 28) for the different F/W_0 , I_{sp} , and y_0 values for both types of solutions. Figures (16 - 24) are the T_1 solutions and Figures (25 - 28) are the T_2 solutions. These graphs were obtained with α_0 being in the interval $\alpha_{0L} < \alpha_0 < \alpha_{0R}$. Unfortunately, we were not able to obtain $\alpha_0 = \alpha_{0L}$ and α_{0R} which would imply the limits on ω , i.e., $\omega = \omega_L$ and $\omega = \omega_R$. However, we were able to obtain ω 's near ω_L and ω_R . Due to this it should be emphasized that the reader of this report should not extrapolate values of $\frac{W_c}{W_0}$ as a function of $\Delta\omega$.

By comparing the T_1 solutions with the T_2 solutions on Figures (16 - 24) with Figures (25 - 28) a distinction is seen between the two sets of solutions. For the T_1 solutions it is seen that the largest portion of the interval on $\Delta\omega$ is on the positive axis, whereas, for the T_2 solutions the largest portion of $\Delta\omega$ is on the negative axis. In other words, there is more time allotted after the optimum ω for the T_1 solutions and more time allotted prior to the optimum ω for the T_2 solutions. The rate of change of ω with respect to time, $\dot{\omega}$, is shown in Figure (29) as a function of y_0 in order that ω may be converted to time.

The reader can easily see the effects that the parameters F/W_0 , I_{sp} , and y_0 have on the size of a launch window.

The trajectory shapes for both types of solutions have been plotted (Figures 30 - 48). For better detail, altitude versus range has been plotted. This has been done for non-optimum and optimum situations. The trajectories shown in Figures (30 and 31) are typical examples for a non-optimum α_0 . These results were obtained with a $F/W_0 = .5$, $I_{sp} = 400$ and 900 sec, and $\alpha_0 = -40^\circ$. Figures (32 and 33) are non-optimum examples similar to Figures (30 and 31) except $F/W_0 = 1$ and $\alpha_0 = -20^\circ$. The optimum trajectories are shown in Figures (34 - 48) for the different F/W_0 and I_{sp} values.

From these illustrations it is seen that the T_2 solutions are initially away from perigee and inject into the terminal

orbit near perigee, whereas, the T_1 solutions are initially near perigee and injection is away from perigee. This result is typical for non-optimum and optimum trajectories.

The angle, χ , between the launch vertical and the vehicle's thrust vector has been plotted as a function of time in Figures (49 - 58). Non-optimum χ programs have been plotted in Figure (49) in order to illustrate the behavior of χ for α_0 's in the interval $\alpha_{0L} < \alpha_0 < \alpha_{0R}$ for both solutions. This is typical for the different values of F/W_0 , I_{sp} , and y_0 . The parameters chosen in this non-optimum example are $F/W_0 = 1$, $I_{sp} = 700$ sec, and $y_0 = 300$ km.

Optimum χ programs are shown in Figures (50 - 58) in terms of the two solutions or only in terms of the T_1 solutions if the T_2 solutions do not apply. The first set of these Figures (50 - 52) are for the non-intersecting case, i.e., $y_0 = 100$ km. Notice in particular for the lower F/W_0 , i.e., .5 in Figure (50) χ appears to be linear in time. In Figures (51 and 52) χ becomes non-linear with the extreme case being the higher $F/W_0 = 2$. Only the T_1 solutions apply to these figures.

In Figure (53) for $y_0 = 200$ km χ appears to be linear in time again for $F/W_0 = .5$. Again, only the T_1 solutions apply to this figure. In Figures (54 and 55) both solutions apply. Notice that the χ programs for both solutions appear linear and are essentially parallel.

Figures (56 - 58) illustrate χ for $y_0 = 300$ km for both types of solutions. Figure (56) shows χ is non-linear for $F/W_0 = .5$. In Figures (57 and 58) the two solutions appear to be linear and parallel.

The angle of attack, α , has been plotted as a function of time in Figures (59 - 68). α is the angle between the velocity vector and the thrust vector measured positive counter-clockwise. These α programs are the typical α -histories associated with the χ programs in Figures (49 - 58).

REFERENCE

1. Davidson, Mirt C., "A Survey of the Influence of Variations In Stage Characteristics on Optimized Trajectory Shaping, Part I: Two Stage Vehicle Injection Into Circular Orbit," MTP-AERO-63-29 dated April 24, 1963.

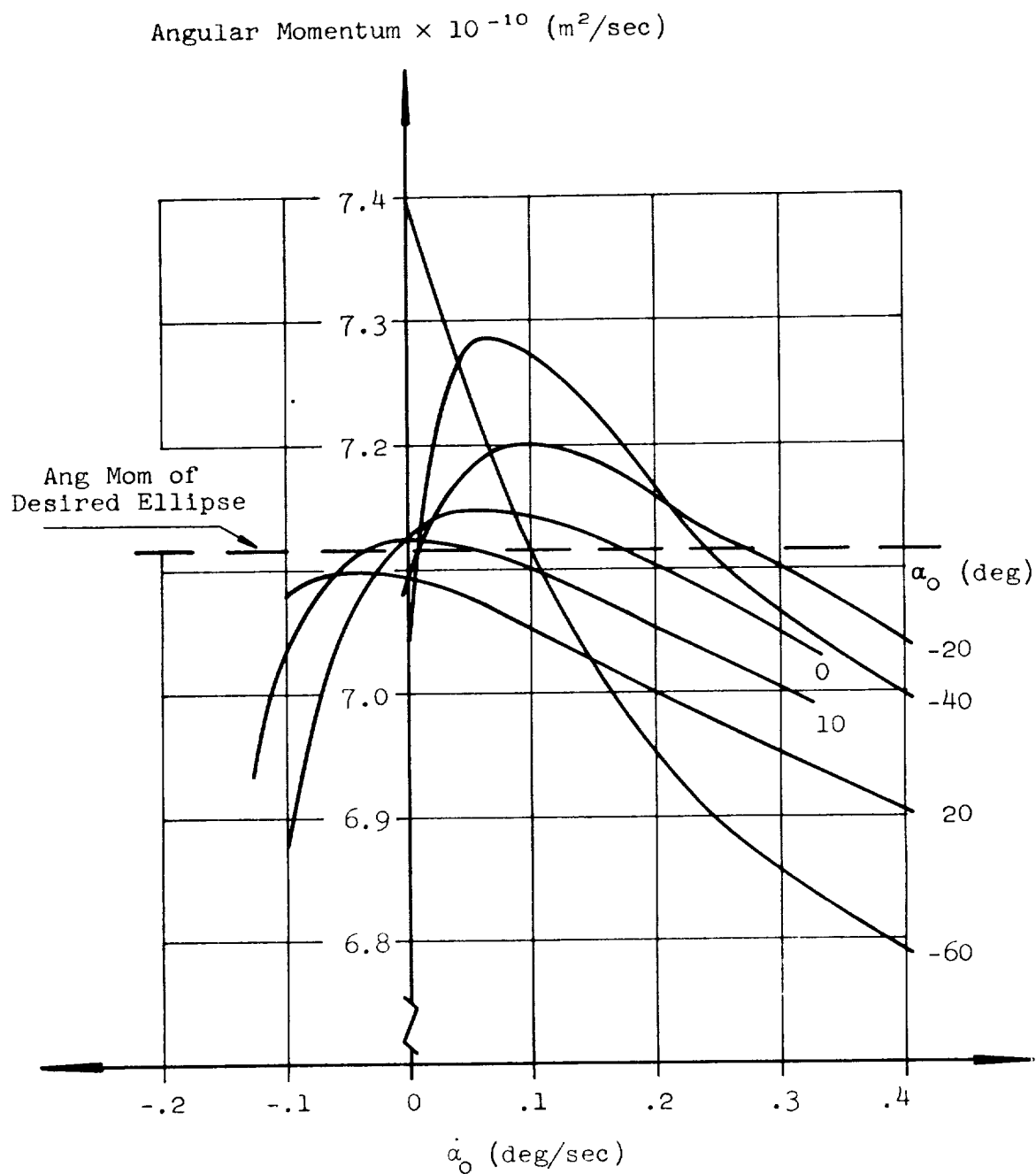


FIG. 1. VARIATION OF TERMINAL ANGULAR MOMENTUM
WITH $\dot{\alpha}_0$ FOR PARAMETERS OF α_0

FOR $F/W_0 = .5$; $y_0 = 100$ km; $I_{sp} = 700$ sec

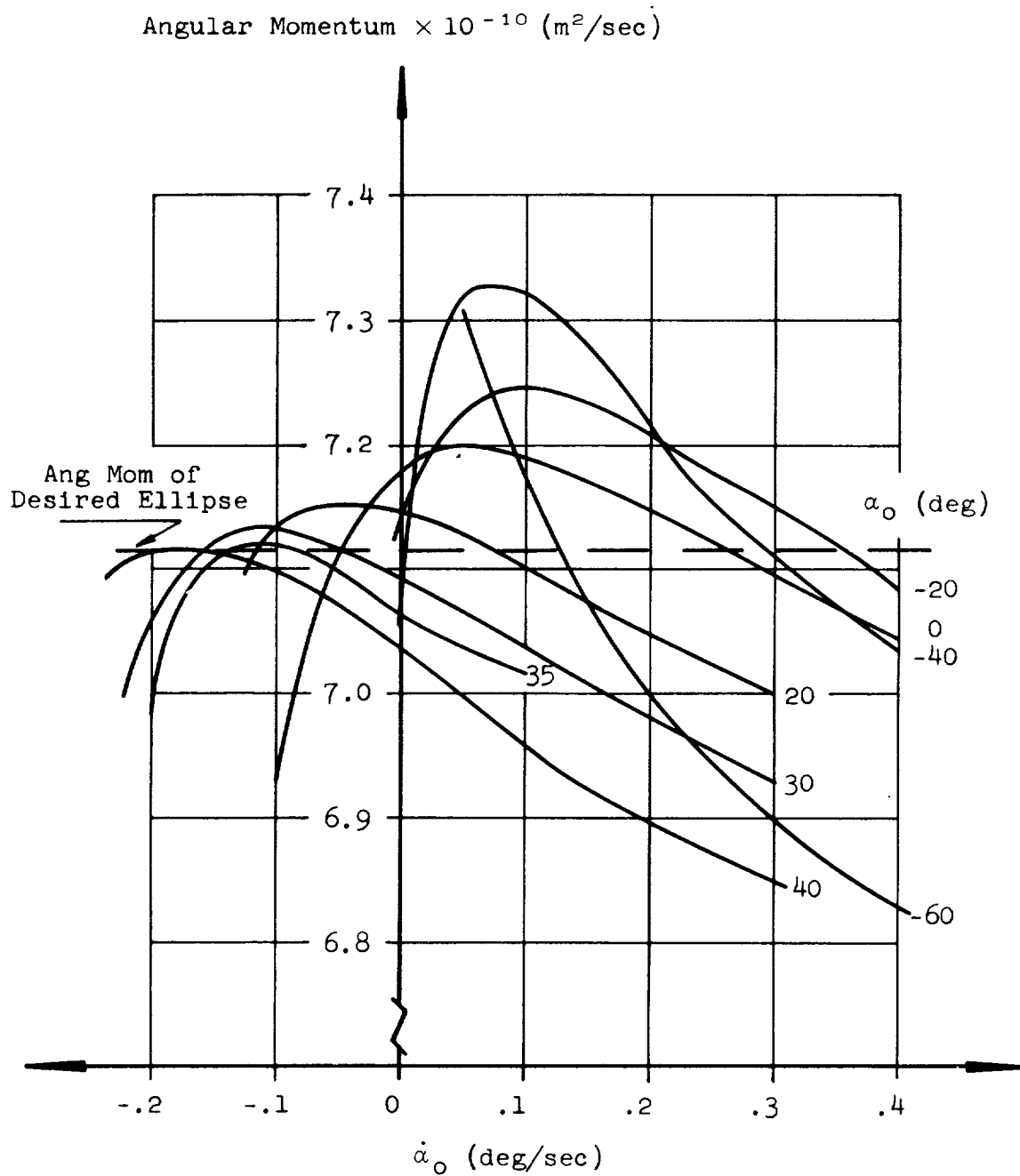


FIG. 2. VARIATION OF TERMINAL ANGULAR MOMENTUM
WITH α_0 FOR PARAMETERS OF α_0
FOR $F/W_0 = .5$; $y_0 = 200$ km; $I_{sp} = 700$ sec

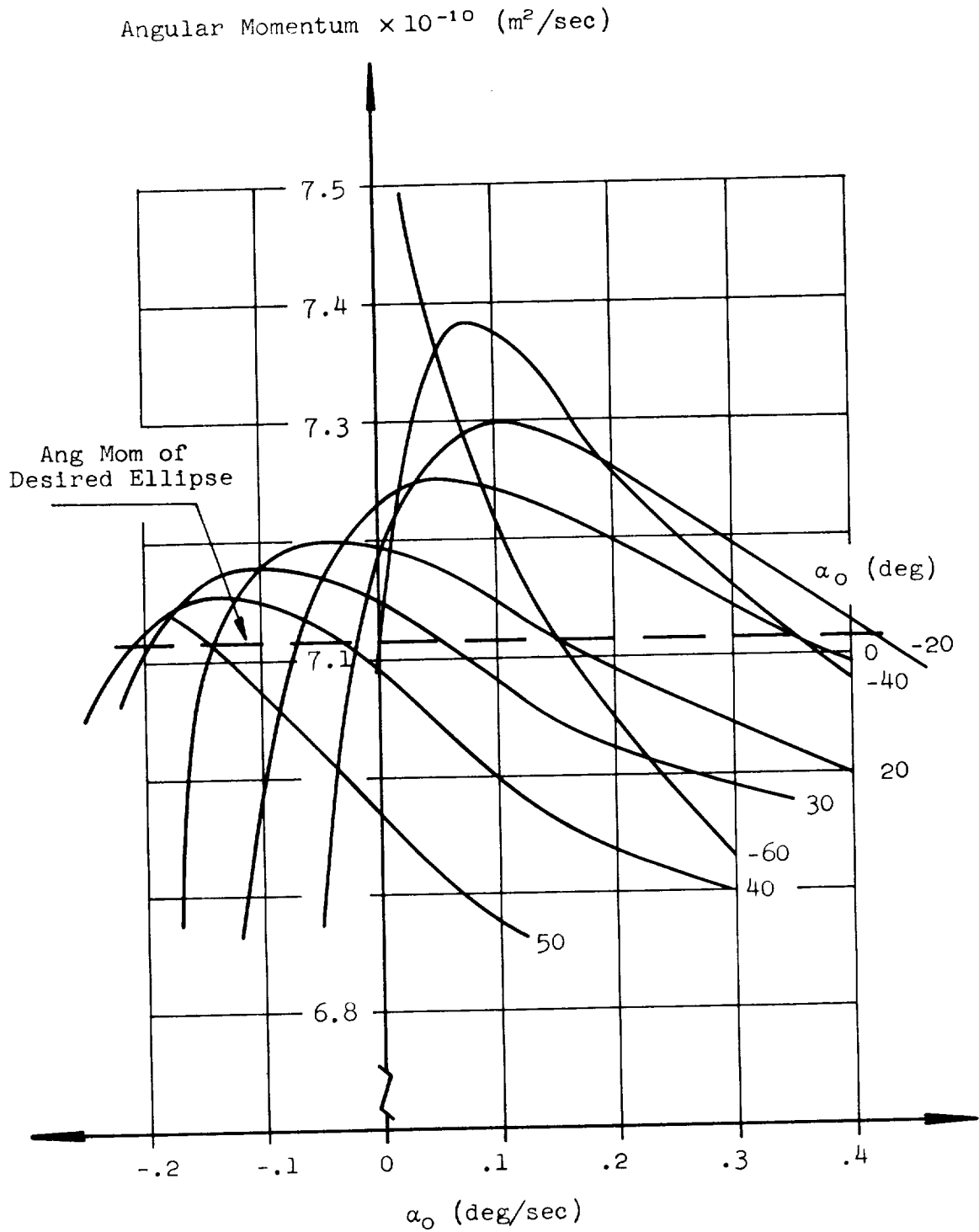


FIG. 3. VARIATION OF TERMINAL ANGULAR MOMENTUM
WITH $\dot{\alpha}_0$ FOR PARAMETERS OF α_0

FOR $F/W_0 = .5$; $y_0 = 300$ km; $I_{sp} = 700$ sec

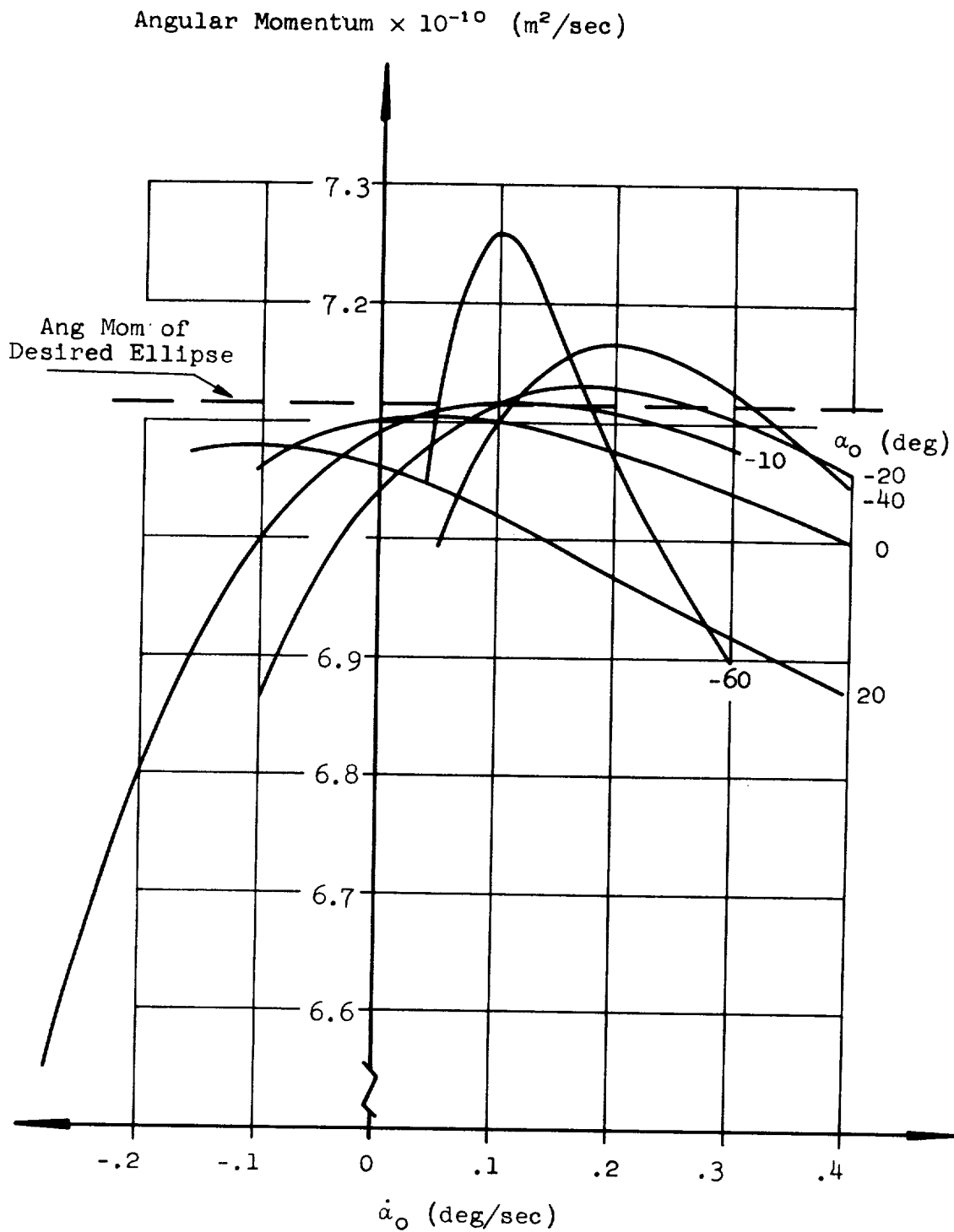


FIG. 4. VARIATION OF TERMINAL ANGULAR MOMENTUM

WITH $\dot{\alpha}_0$ FOR PARAMETERS OF α_0

FOR $F/W_0 = 1$; $y_0 = 100$ km; $I_{sp} = 700$ sec

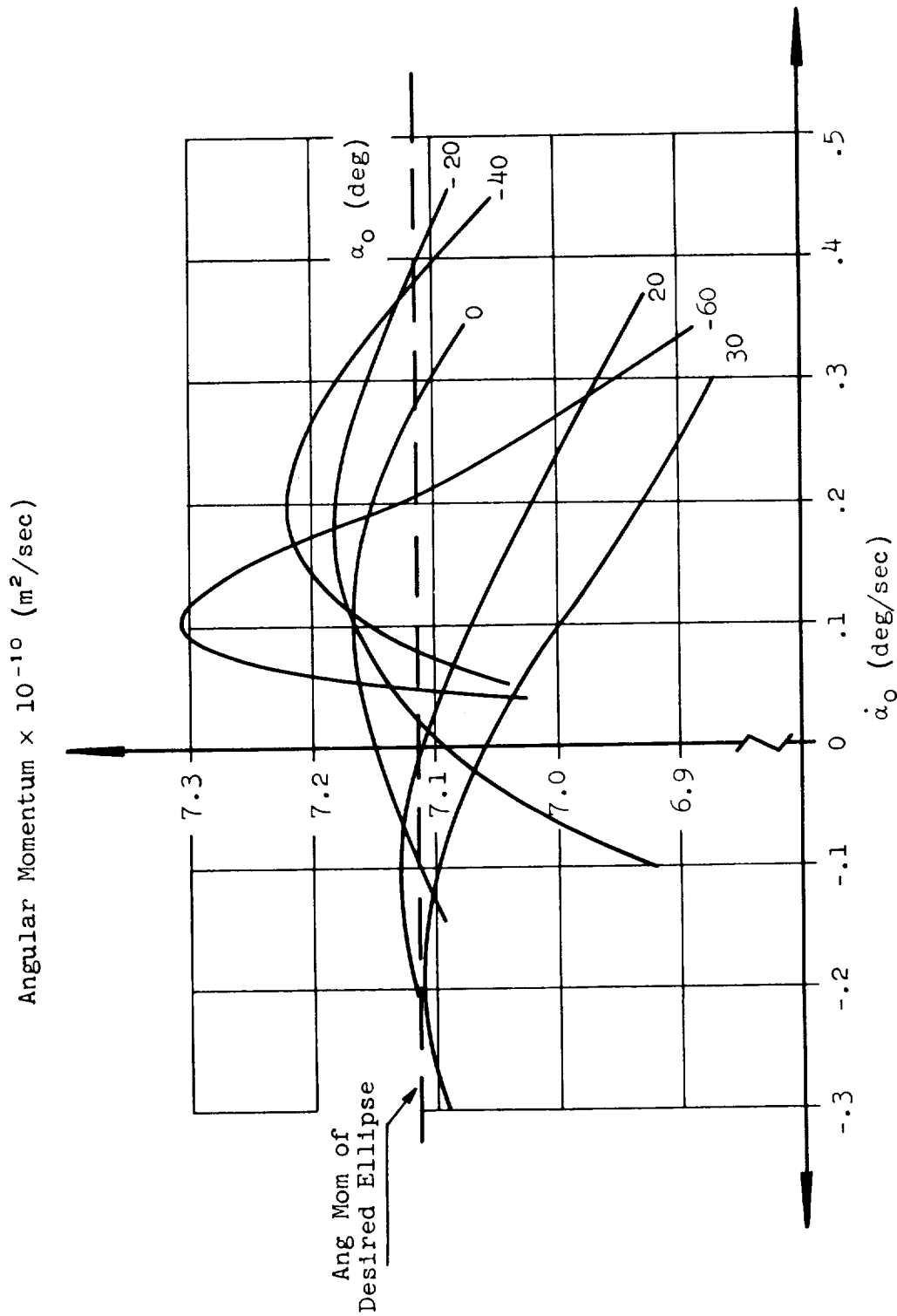


FIG. 5. VARIATION OF TERMINAL ANGULAR MOMENTUM WITH $\dot{\alpha}_0$ FOR PARAMETERS OF α_0

FOR $F/W_0 = 1$; $y_0 = 200$ km; $I_{sp} = 700$ sec

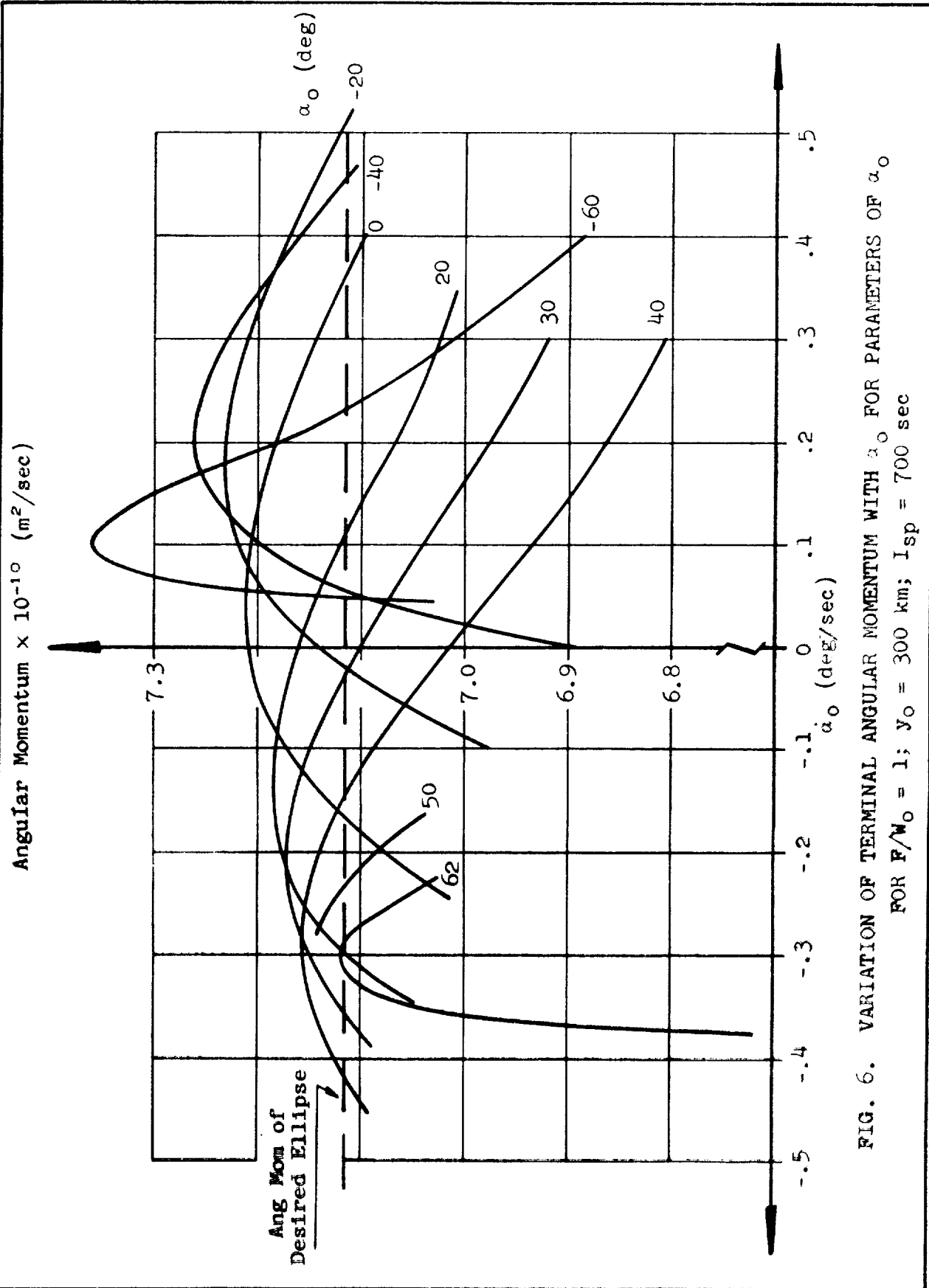


FIG. 6. VARIATION OF TERMINAL ANGULAR MOMENTUM WITH α_0 FOR PARAMETERS OF α_0
 FOR $P/W_0 = 1$; $y_0 = 300$ km; $I_{sp} = 700$ sec

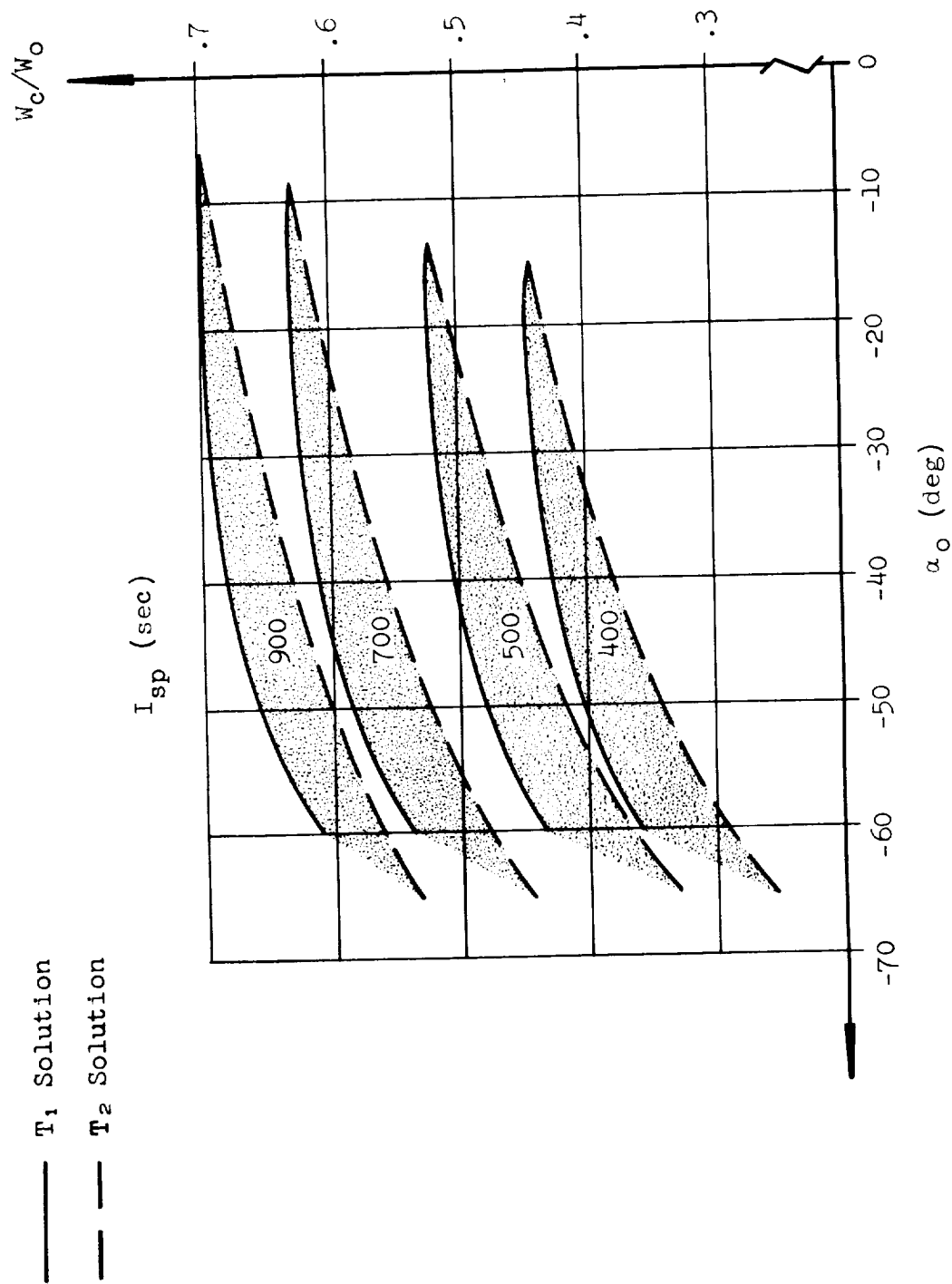


FIG. 7. RATIO OF THE CUTOFF WEIGHT TO THE INITIAL WEIGHT AS A FUNCTION OF α_o
 FOR PARAMETERS OF I_{sp} WITH $F/W_o = 1$; $y_o = 100$ km

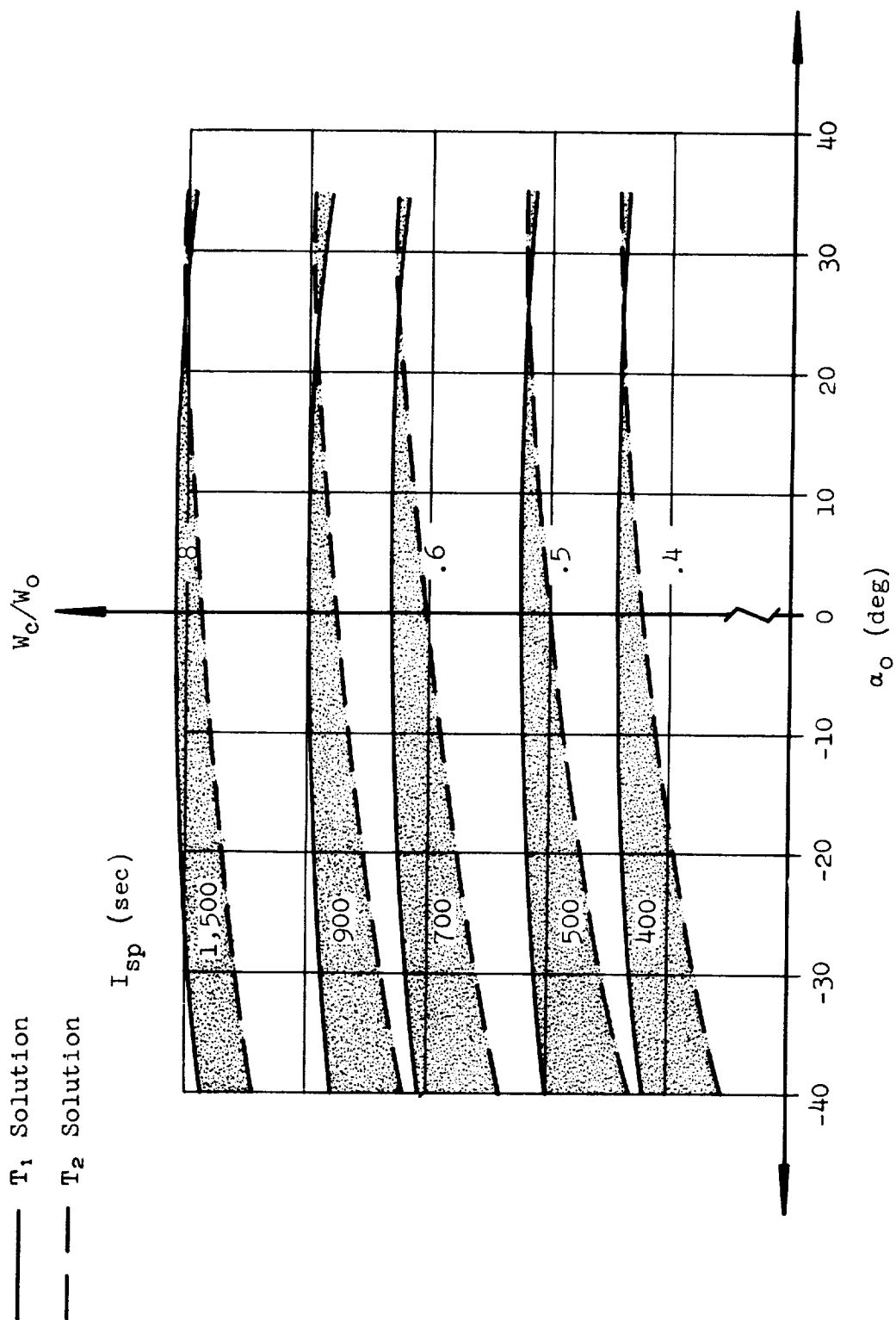


FIG. 8. RATIO OF THE CUTOFF WEIGHT TO THE INITIAL WEIGHT AS A FUNCTION OF α_o

FOR PARAMETERS OF I_{sp} WITH $F/W_o = 1$; $y_o = 200$ km

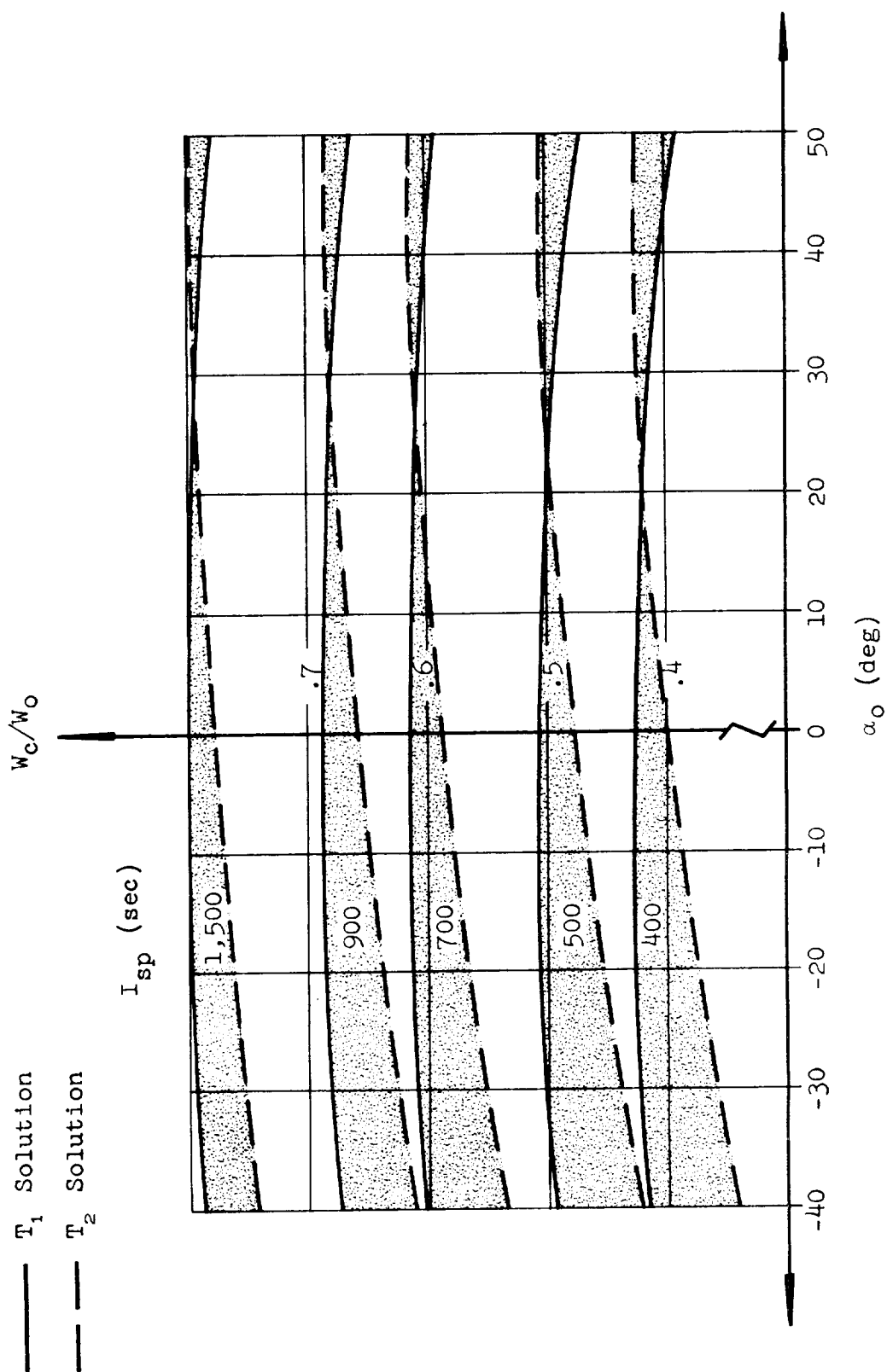


FIG. 9. RATIO OF THE CUTOFF WEIGHT TO THE INITIAL WEIGHT AS A FUNCTION OF α_0

FOR PARAMETERS OF I_{sp} WITH $F/W_0 = 1$; $y_0 = 300$ km

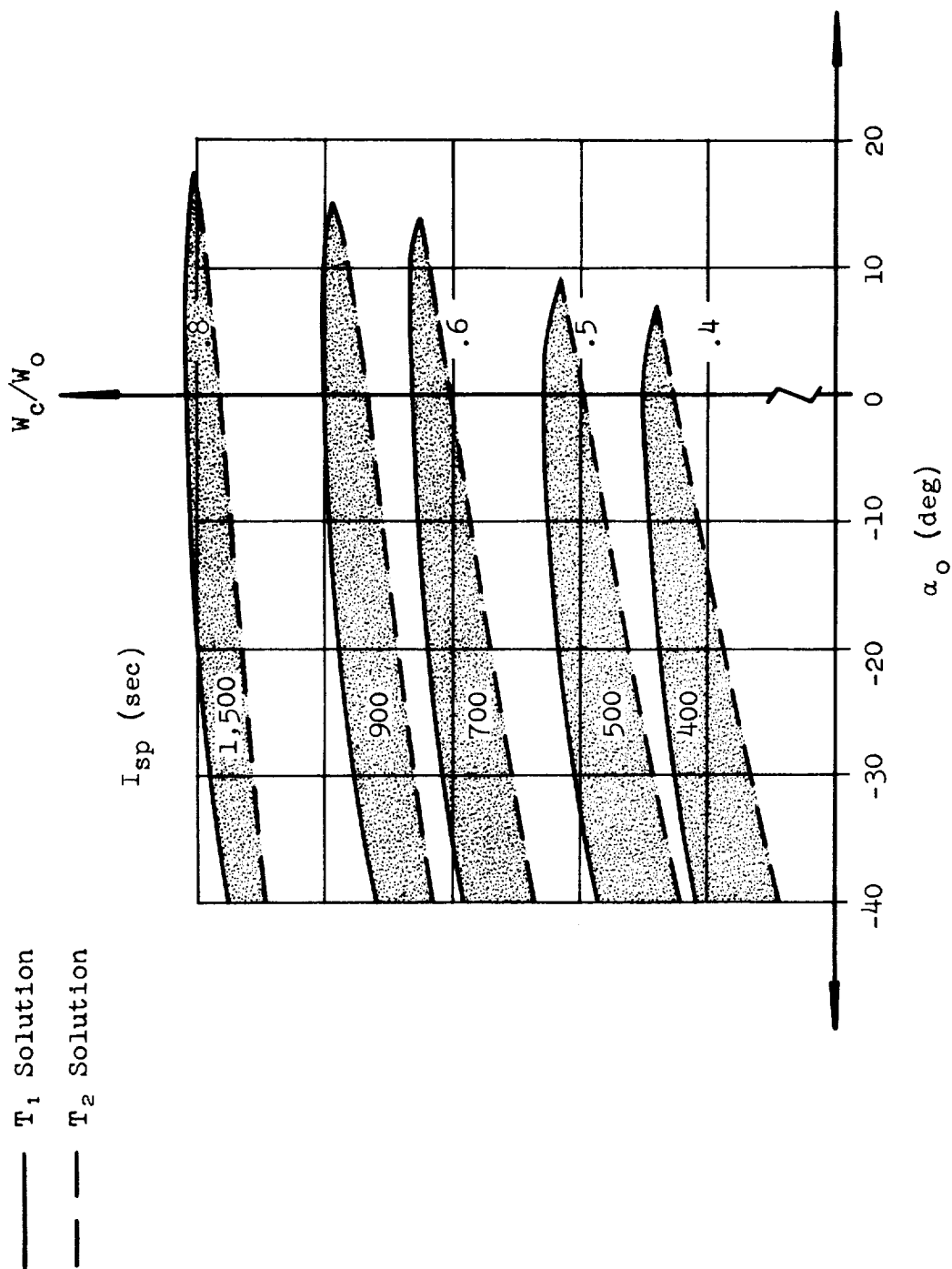


FIG. 10. RATIO OF THE CUTOFF WEIGHT TO THE INITIAL WEIGHT AS A FUNCTION OF α_o

FOR PARAMETERS OF I_{sp} WITH $F/W_o = .5$; $y_o = 100$ km

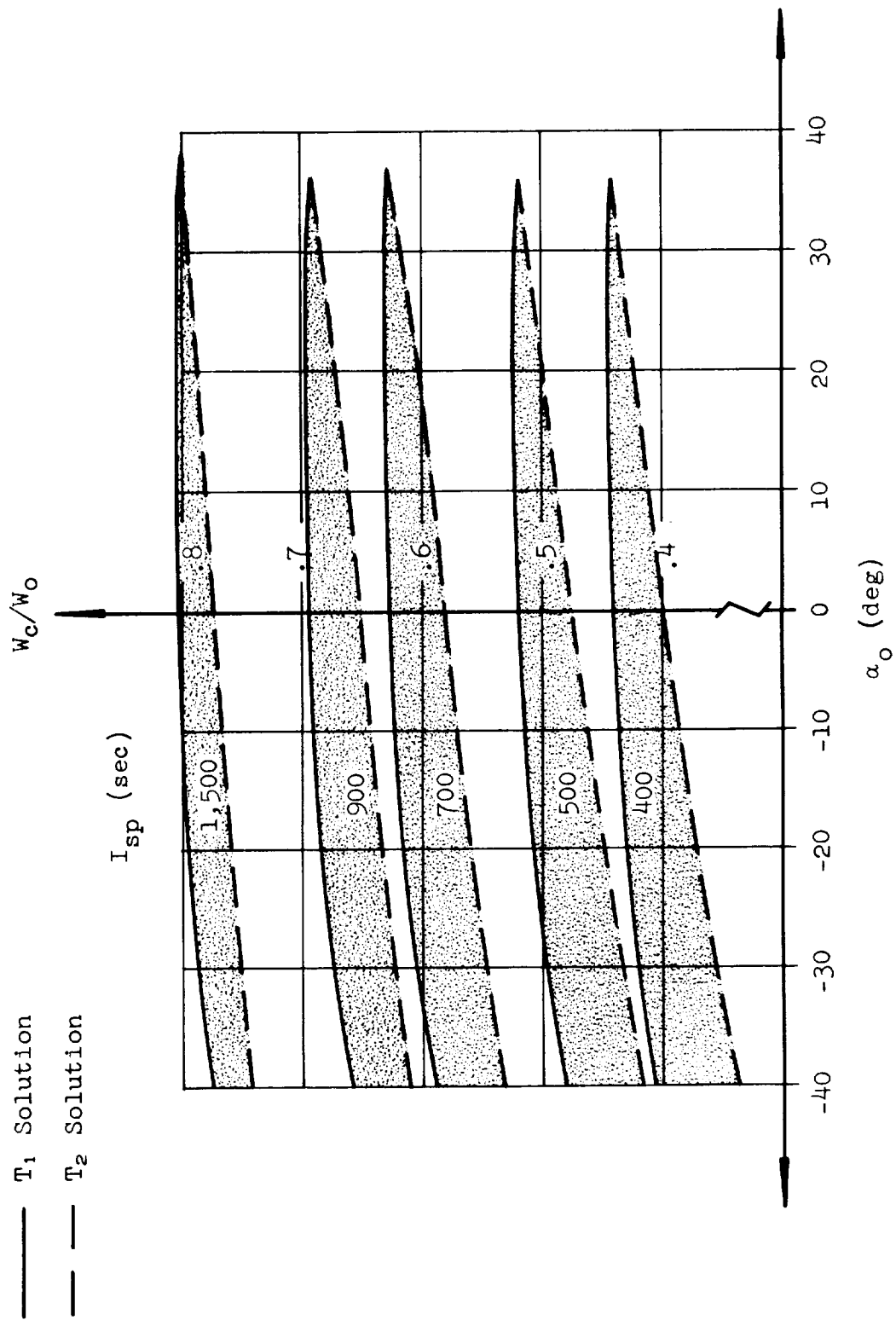


FIG. 11. RATIO OF THE CUTOFF WEIGHT TO THE INITIAL WEIGHT AS A FUNCTION OF α_o
 FOR PARAMETERS OF I_{sp} WITH $F/W_o = .5$; $y_o = 200$ km

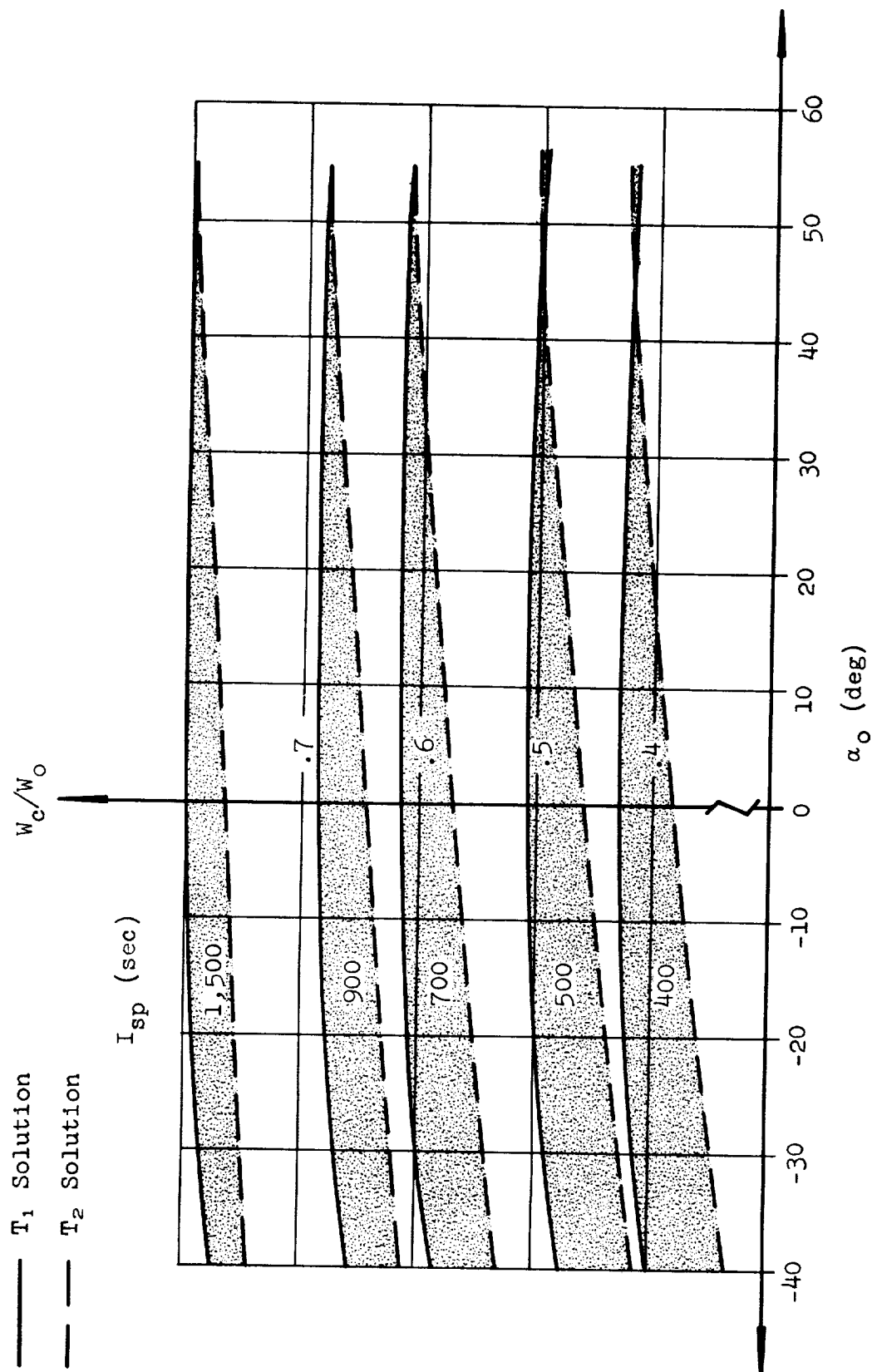


FIG. 12. RATIO OF THE CUTOFF WEIGHT TO THE INITIAL WEIGHT AS A FUNCTION OF α_o
 FOR PARAMETERS OF I_{sp} WITH $F/W_o = .5$; $y_o = 300$ km

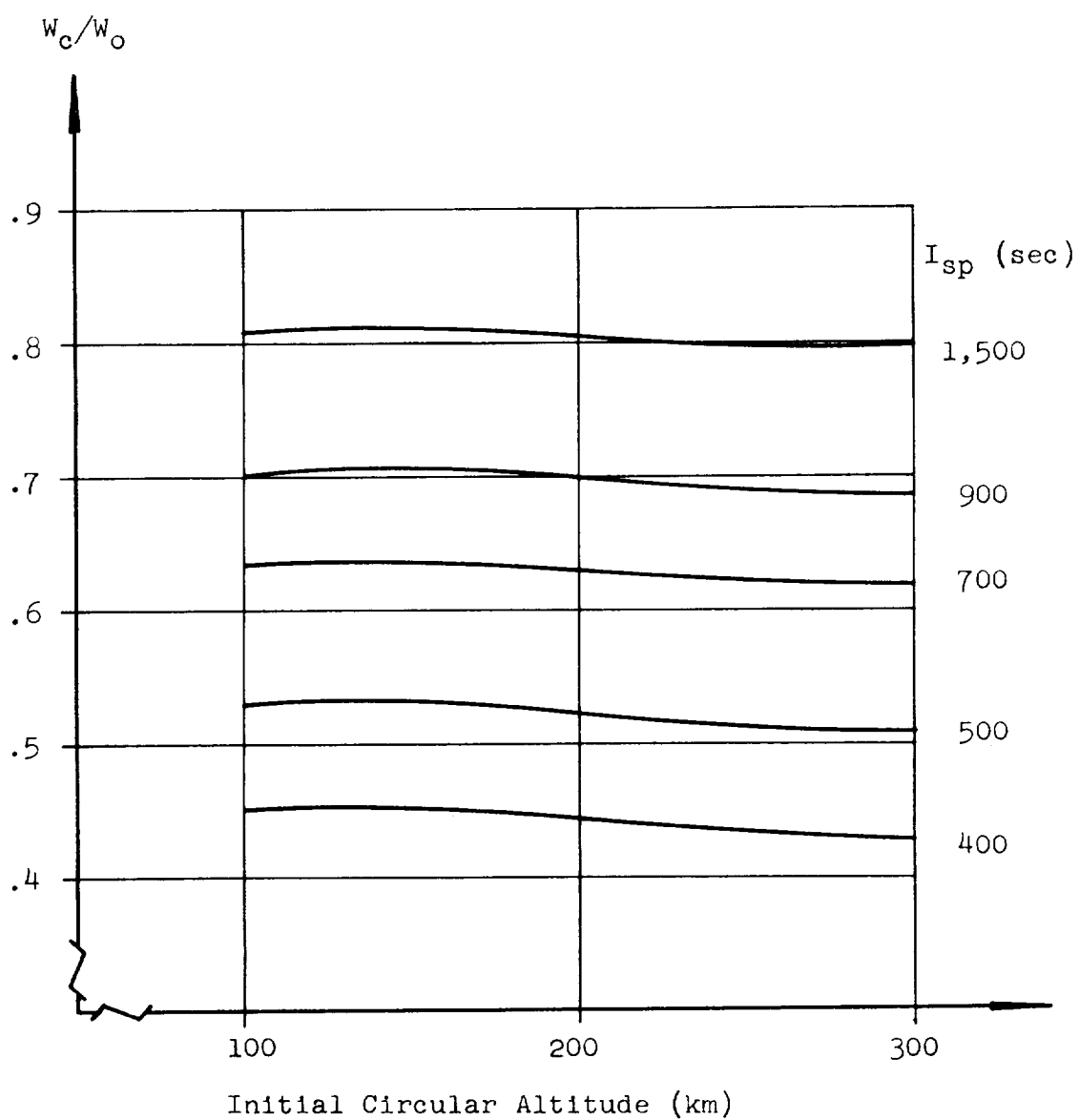


FIG. 13. RATIO OF THE CUTOFF WEIGHT TO THE INITIAL WEIGHT
AS A FUNCTION OF y_o FOR THE OPTIMUM α_o AND
THE T_1 SOLUTIONS FOR $F/W_o = .5$ AND PARAMETERS OF I_{sp}

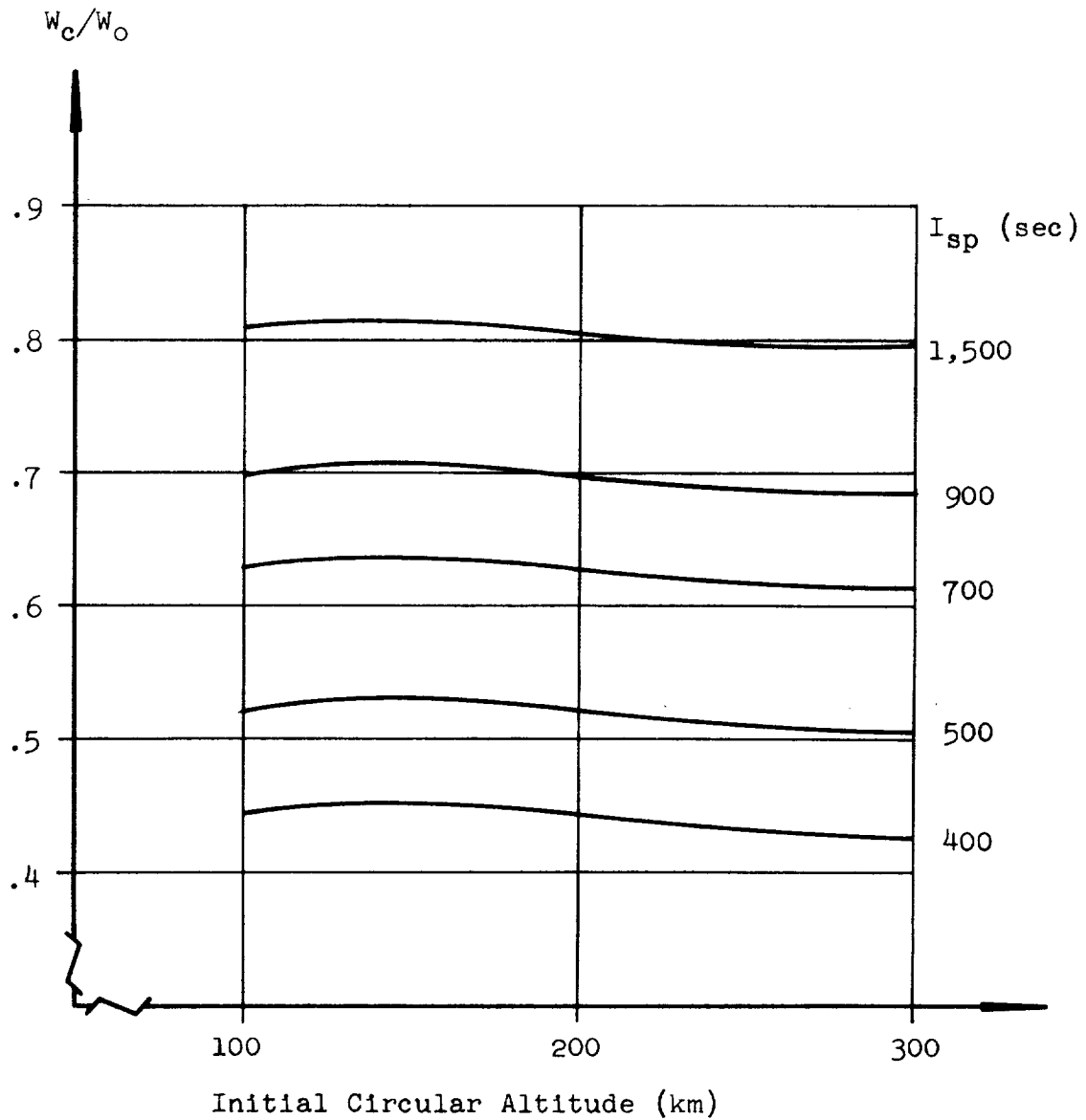


FIG. 14. RATIO OF THE CUTOFF WEIGHT TO THE INITIAL WEIGHT
 AS A FUNCTION OF y_o FOR THE OPTIMUM α_o AND
 THE T_1 SOLUTIONS FOR $F/W_o = 1$ AND PARAMETERS OF I_{sp}

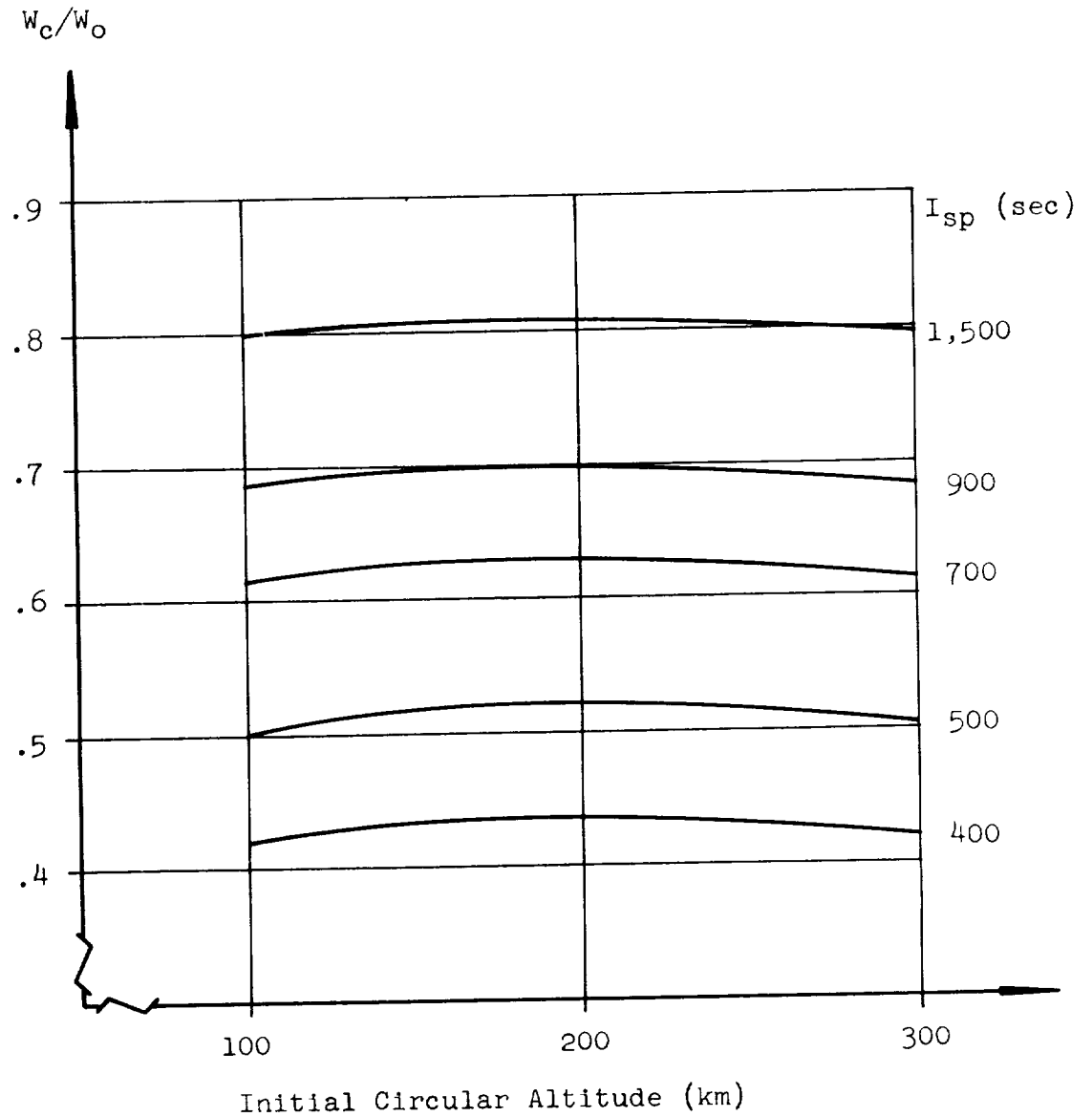


FIG. 15. RATIO OF THE CUTOFF WEIGHT TO THE INITIAL WEIGHT
AS A FUNCTION OF y_o FOR THE OPTIMUM α_o AND
THE T_1 SOLUTIONS FOR $F/W_o = 2$ AND PARAMETERS OF I_{sp}

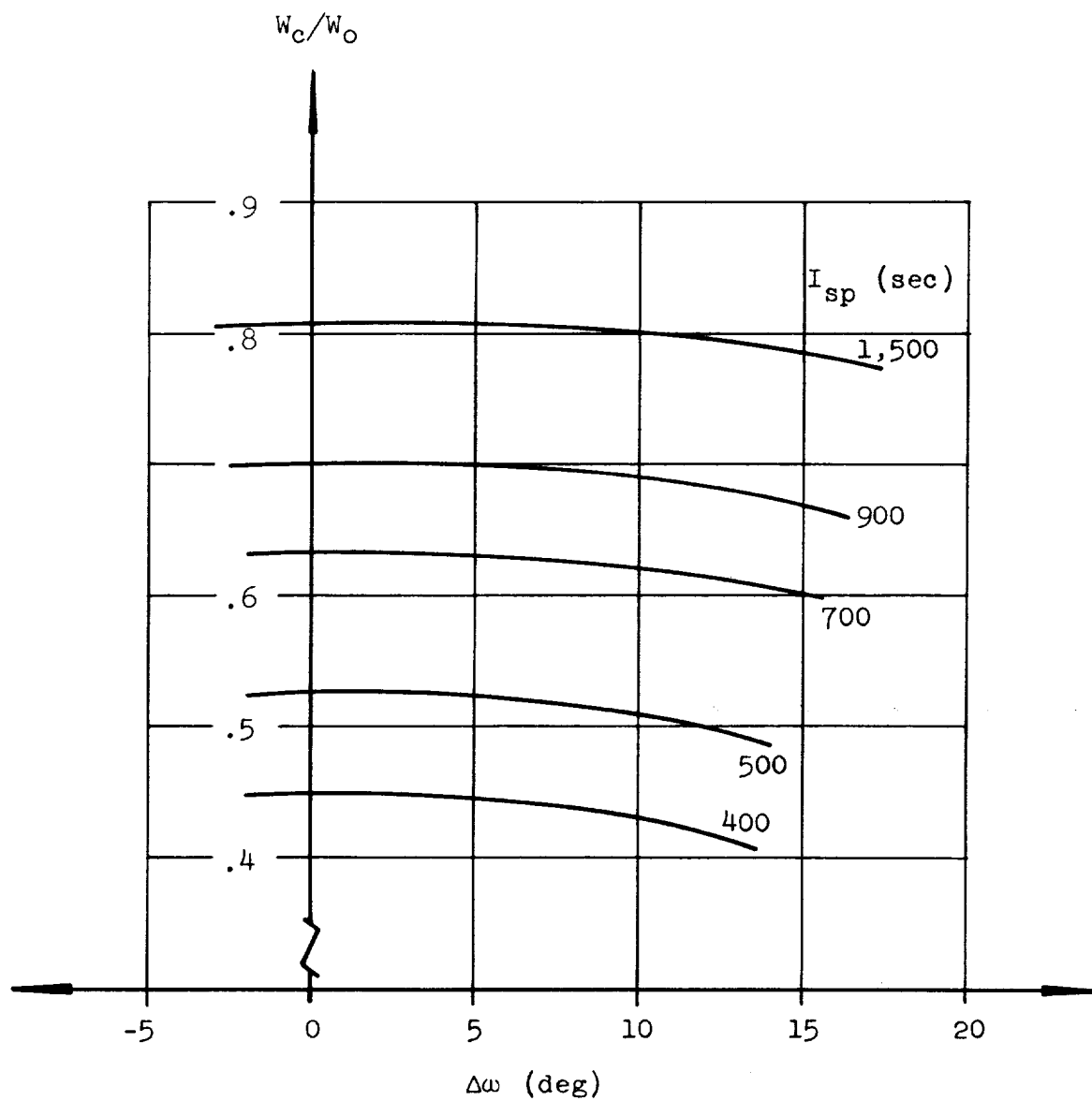


FIG. 16. W_c/W_o AS A FUNCTION OF THE DEVIATION OF
THE DEPARTURE ANGLE ω FROM THE OPTIMUM ω FOR THE T_1 SOLUTIONS
WITH $F/W_o = .5$; $y_o = 100$ km

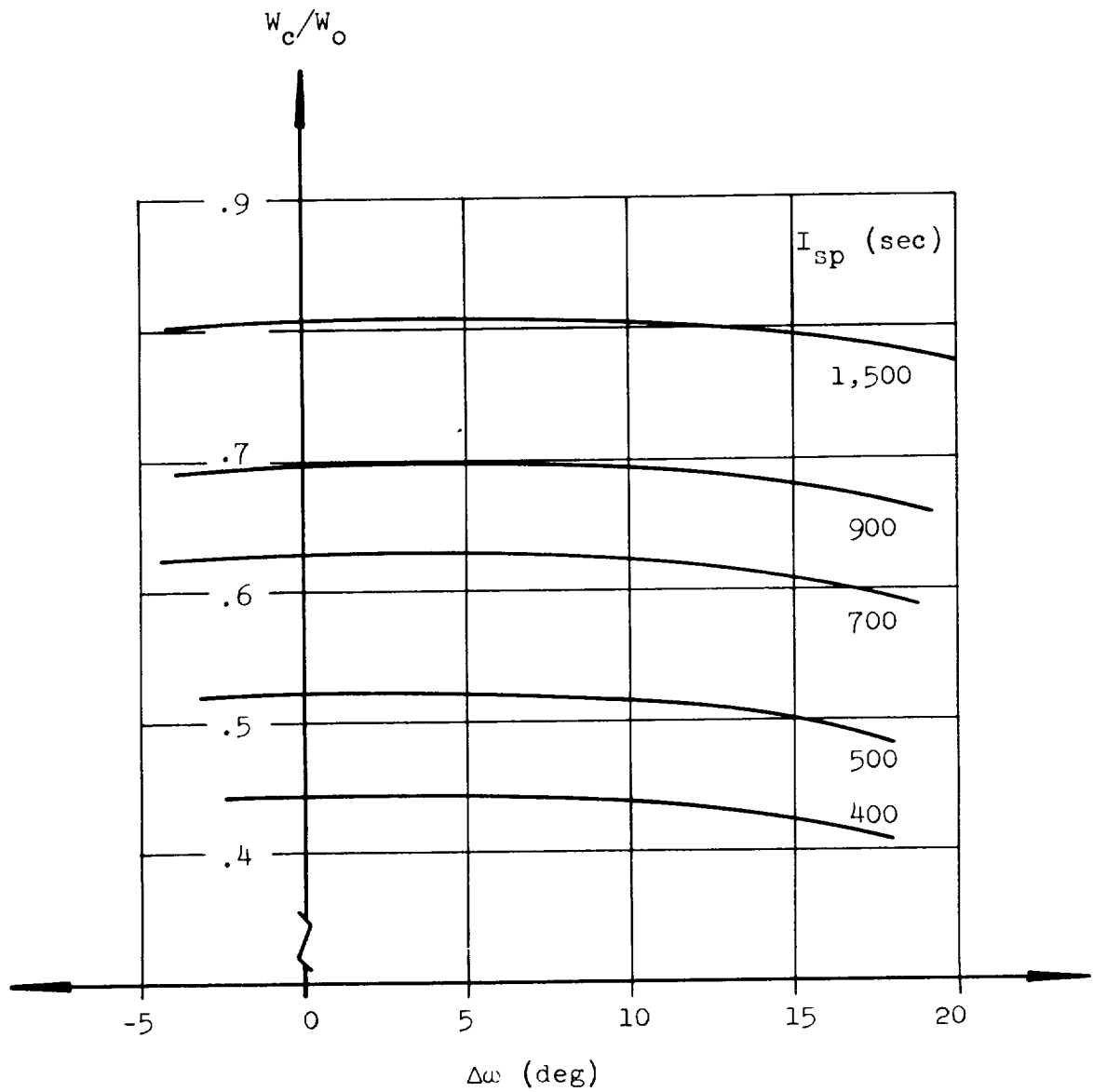


FIG. 17. W_c/W_o AS A FUNCTION OF THE DEVIATION OF
THE DEPARTURE ANGLE ω FROM THE OPTIMUM ω FOR THE T_1 SOLUTIONS
WITH $F/W_o = .5$; $y_o = 200$ km

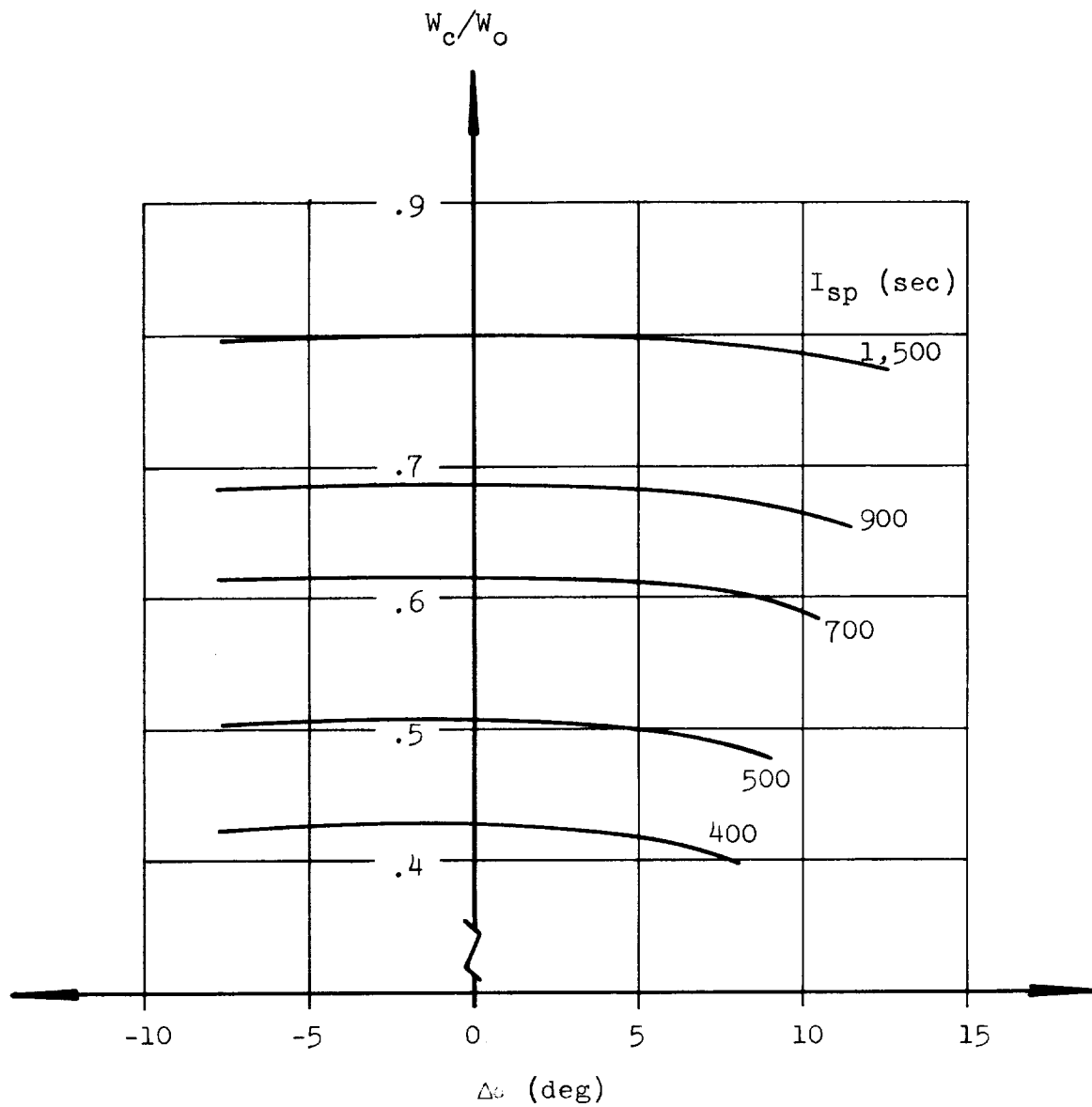


FIG. 18. W_c/W_o AS A FUNCTION OF THE DEVIATION OF THE DEPARTURE ANGLE α FROM THE OPTIMUM α_o FOR THE T_1 SOLUTIONS WITH $F/W_o = .5$; $y_o = 300$ km

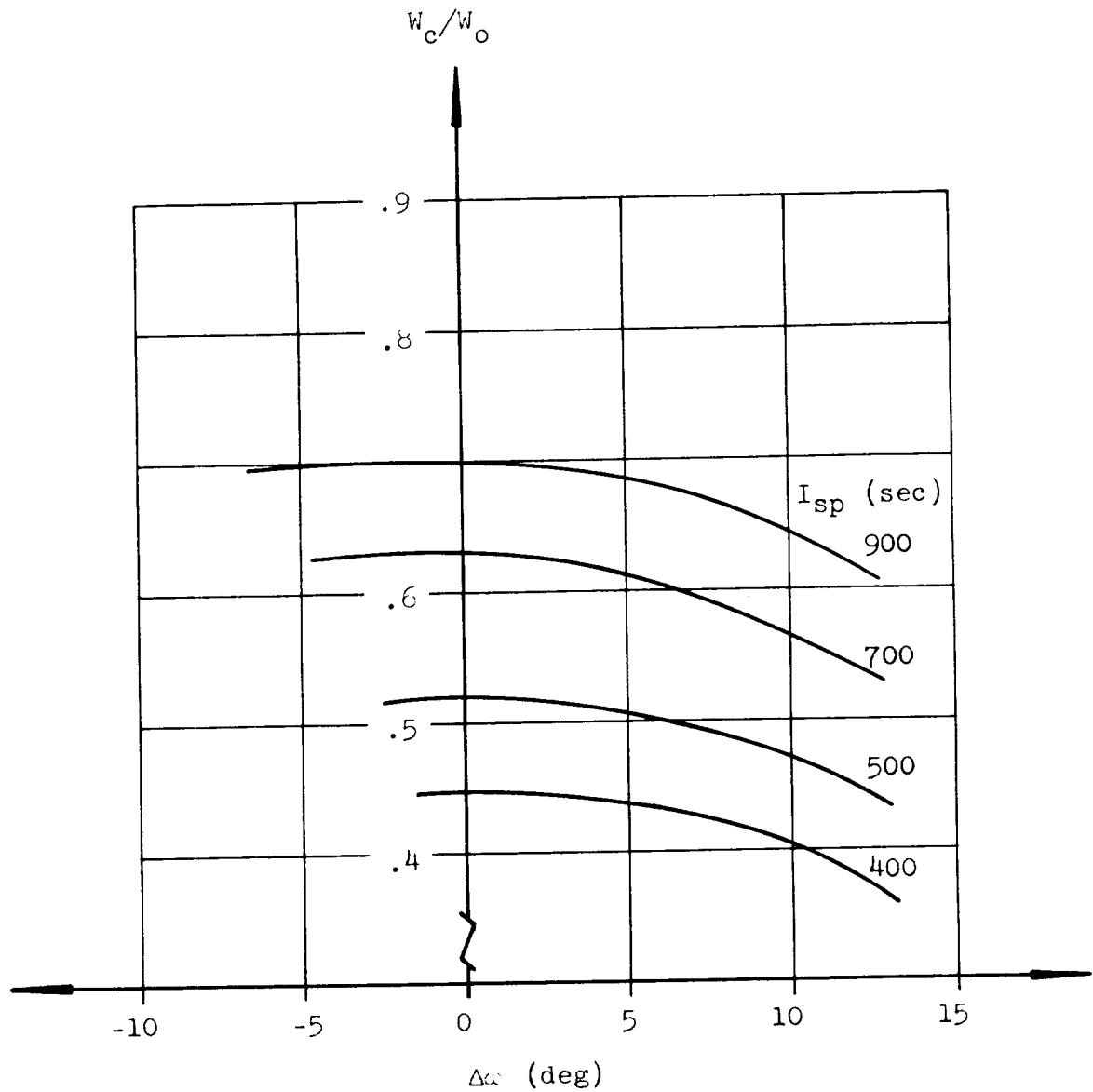


FIG. 19. W_c/W_o AS A FUNCTION OF THE DEVIATION OF THE DEPARTURE ANGLE α FROM THE OPTIMUM α FOR THE T_1 SOLUTIONS WITH $F/W_o = 1$; $y_o = 100$ km

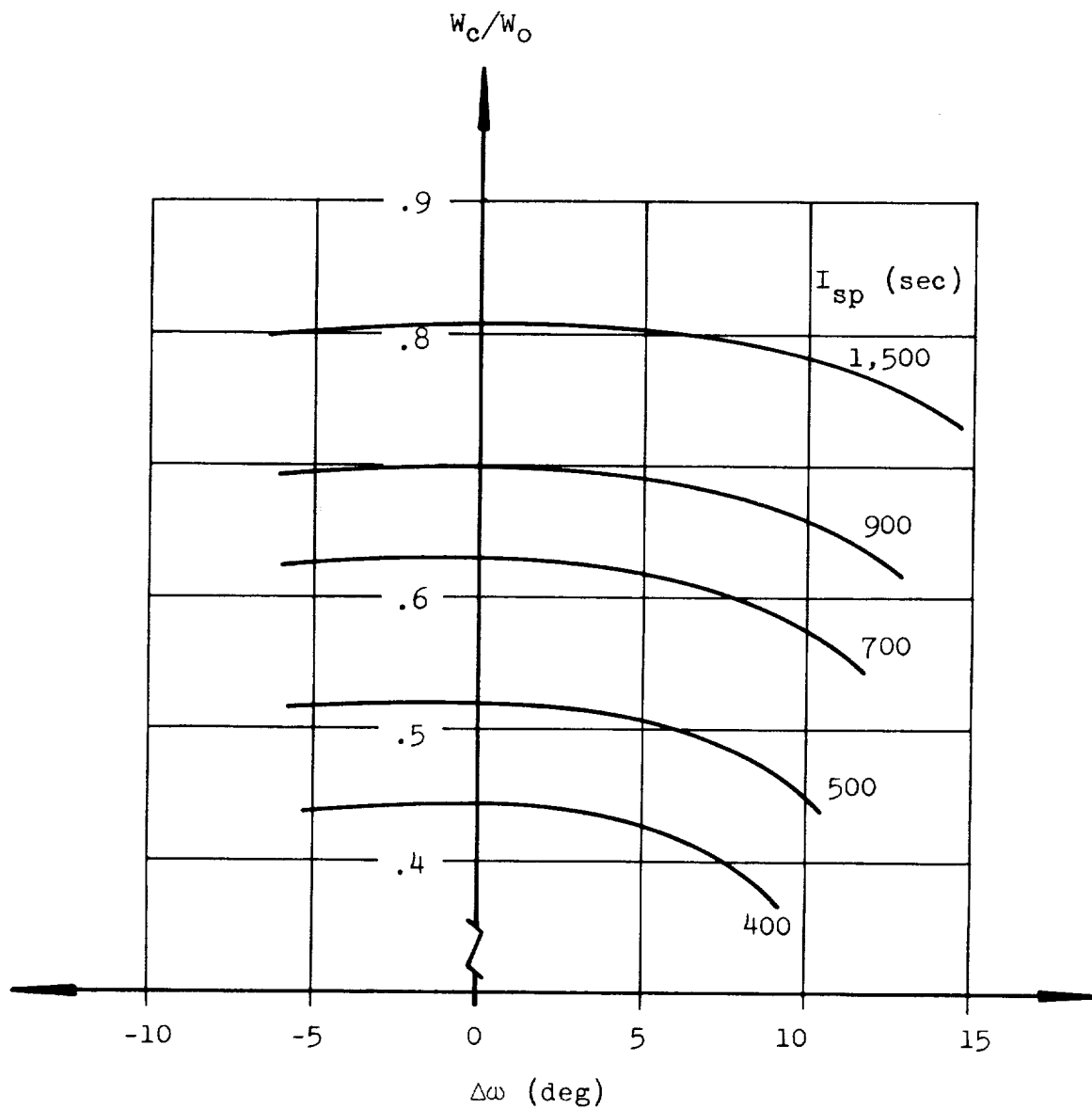


FIG. 20. W_c/W_o AS A FUNCTION OF THE DEVIATION OF
THE DEPARTURE ANGLE ω FROM THE OPTIMUM ω FOR THE T_1 SOLUTIONS
WITH $F/W_o = 1$; $y_o = 200$ km

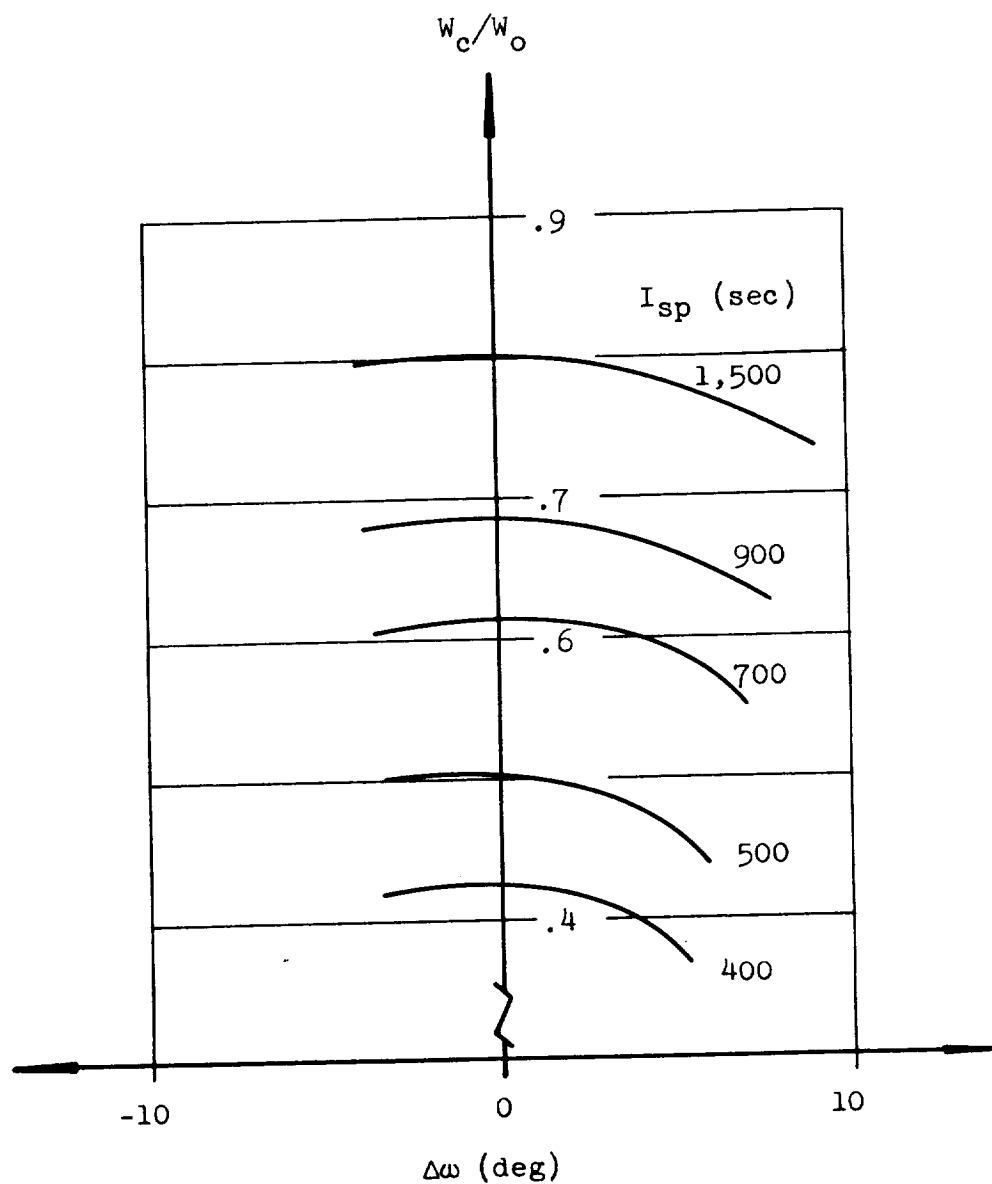


FIG. 21. W_c/W_0 AS A FUNCTION OF THE DEVIATION OF THE DEPARTURE ANGLE ω FROM THE OPTIMUM ω FOR THE T_1 SOLUTIONS WITH $F/W_0 = 1$; $y_0 = 300$ km

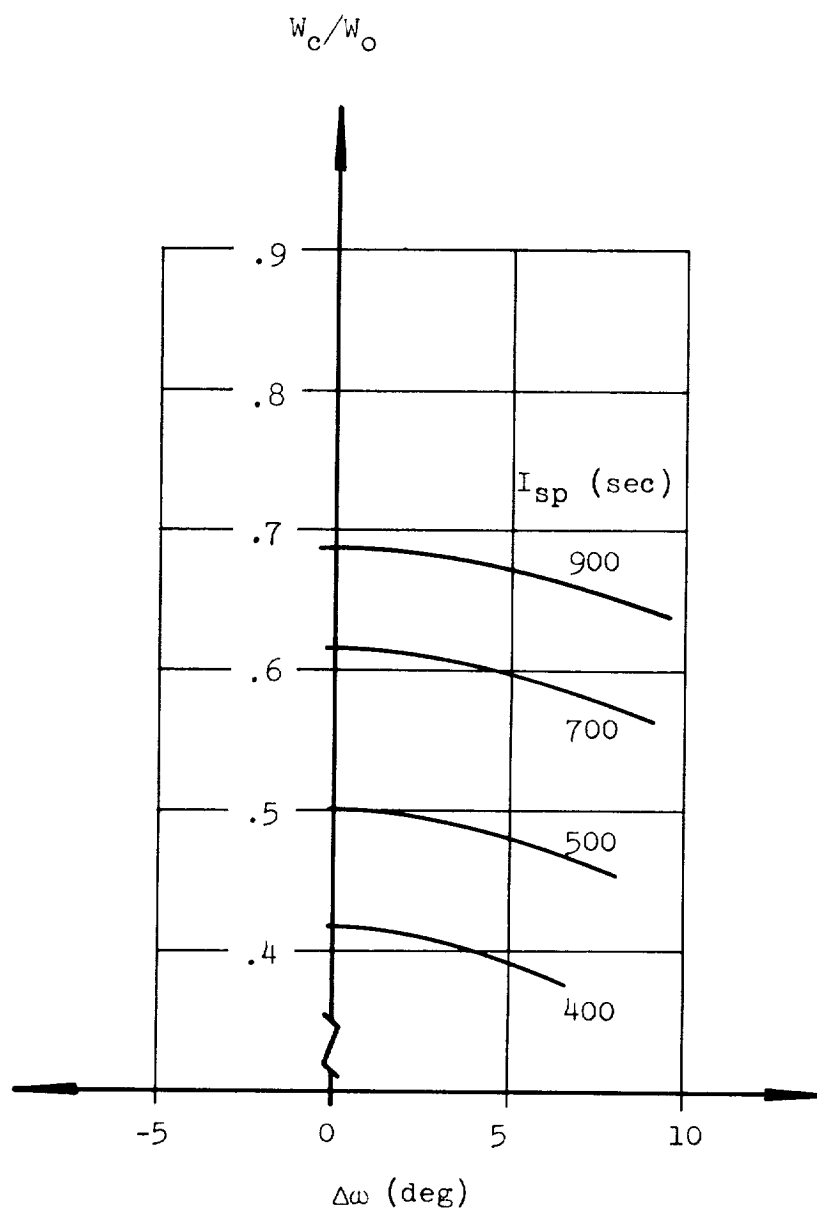


FIG. 22. W_c/W_o AS A FUNCTION OF THE DEVIATION OF THE DEPARTURE ANGLE ω FROM THE OPTIMUM ω FOR THE T_1 SOLUTIONS WITH $F/W_o = 2$; $y_o = 100$ km

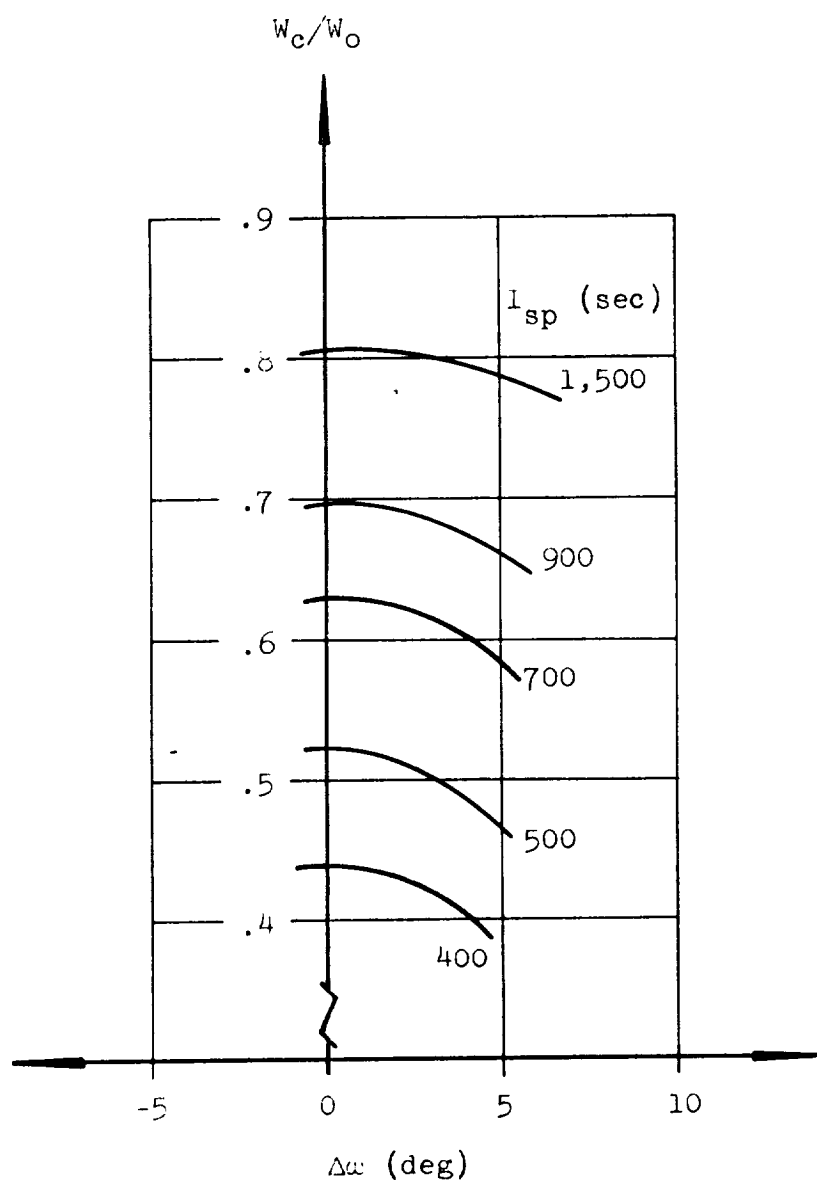


FIG. 23. W_c/W_0 AS A FUNCTION OF THE DEVIATION OF THE DEPARTURE ANGLE ω FROM THE OPTIMUM ω FOR THE T_1 SOLUTIONS WITH $F/W_0 = 2$; $y_0 = 200$ km

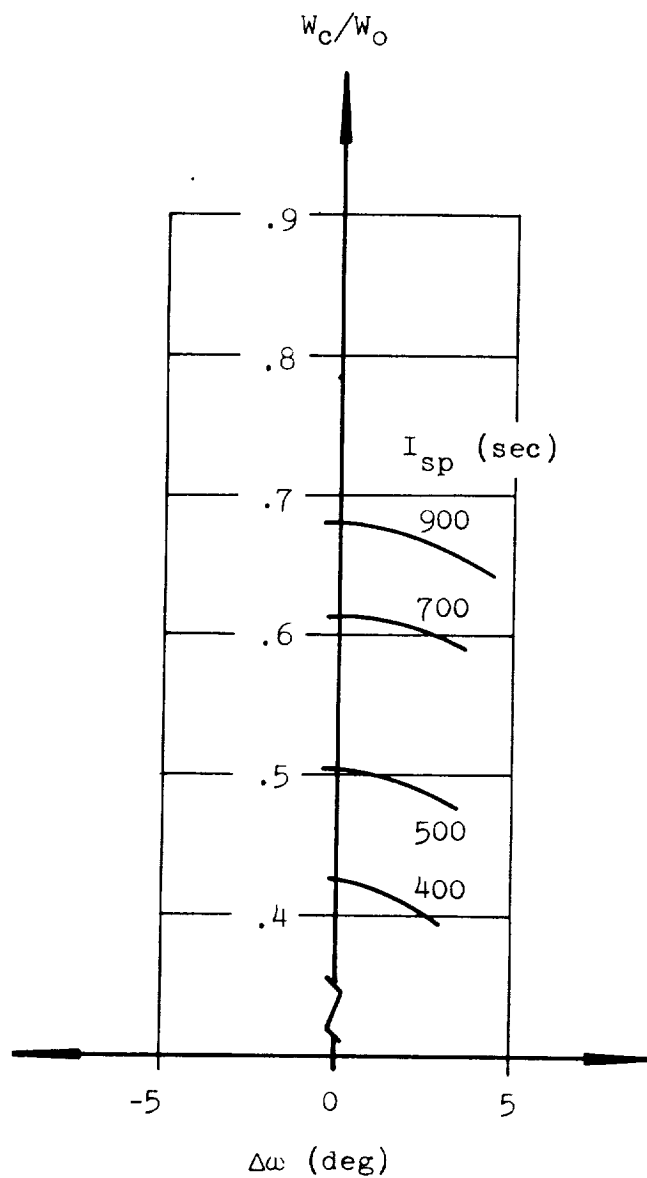


FIG. 24. W_c/W_o AS A FUNCTION OF THE DEVIATION OF THE DEPARTURE ANGLE ω FROM THE OPTIMUM ω FOR THE T_1 SOLUTIONS WITH $F/W_o = 2$; $y_o = 300$ km

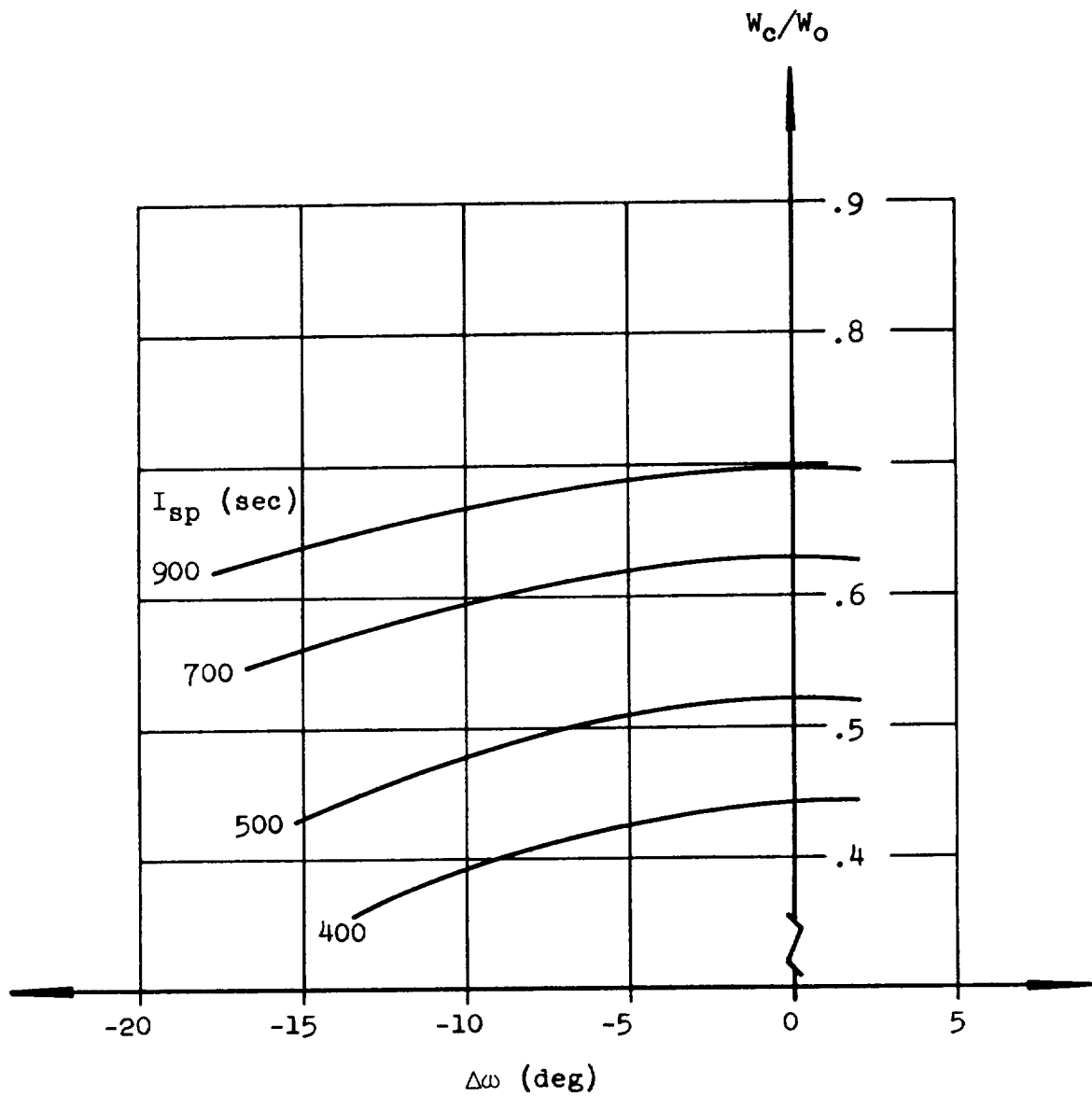


FIG. 25. W_c/W_0 AS A FUNCTION OF THE DEVIATION OF THE DEPARTURE ANGLE ω FROM THE OPTIMUM ω FOR THE T_2 SOLUTIONS WITH $F/W_0 = 1$; $y_0 = 200$ km

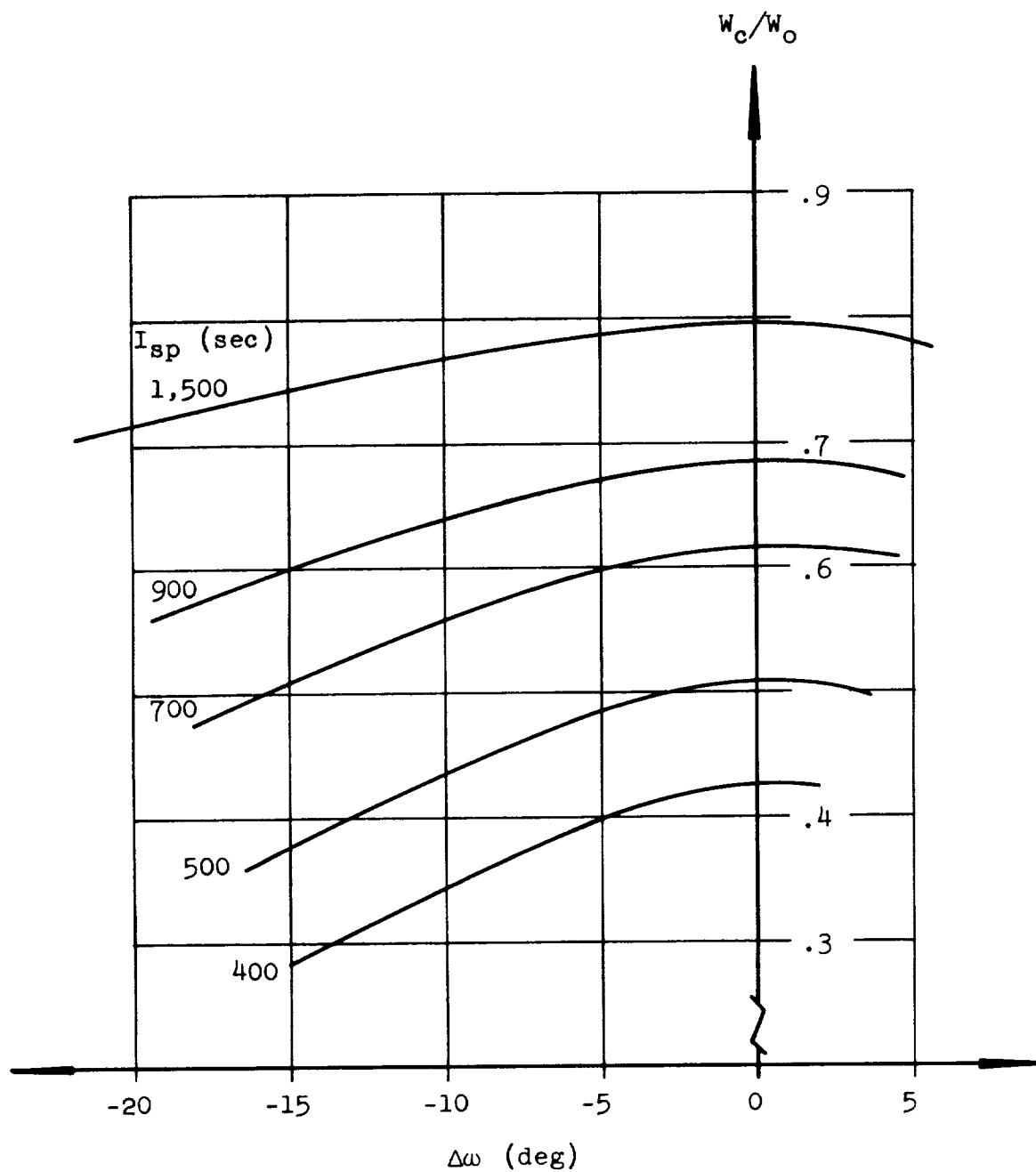


FIG. 26. W_c/W_o AS A FUNCTION OF THE DEVIATION OF
THE DEPARTURE ANGLE ω FROM THE OPTIMUM ω FOR THE T_2 SOLUTIONS
WITH $F/W_o = 1$; $y_o = 300$ km

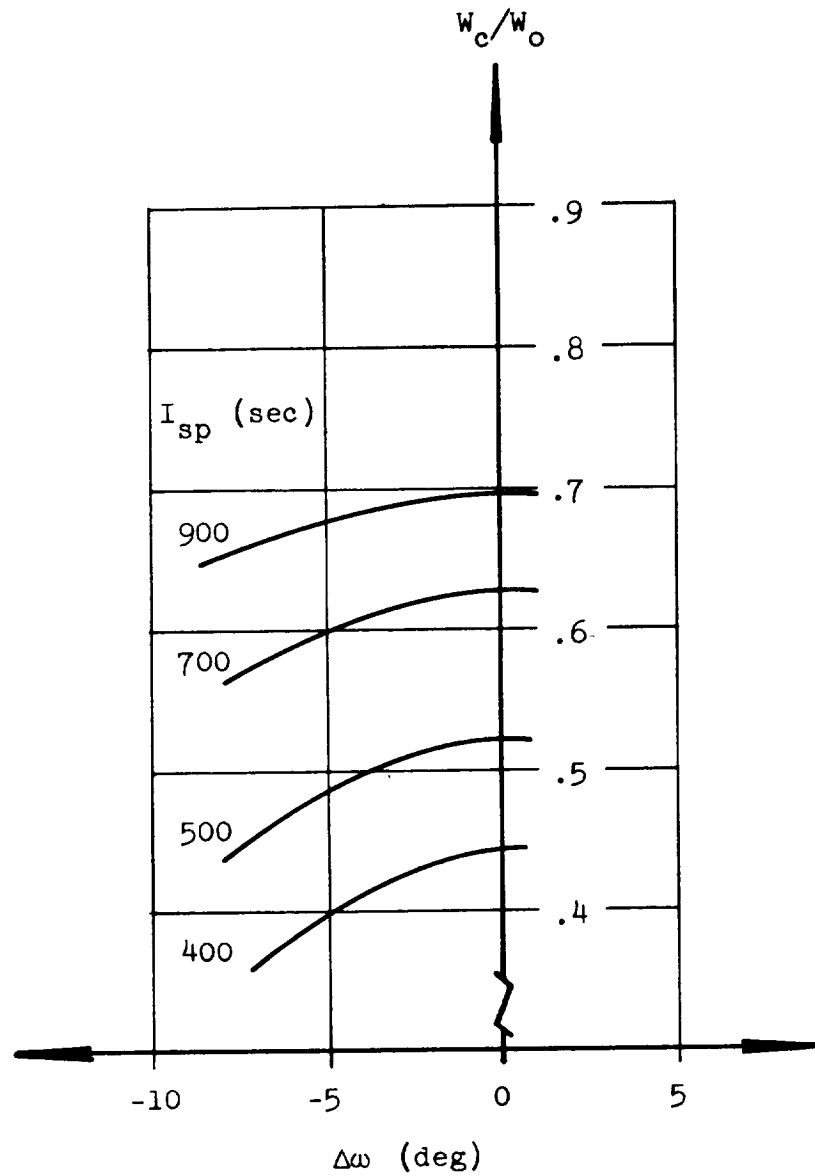


FIG. 27. W_c/W_o AS A FUNCTION OF THE DEVIATION OF THE DEPARTURE ANGLE ω FROM THE OPTIMUM ω FOR THE T_2 SOLUTIONS WITH $F/W_o = 2$; $y_o = 200$ km

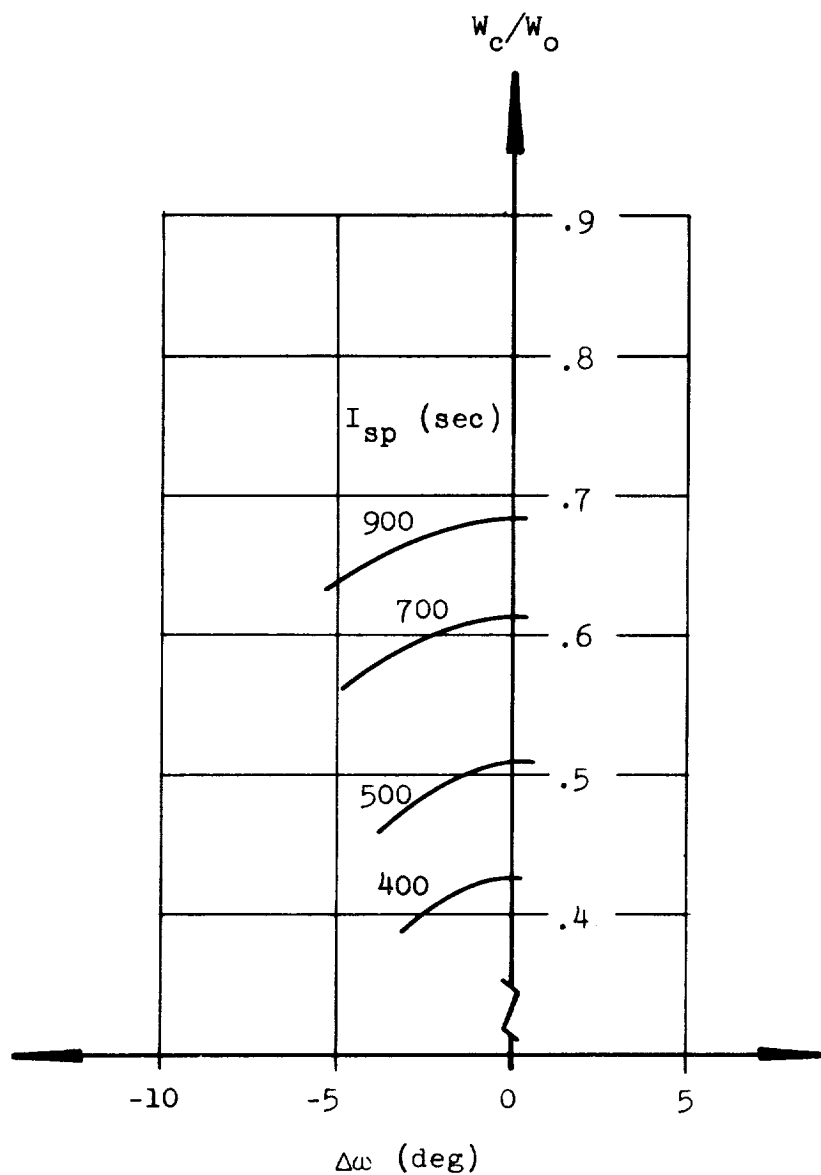


FIG. 28. W_c/W_o AS A FUNCTION OF THE DEVIATION OF
THE DEPARTURE ANGLE ω FROM THE OPTIMUM ω FOR THE T_2 SOLUTIONS
WITH $F/W_o = 2$; $y_o = 300$ km

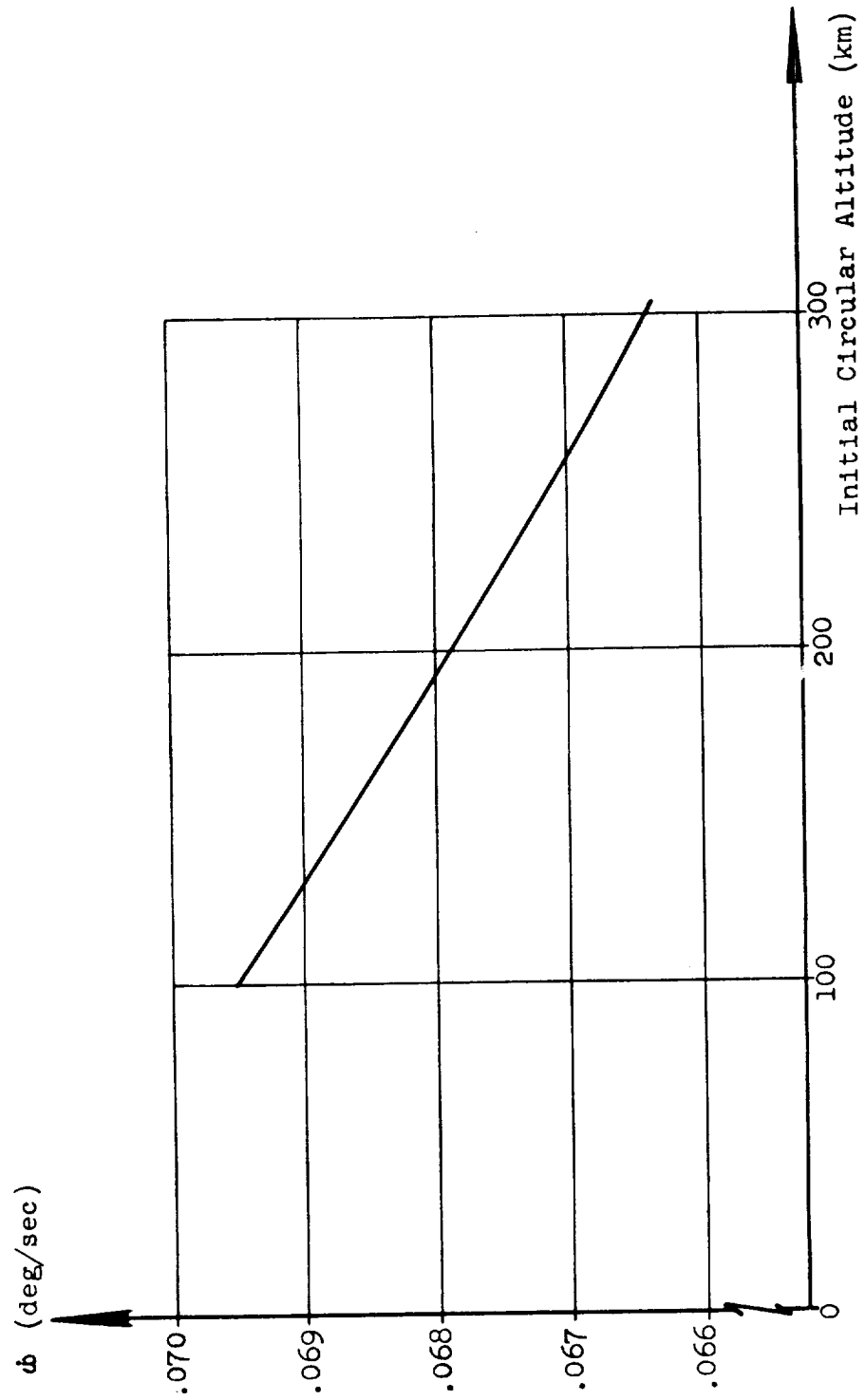


FIG. 29. THE RATE OF CHANGE OF THE DEPARTURE ANGLE $\dot{\psi}$ WITH RESPECT TO TIME
AS A FUNCTION OF THE INITIAL CIRCULAR ALTITUDE

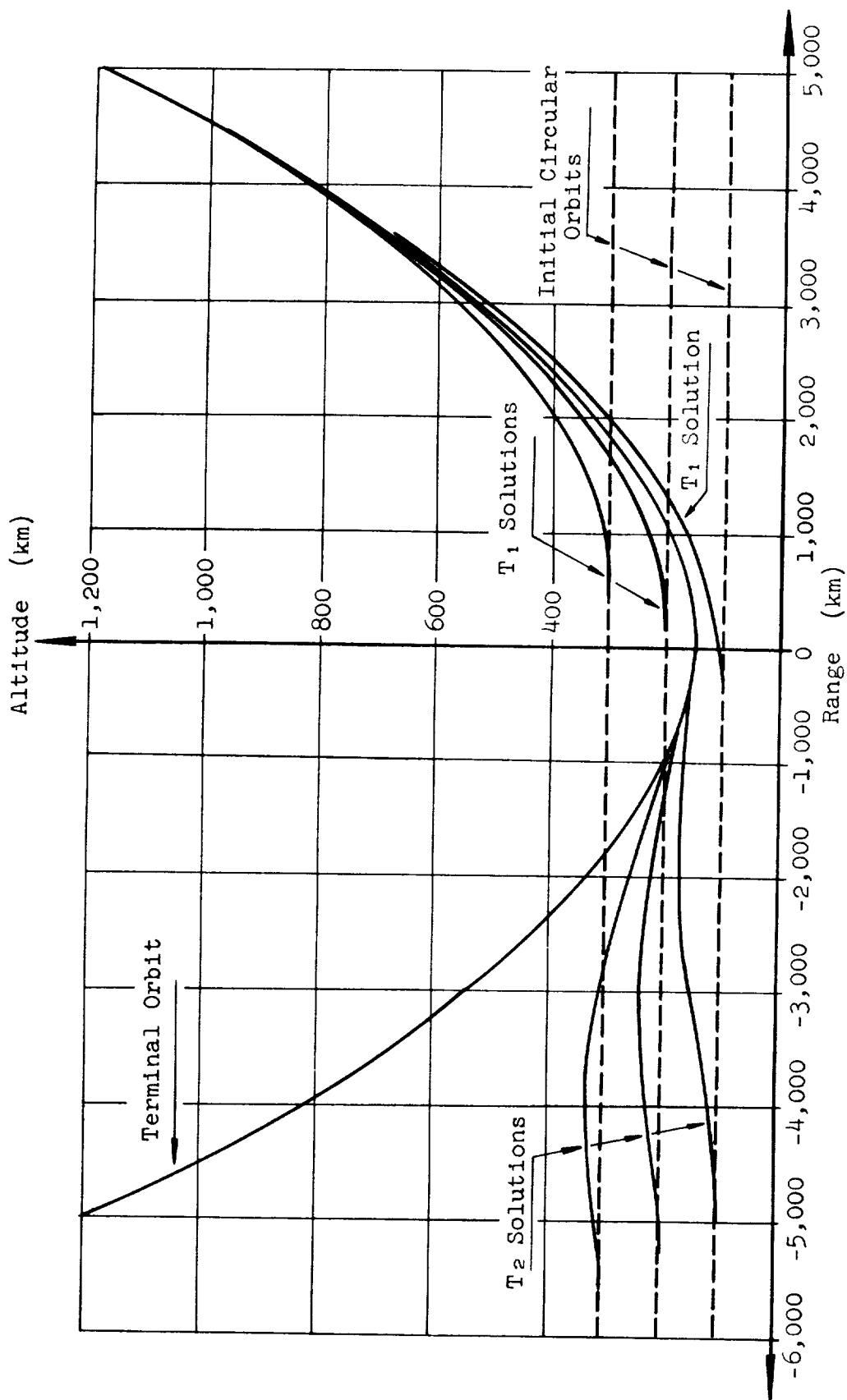


FIG. 30. NON-OPTIMUM TRAJECTORIES FOR BOTH TYPES OF SOLUTIONS

FOR $F/w_0 = .5$; $I_{sp} = 400$ SEC; $\alpha_0 = -40$ DEG

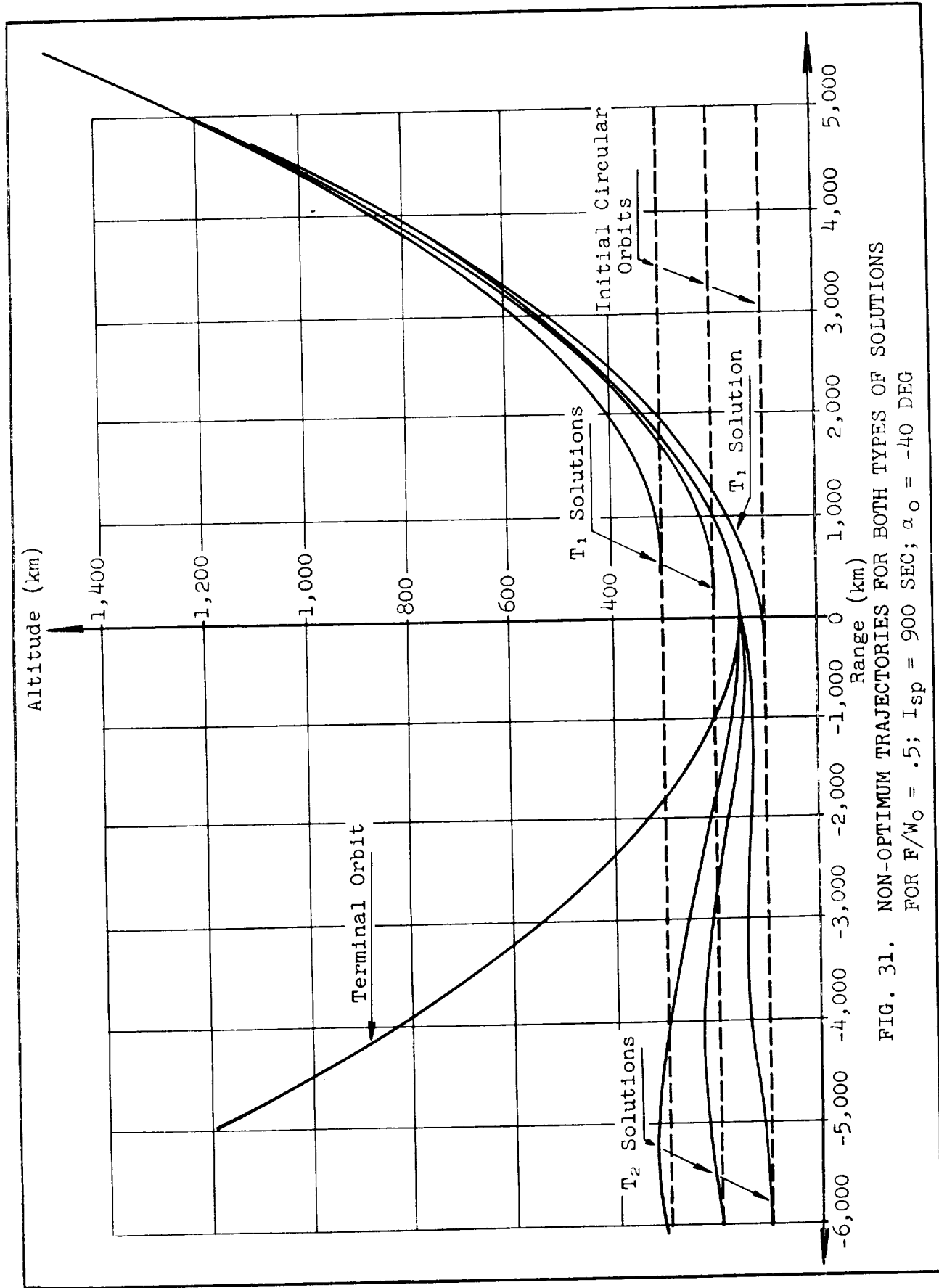


FIG. 31. NON-OPTIMUM TRAJECTORIES FOR BOTH TYPES OF SOLUTIONS
 FOR $F/w_0 = .5$; $I_{sp} = 900$ SEC; $\alpha_0 = -40$ DEG

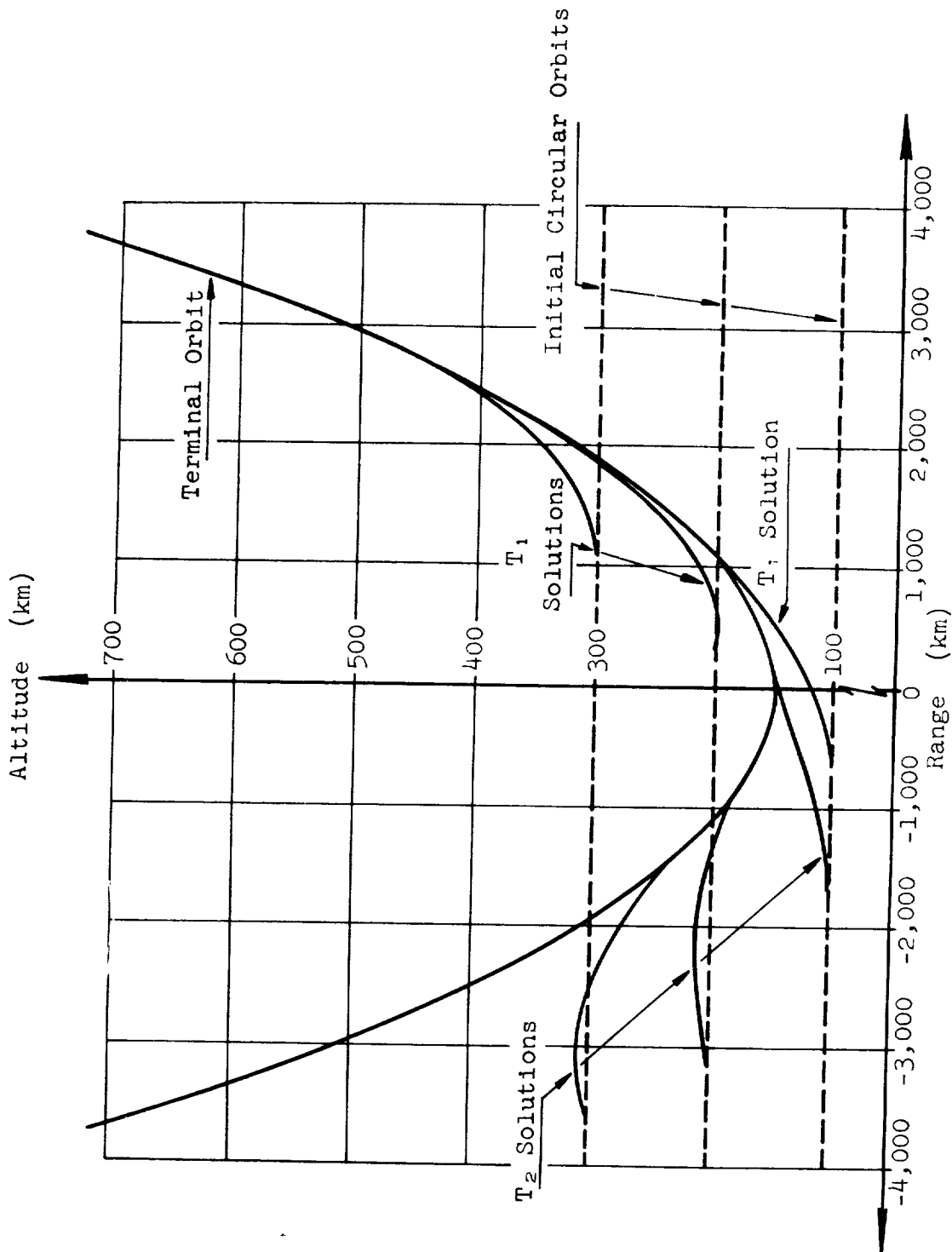


FIG. 32. NON-OPTIMUM TRAJECTORIES FOR BOTH TYPES OF SOLUTIONS
 FOR $F/W_0 = 1$; $I_{sp} = 400$ SEC; $\alpha_0 = -20$ DEG

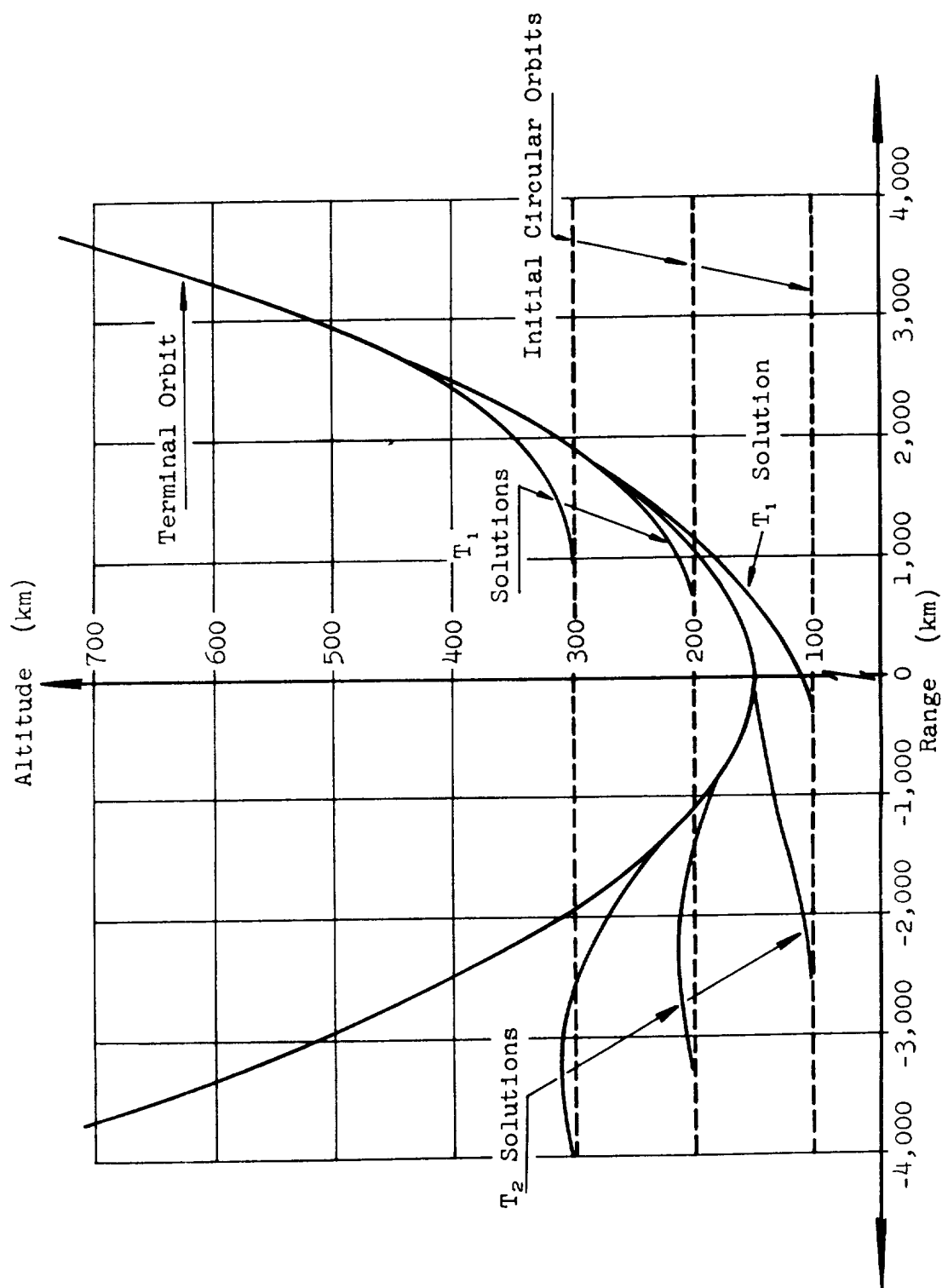


FIG. 33. NON-OPTIMUM TRAJECTORIES FOR BOTH TYPES OF SOLUTIONS

FOR $F/W_0 = 1$; $I_{sp} = 900$ SEC; $\alpha_0 = -20$ DEG

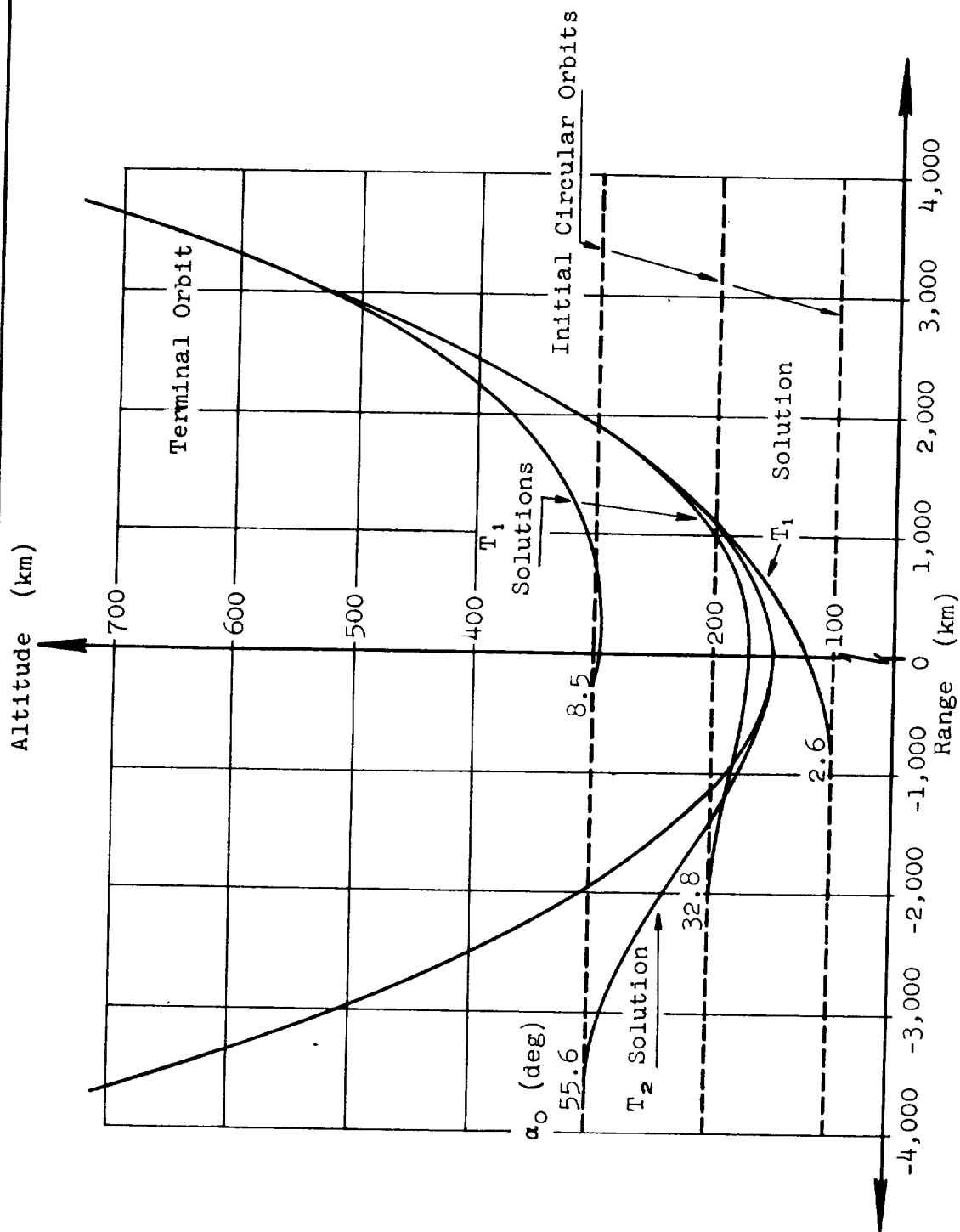


FIG. 34. OPTIMUM TRAJECTORIES FOR BOTH TYPES OF SOLUTIONS
FOR $F/W_0 = .5$; $I_{sp} = 400$ SEC

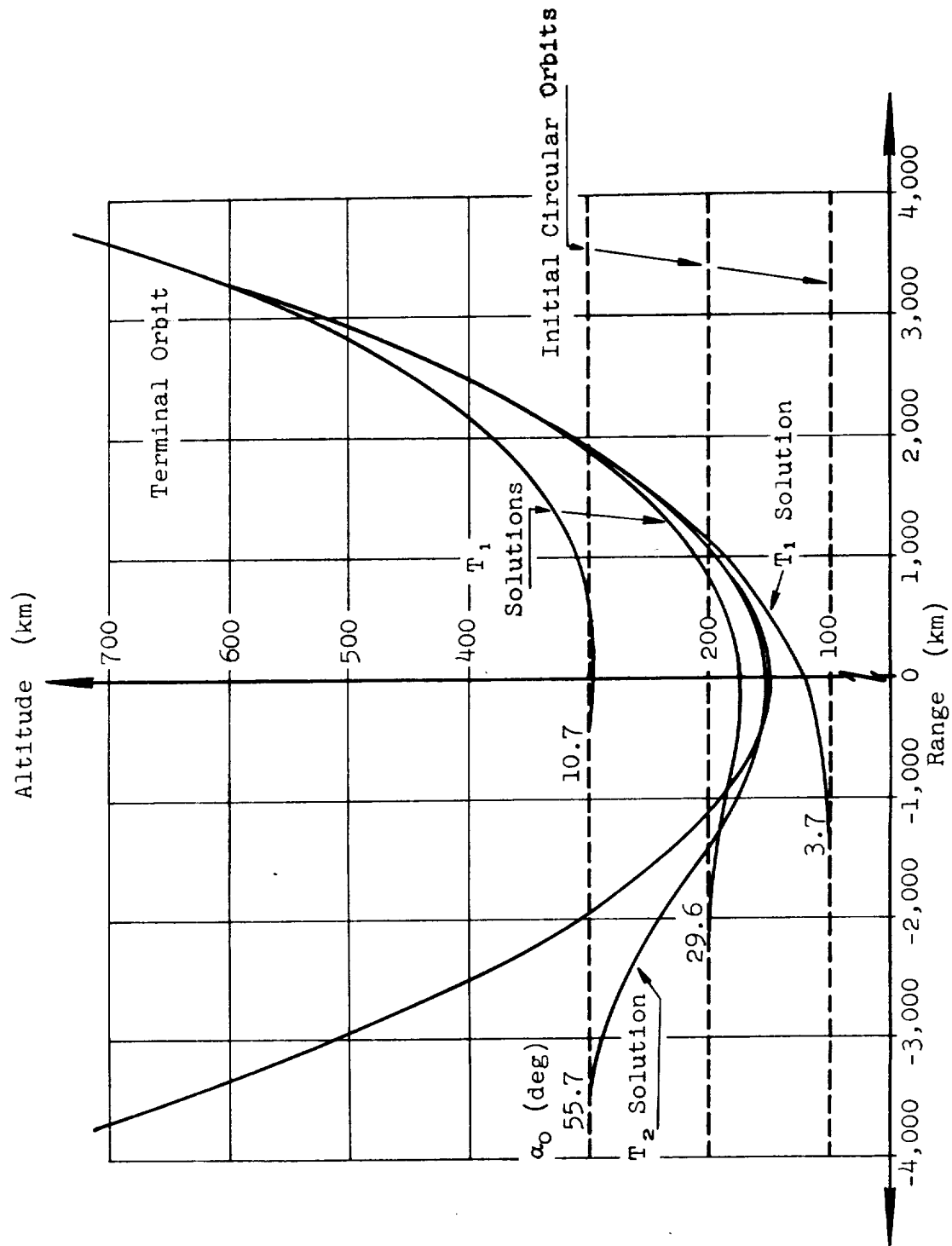


FIG. 35. OPTIMUM TRAJECTORIES FOR BOTH TYPES OF SOLUTIONS

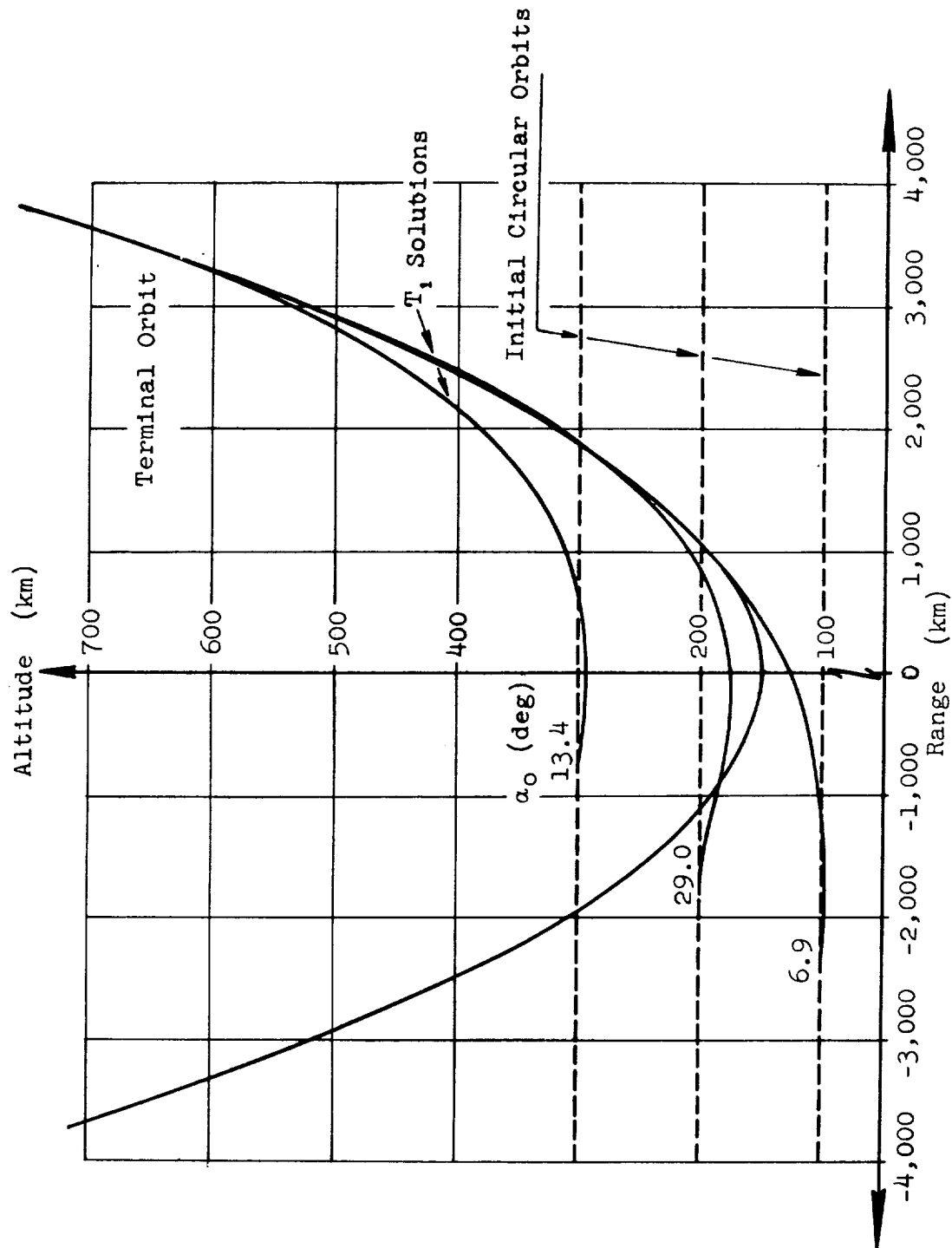


FIG. 36. OPTIMUM TRAJECTORIES FOR T_1 SOLUTIONS
 FOR $F/W_o = .5$; $I_{sp} = 700$ SEC

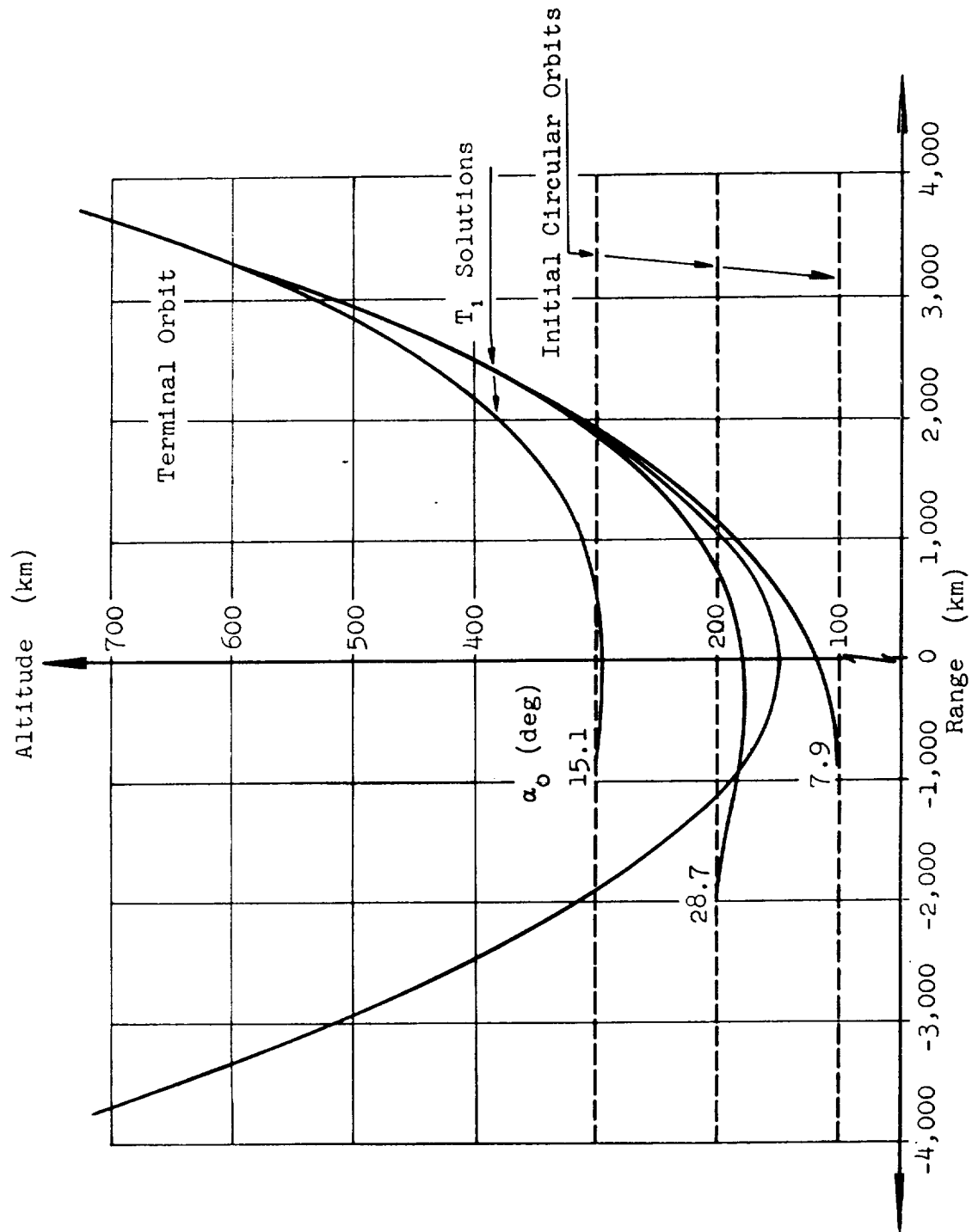


FIG. 37. OPTIMUM TRAJECTORIES FOR T_1 SOLUTIONS

FOR $F/W = .5$; $I_{sp} = 900$ SEC

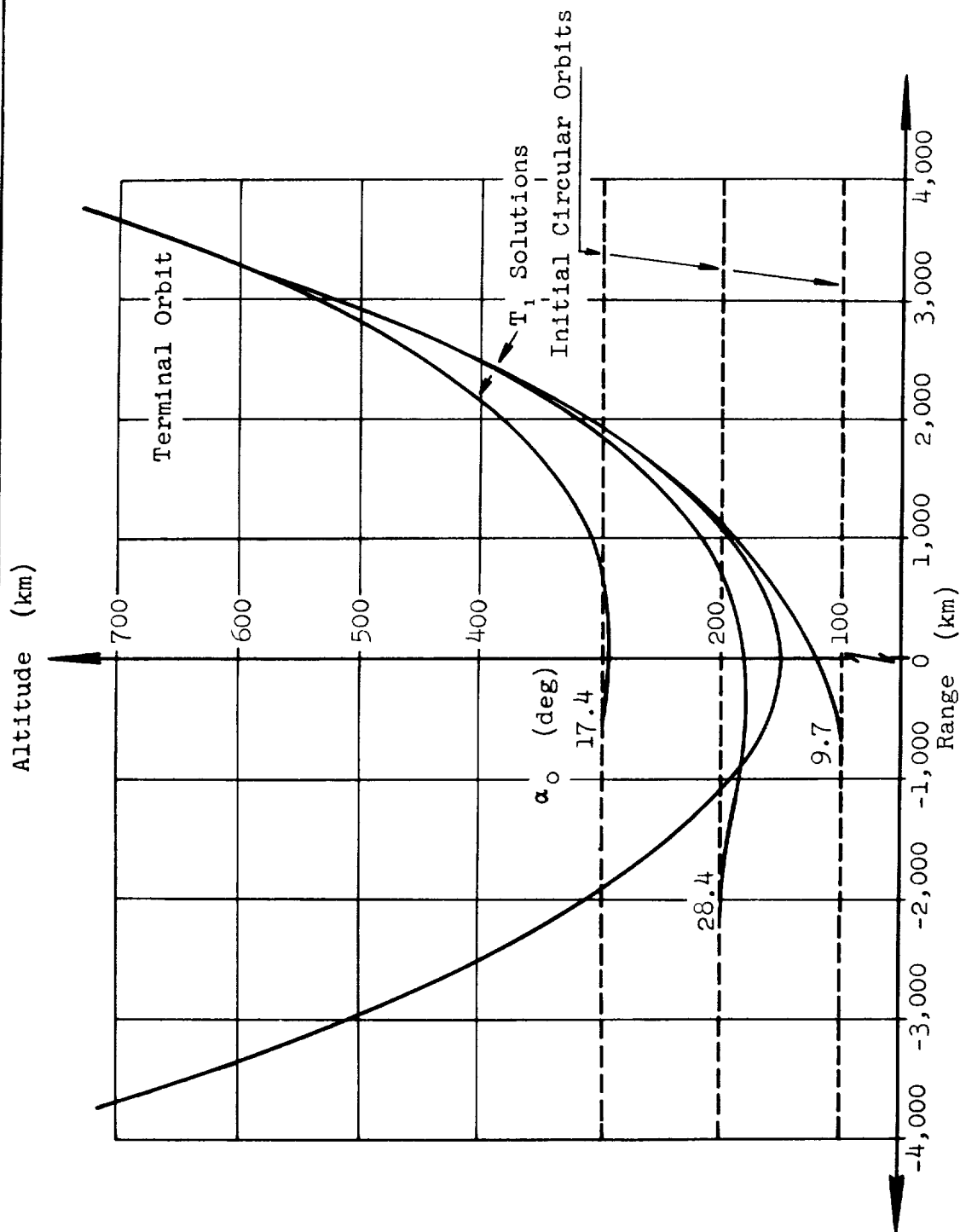


FIG. 38. OPTIMUM TRAJECTORIES FOR T_1 SOLUTIONS
FOR $F/w_0 = .5$; $I_{sp} = 1,500$ SEC

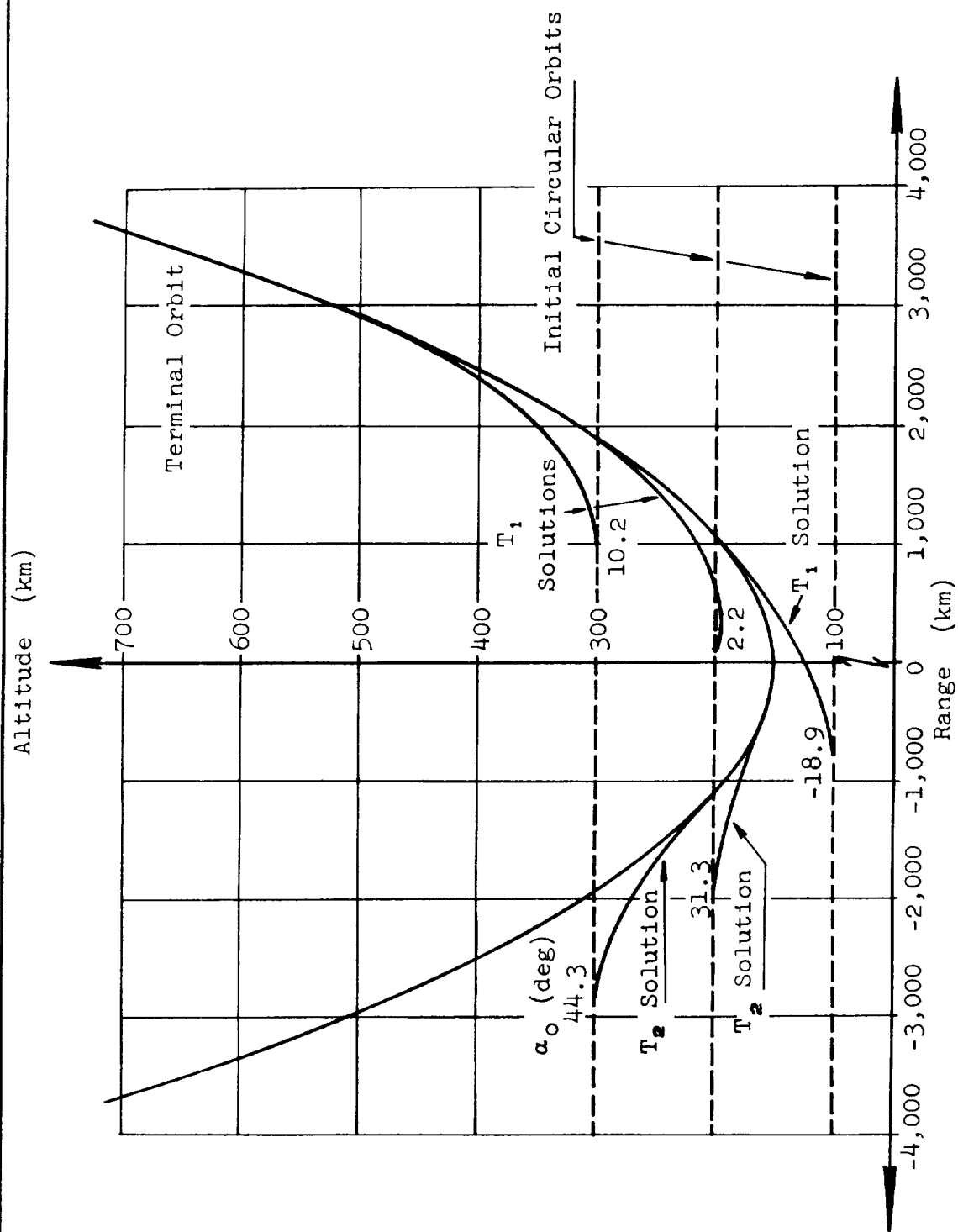


FIG. 39. OPTIMUM TRAJECTORIES FOR BOTH TYPES OF SOLUTIONS
FOR $F/W_0 = 1$; $I_{sp} = 400$ SEC

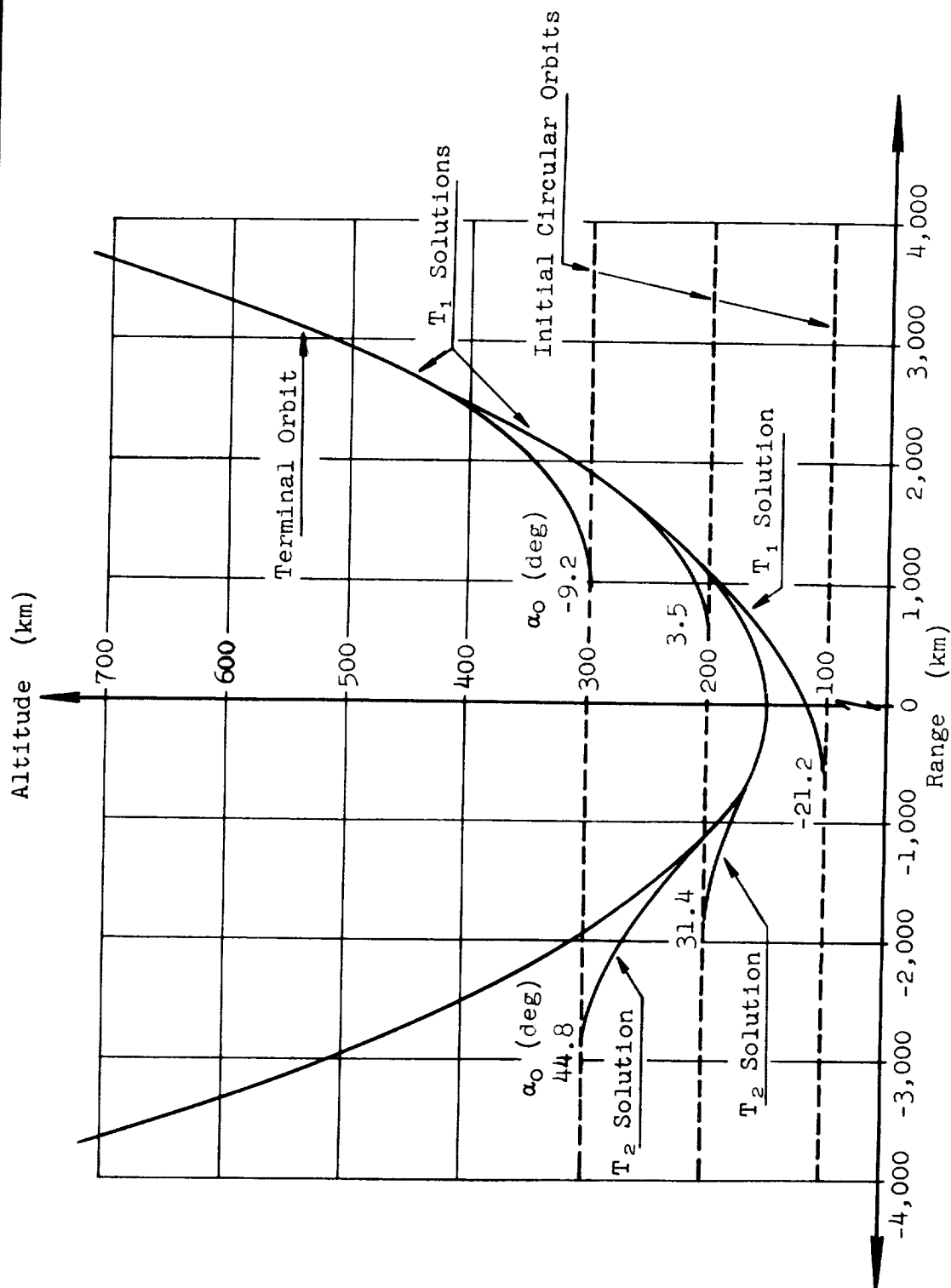


FIG. 40. OPTIMUM TRAJECTORIES FOR BOTH TYPES OF SOLUTIONS

FOR $F/W_0 = 1$; $I_{sp} = 500$ SEC

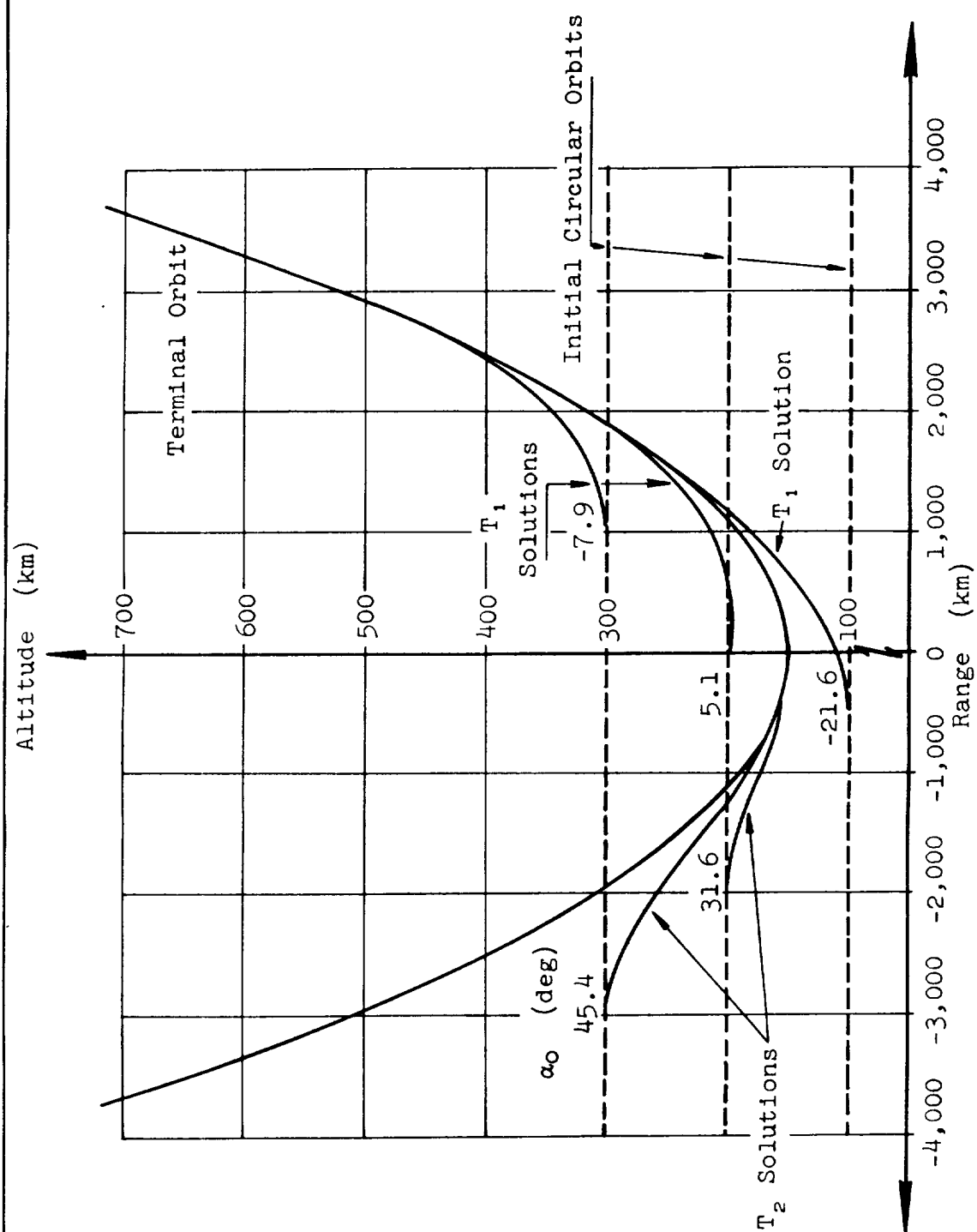


FIG. 41. OPTIMUM TRAJECTORIES FOR BOTH TYPES OF SOLUTIONS

FOR $F/W_0 = 1$; $I_{sp} = 700$ SEC

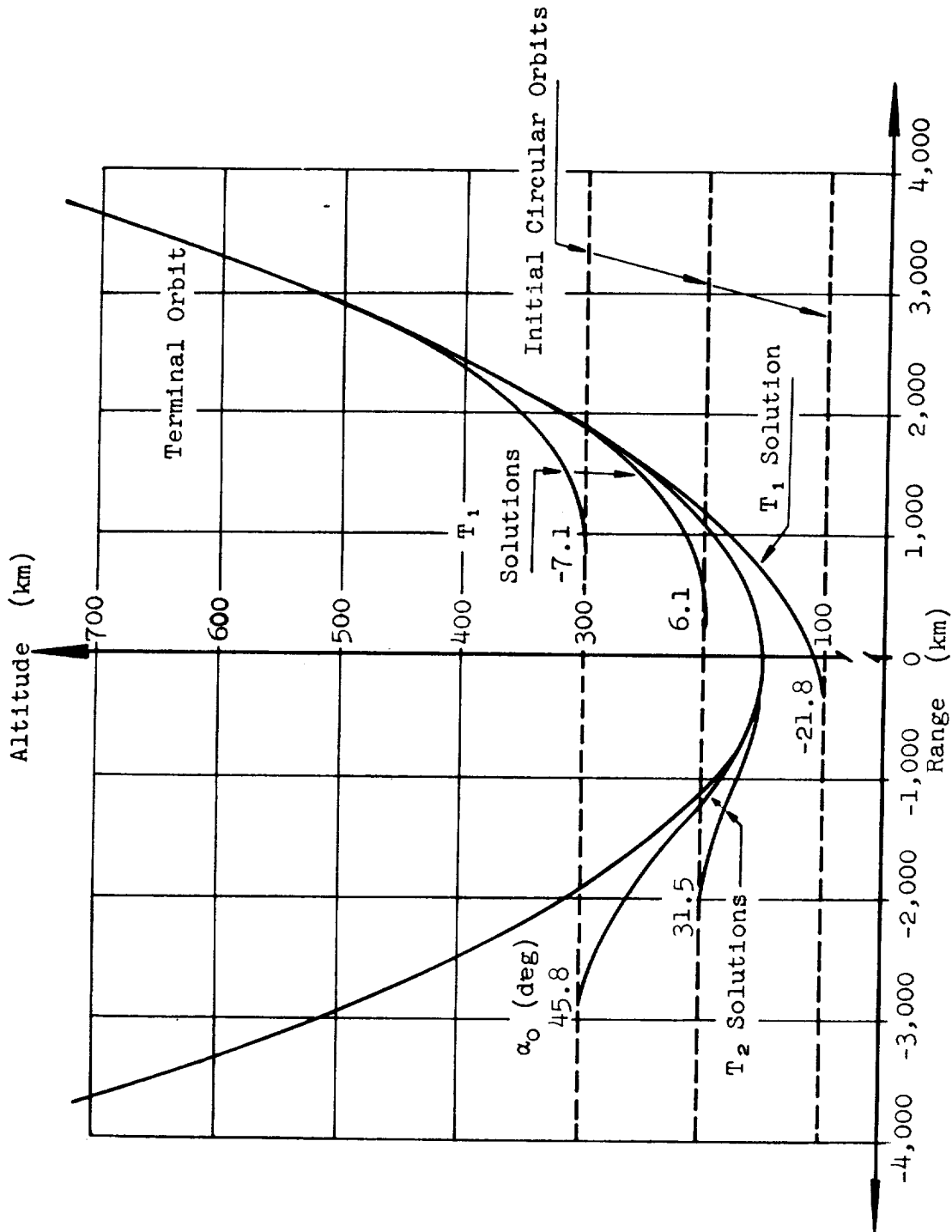


FIG. 42. OPTIMUM TRAJECTORIES FOR BOTH TYPES OF SOLUTIONS
FOR $F/W_0 = 1$; $I_{sp} = 900$ SEC

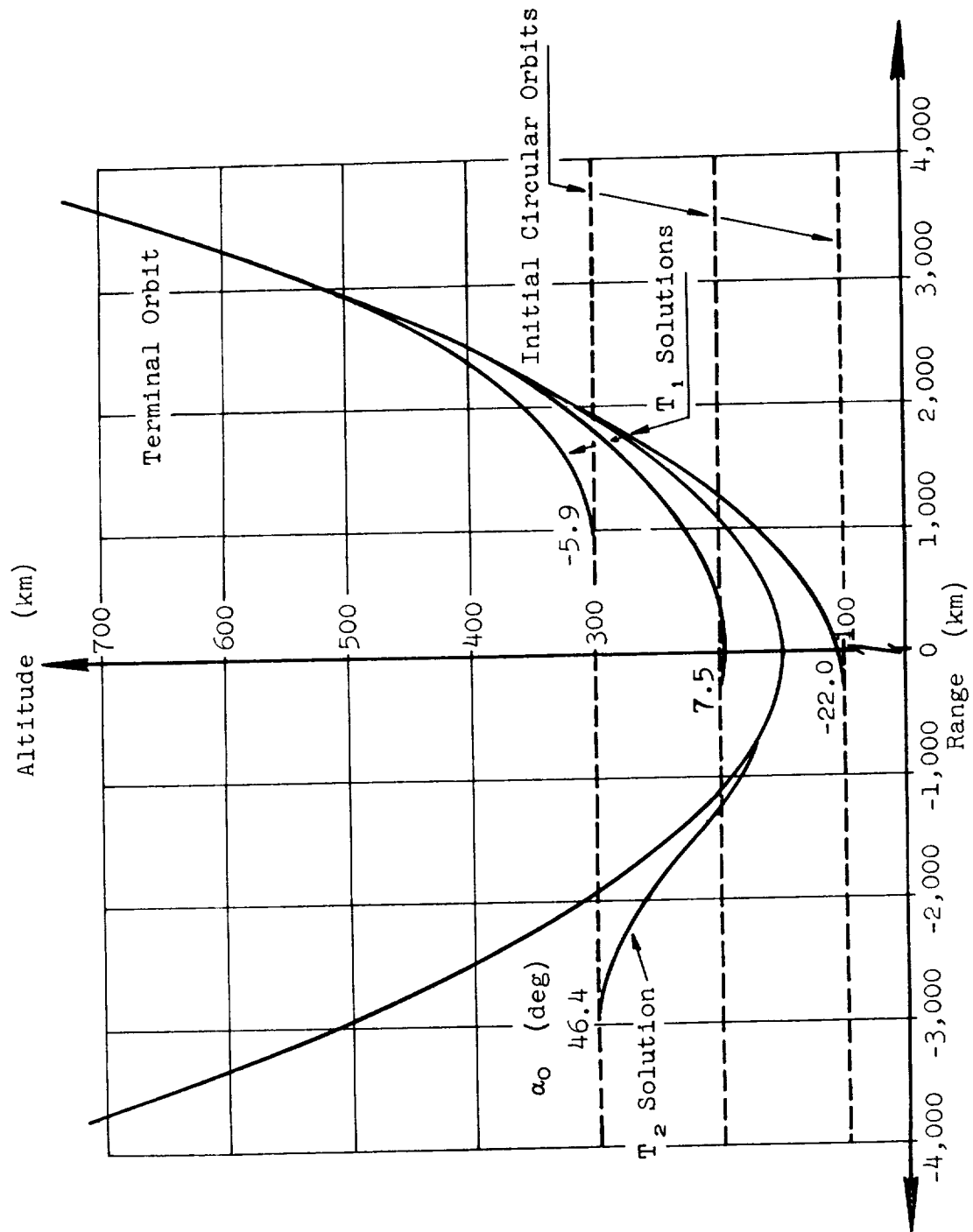


FIG. 43. OPTIMUM TRAJECTORIES FOR BOTH TYPES OF SOLUTIONS

FOR $F/W_0 = 1$; $I_{sp} = 1,500$ SEC

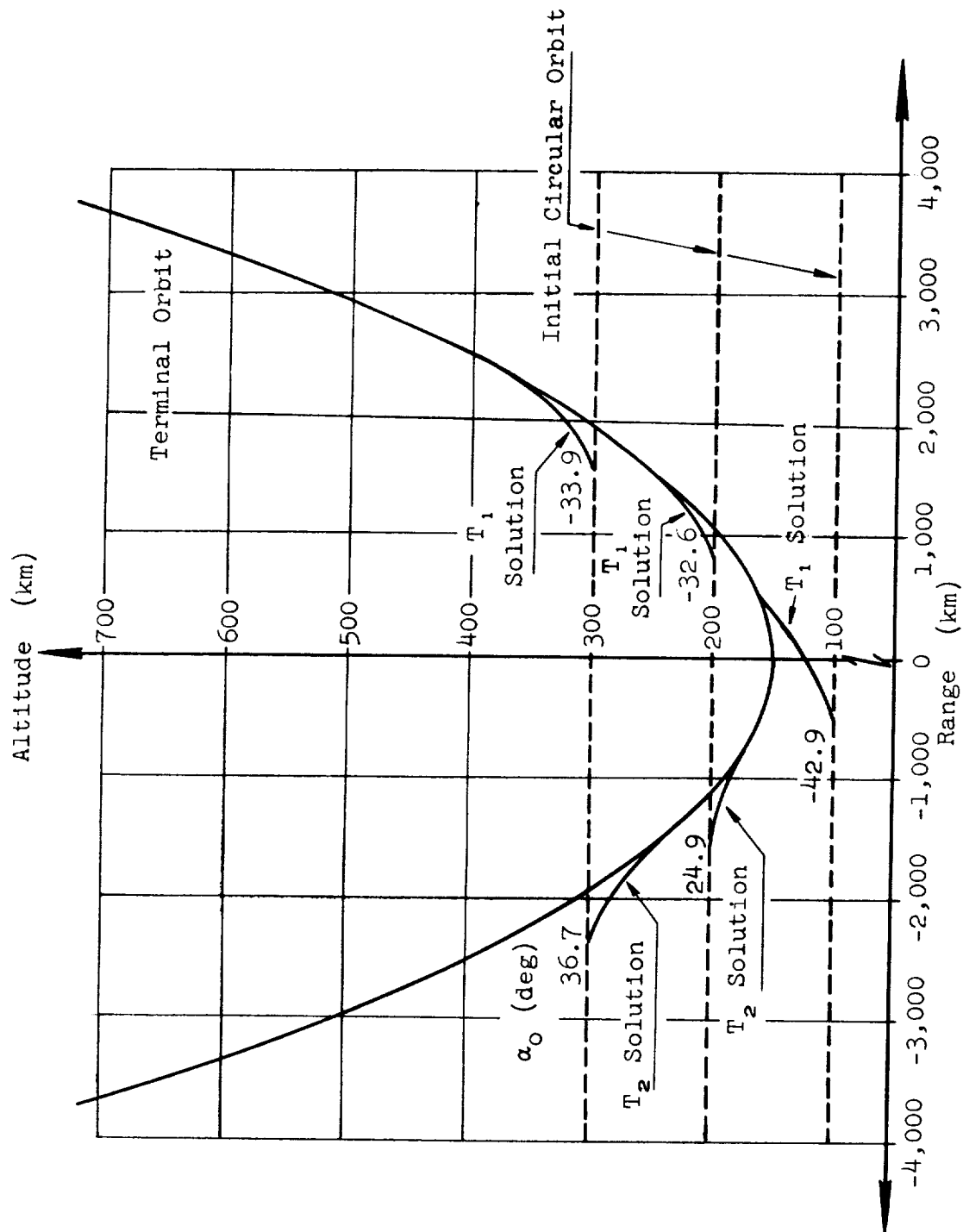


FIG. 44. OPTIMUM TRAJECTORIES FOR BOTH TYPES OF SOLUTIONS

FOR $F/W_0 = 2$; $I_{sp} = 400$ SEC

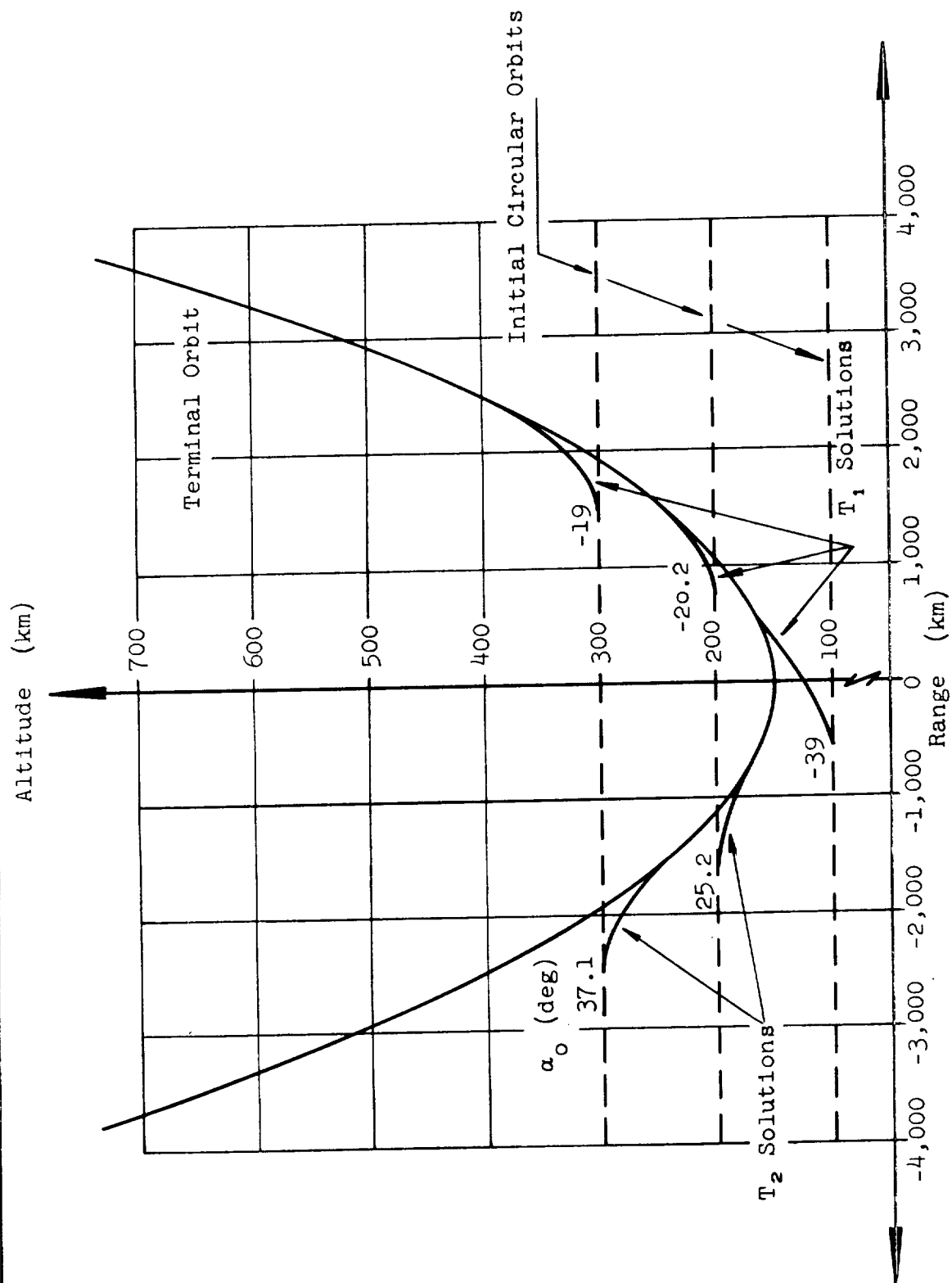


FIG. 45. OPTIMUM TRAJECTORIES FOR BOTH TYPES OF SOLUTIONS
FOR $F/W_0 = 2$; $I_{sp} = 500$ SEC

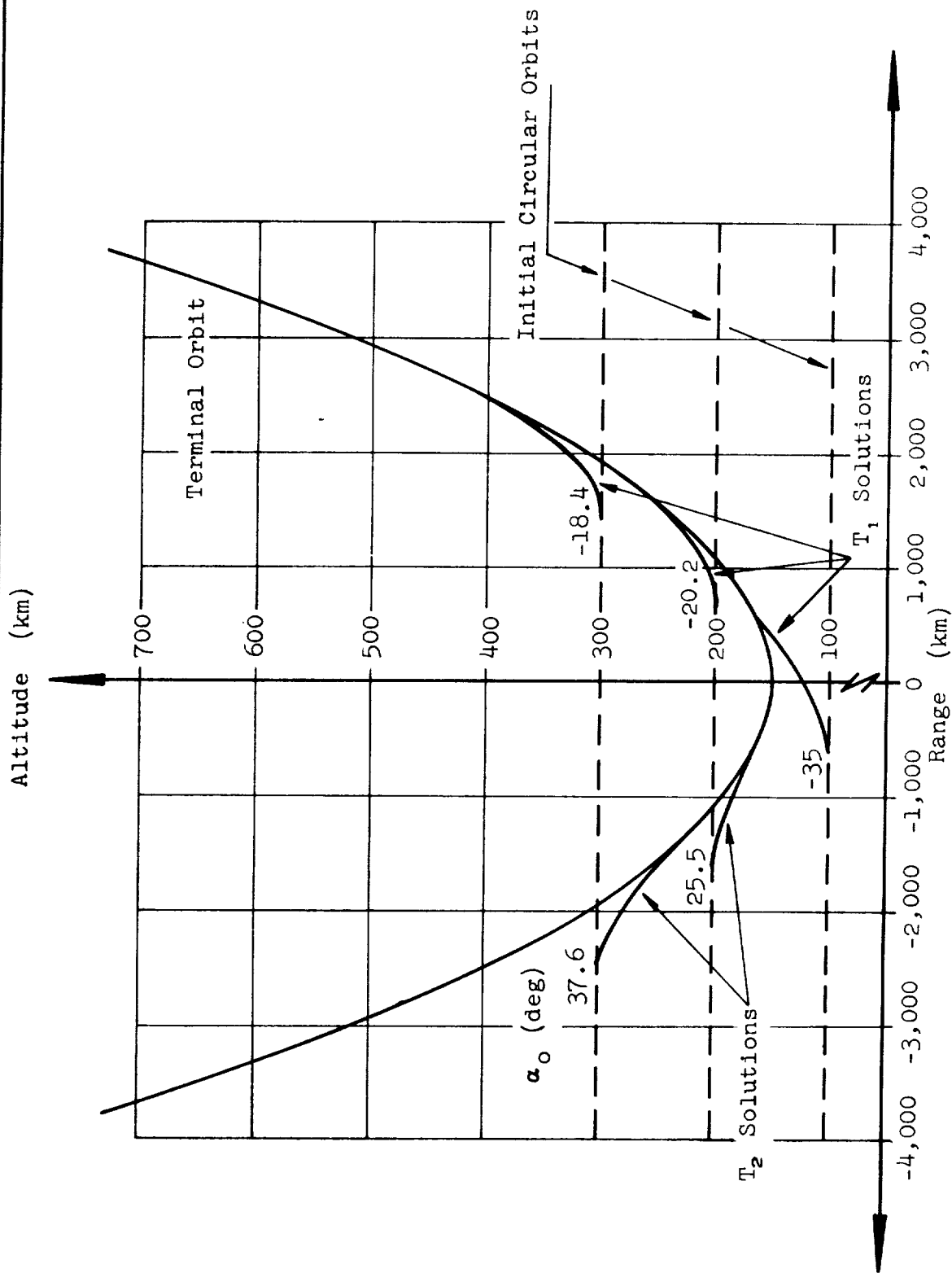


FIG. 46. OPTIMUM TRAJECTORIES FOR BOTH TYPES OF SOLUTIONS

FOR $F/W_0 = 2$; $I_{sp} = 700$ SEC

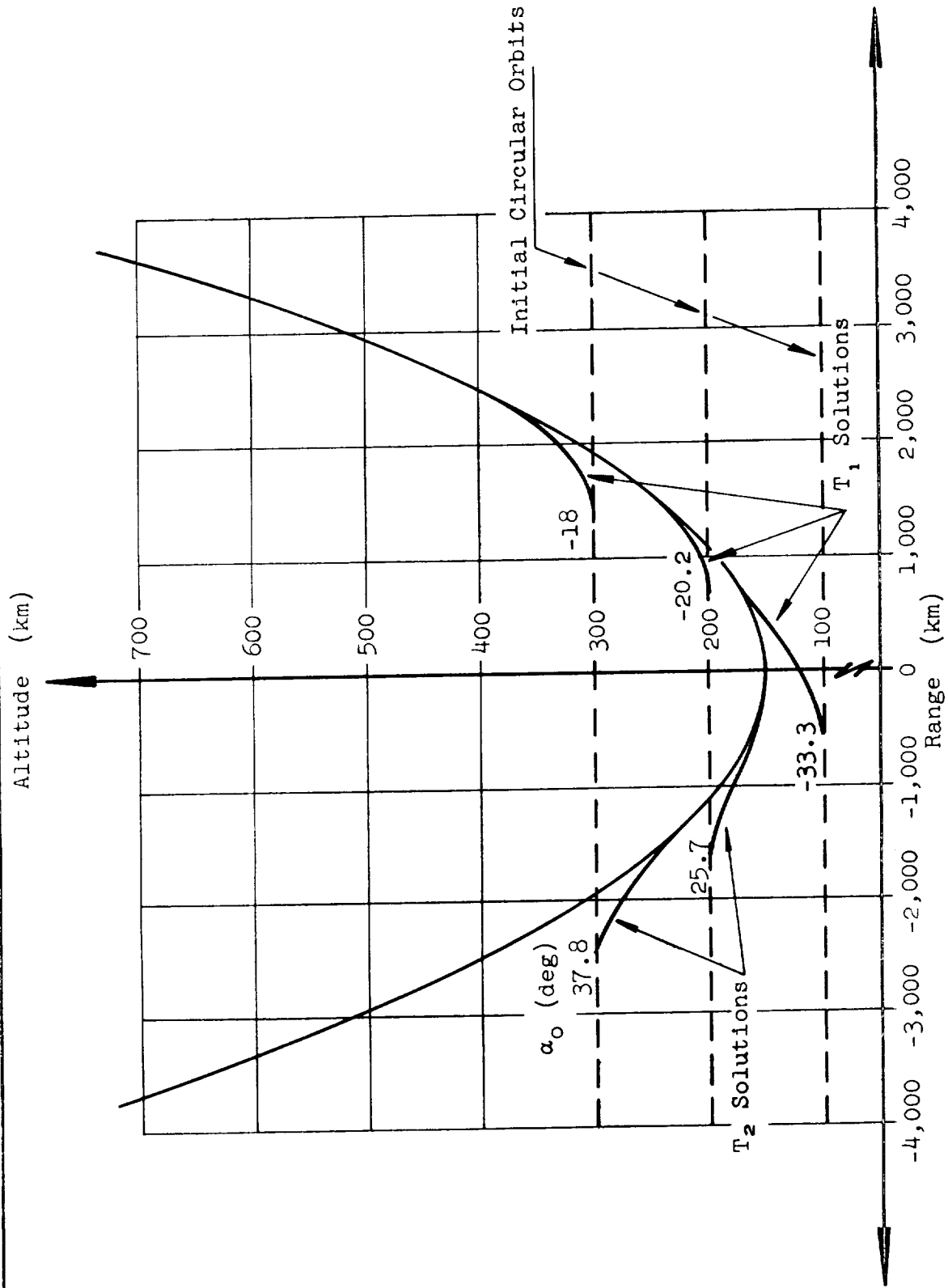


FIG. 47. OPTIMUM TRAJECTORIES FOR BOTH TYPES OF SOLUTIONS

FOR $F/W_0 = 2$; $I_{sp} = 900$ SEC

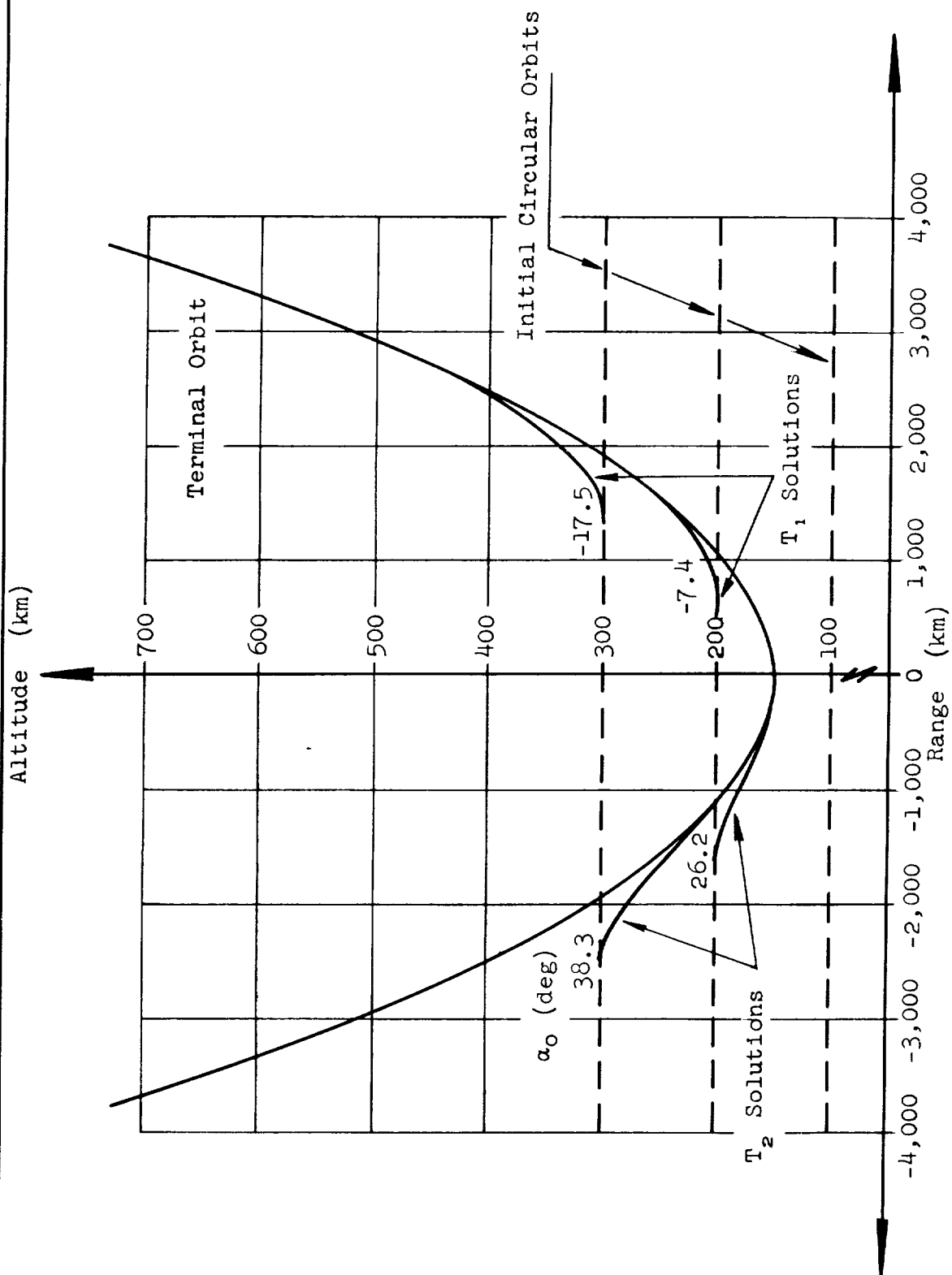


FIG. 48. OPTIMUM TRAJECTORIES FOR BOTH TYPES OF SOLUTIONS
FOR $F/W_0 = 2$; $I_{sp} = 1,500$ SEC

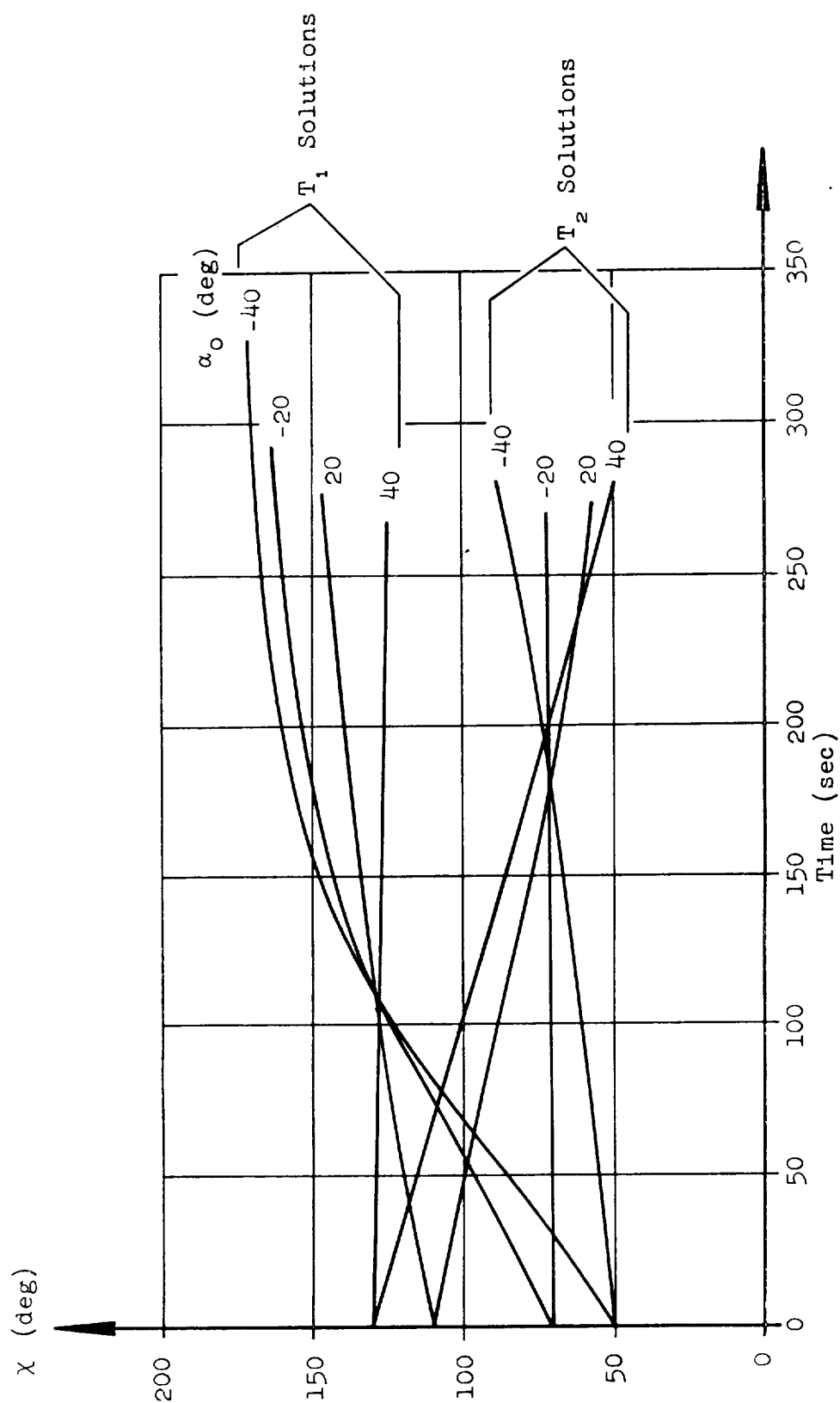


FIG. 49. NON-OPTIMUM CONTROL HISTORIES FOR PARAMETERS OF α_0

FOR $F/w_0 = 1$; $I_{sp} = 700$ sec; $y_0 = 300$ km

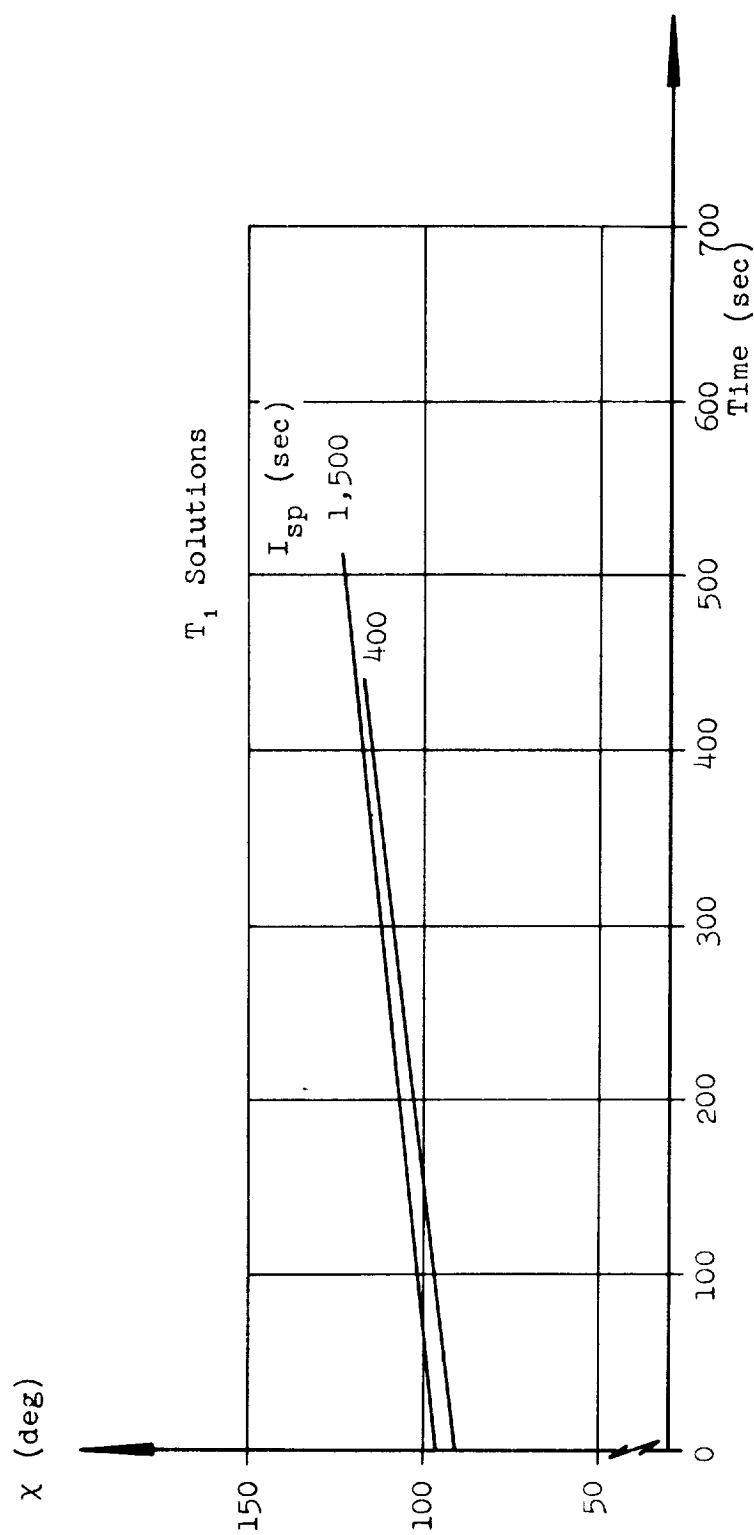


FIG. 50. OPTIMUM CONTROL HISTORIES FOR PARAMETERS OF I_{sp}

FOR $F/w_0 = .5$; $y_0 = 100$ km

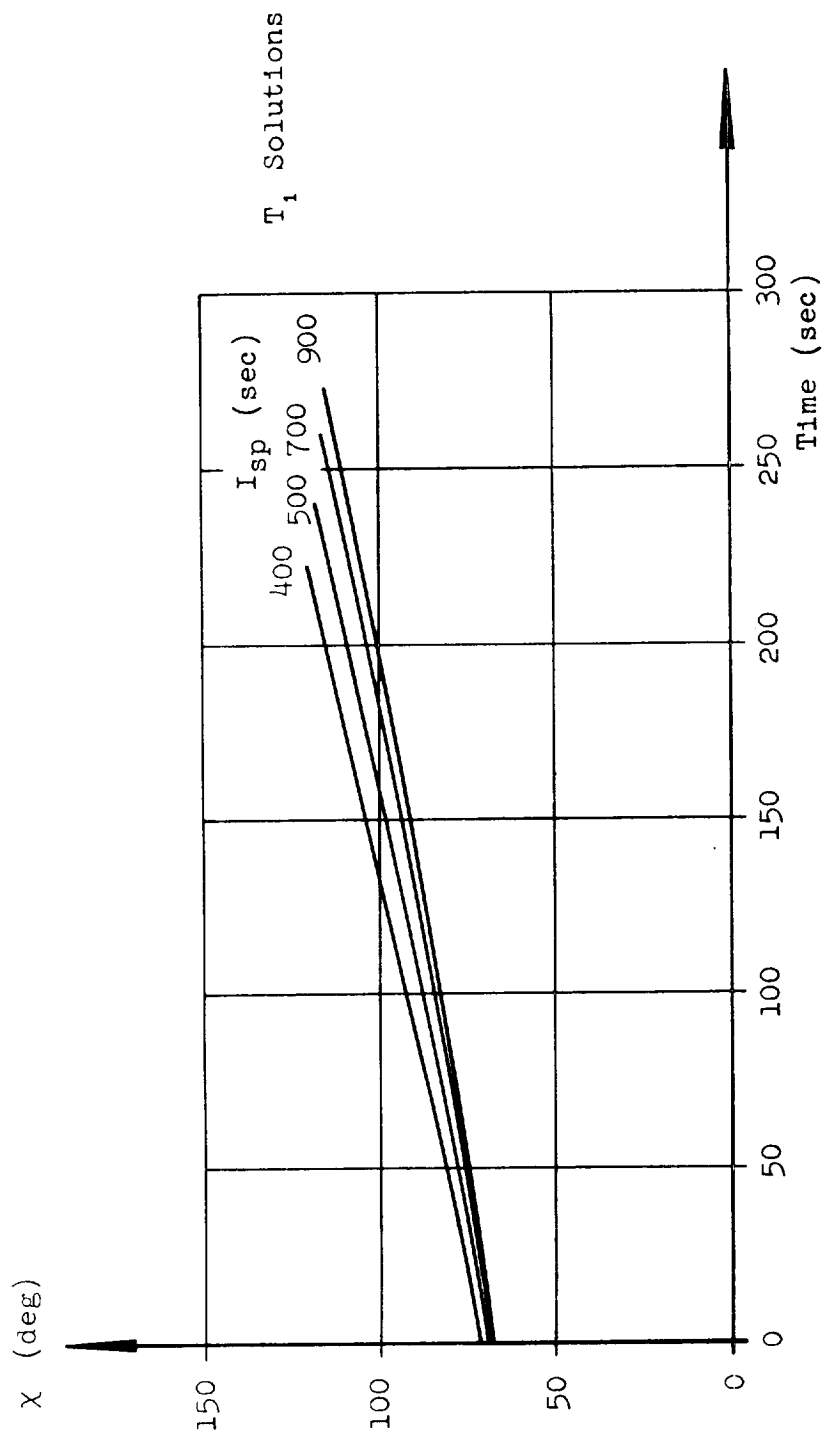


FIG. 51. OPTIMUM CONTROL HISTORIES FOR PARAMETERS OF I_{sp}

FOR $F/W_0 = 1$; $y_0 = 100$ km

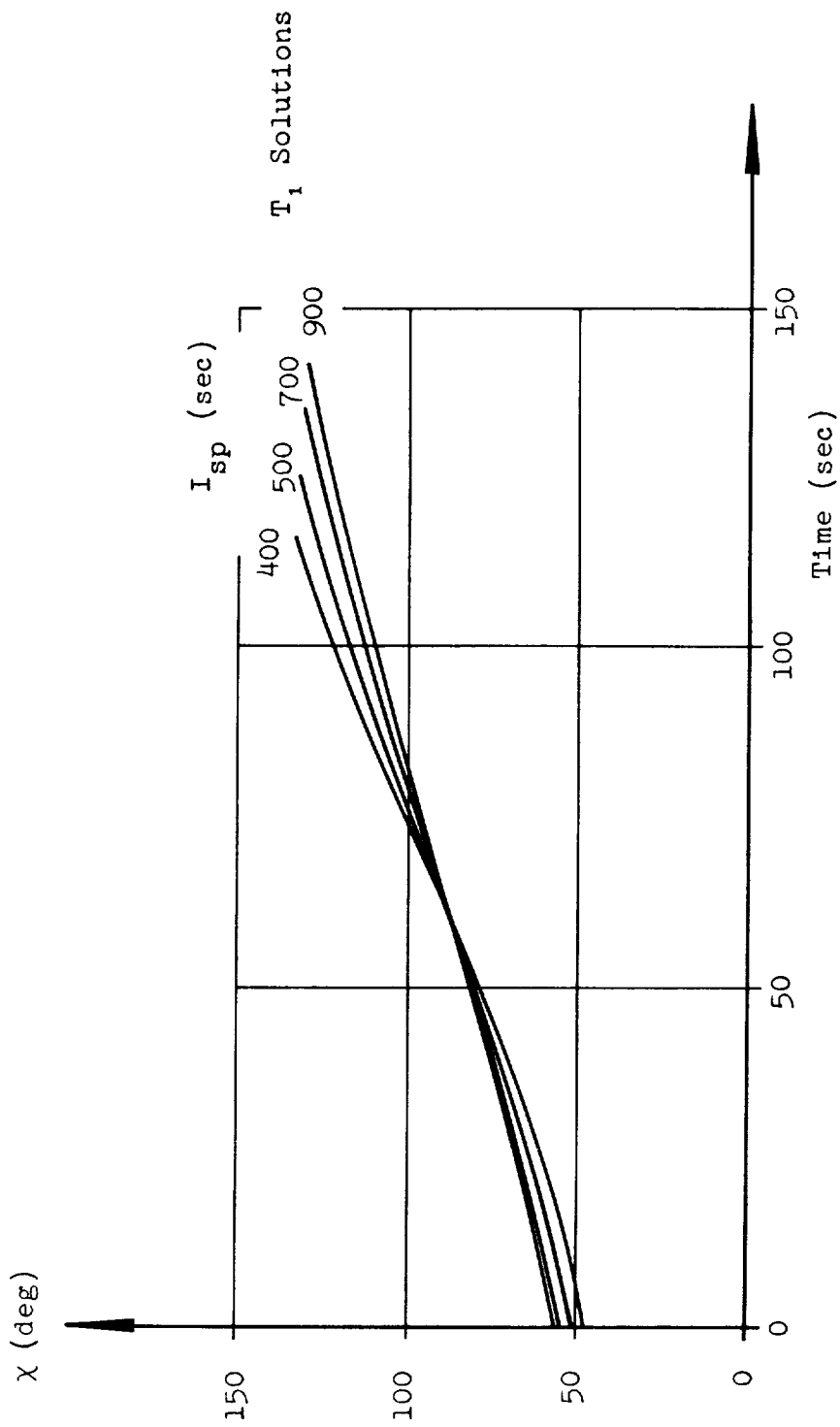


FIG. 52. OPTIMUM CONTROL HISTORIES FOR PARAMETERS OF I_{sp}

FOR $F/W_0 = 2$; $y_0 = 100$ km

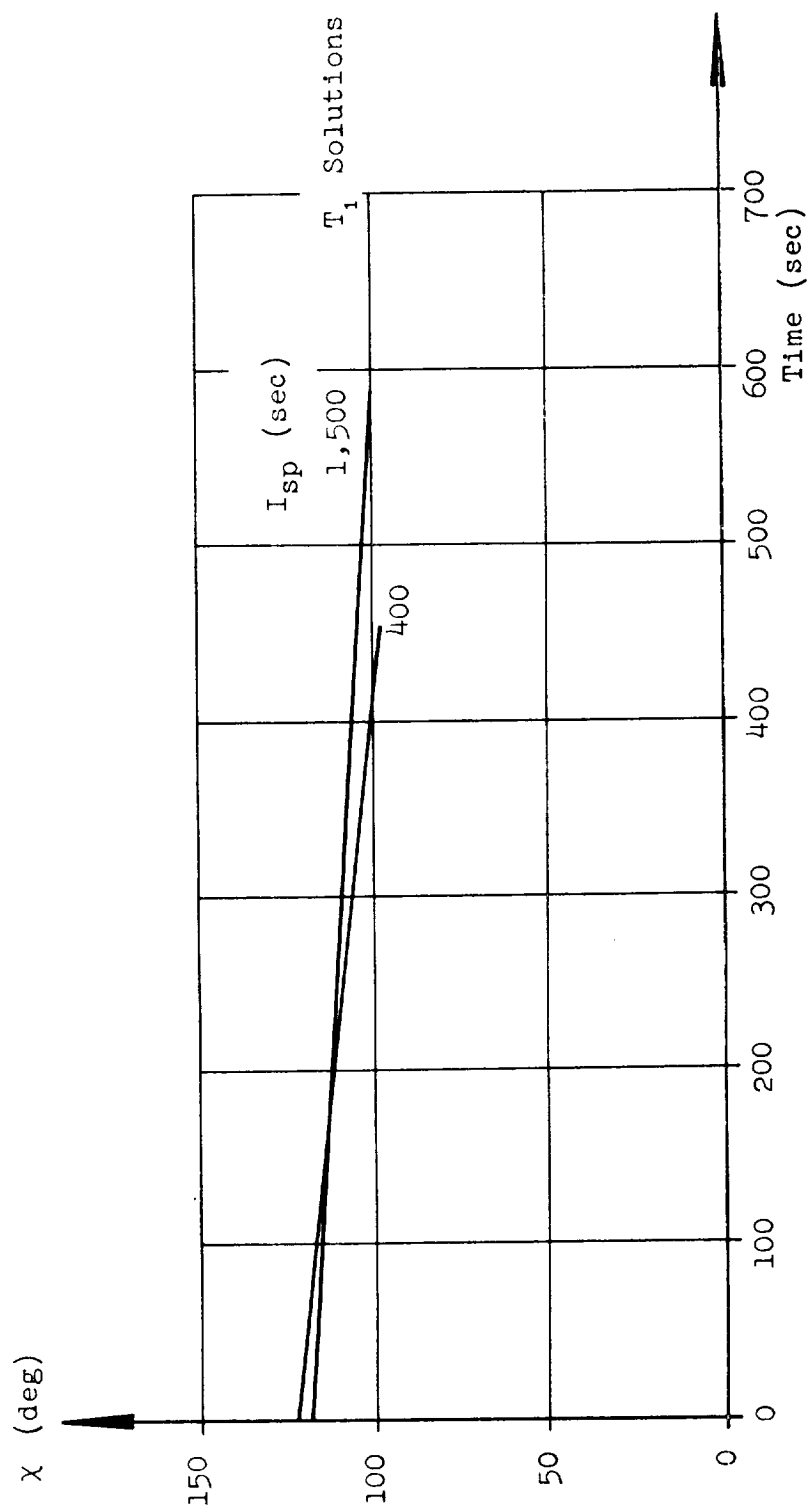


FIG. 53. OPTIMUM CONTROL HISTORIES FOR PARAMETERS OF I_{sp}

FOR $F/W_0 = .5$; $y_0 = 200$ km

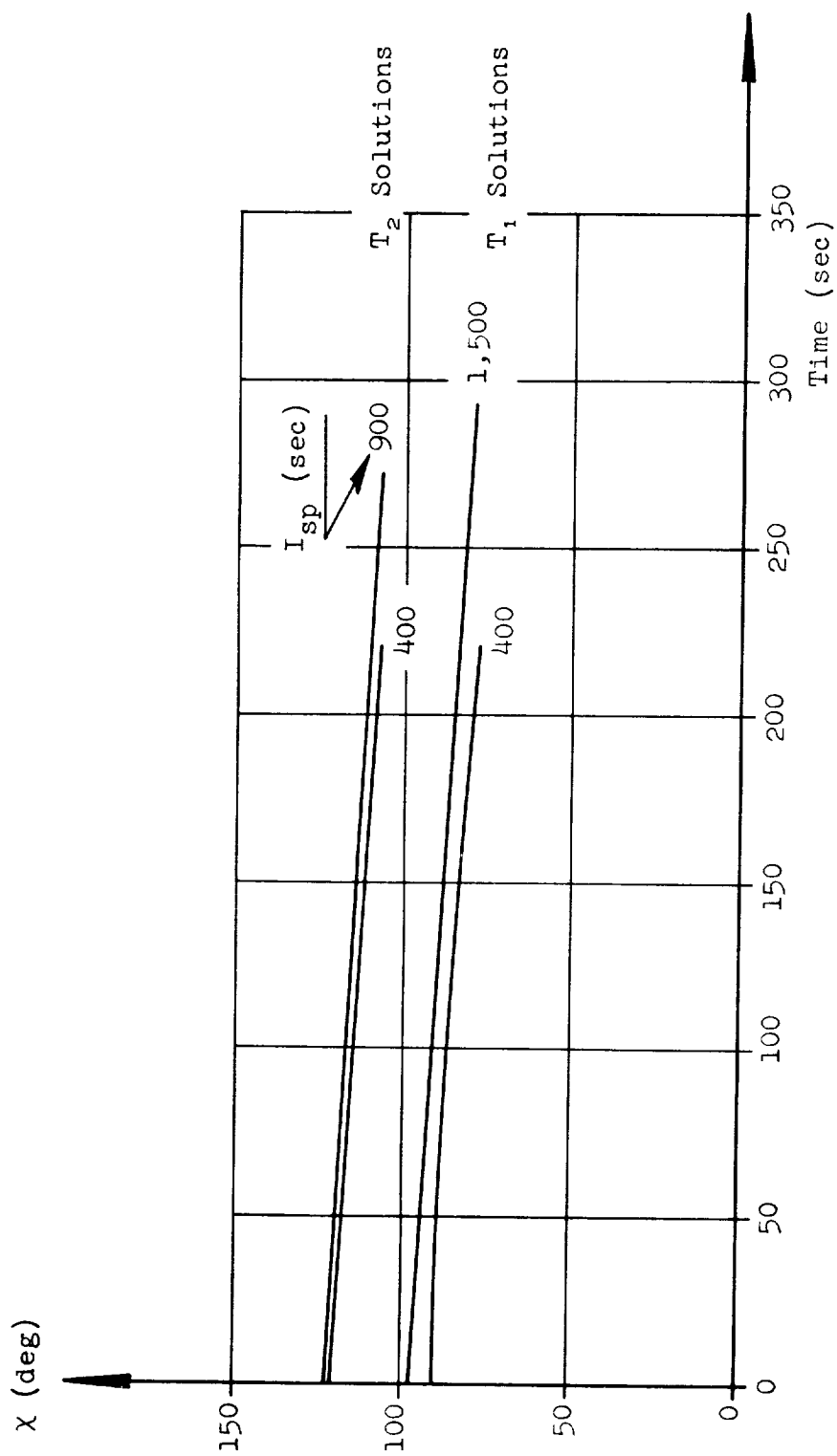


FIG. 54. OPTIMUM CONTROL HISTORIES FOR PARAMETERS OF I_{sp}

FOR $F/W_0 = 1$; $y_0 = 200$ km

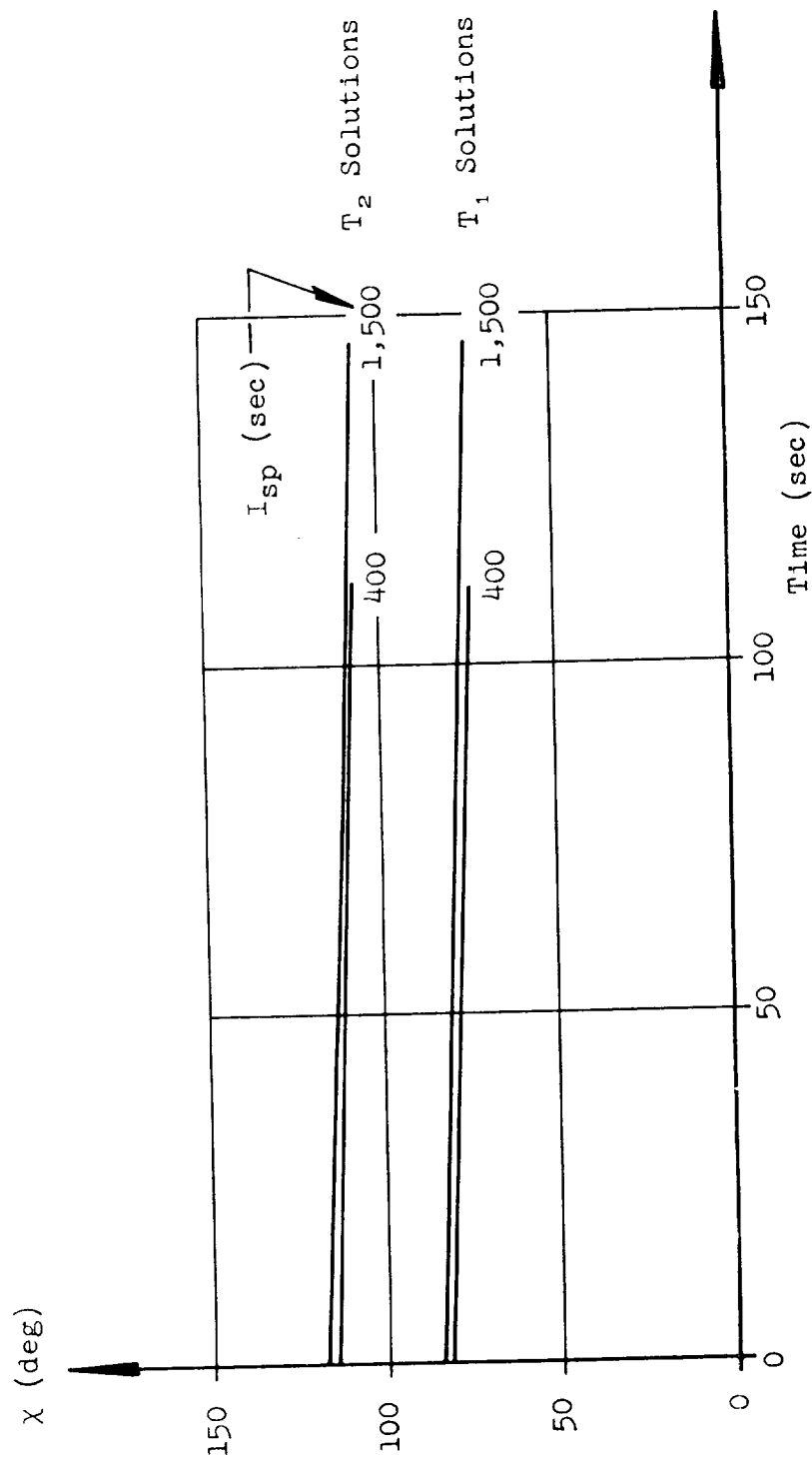


FIG. 55. OPTIMUM CONTROL HISTORIES FOR PARAMETERS OF I_{sp}

FOR $F/w_0 = 2$; $y_0 = 200$ km

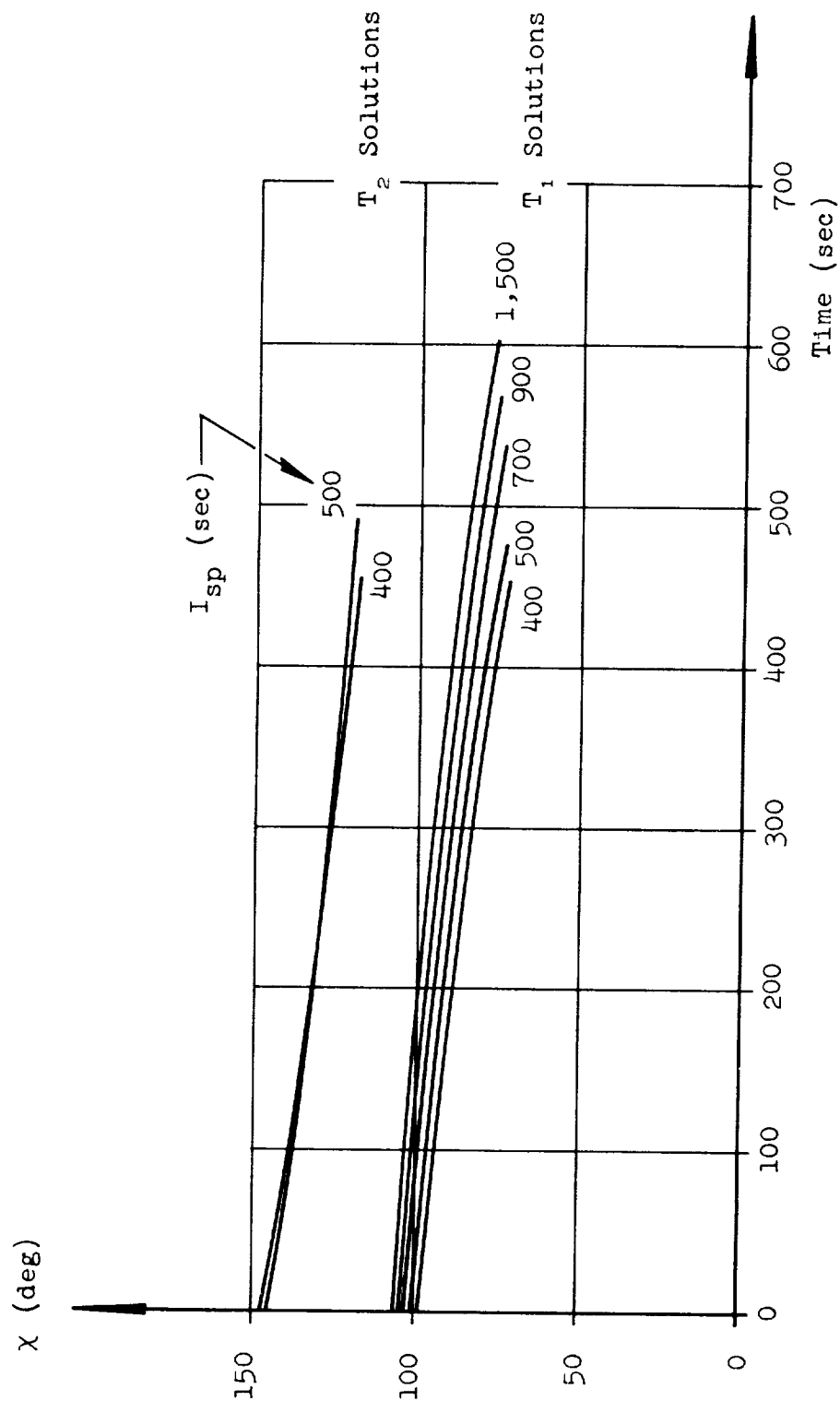


FIG. 56. OPTIMUM CONTROL HISTORIES FOR PARAMETERS OF I_{sp}

FOR $F/W_0 = .5$; $y_0 = 300$ km

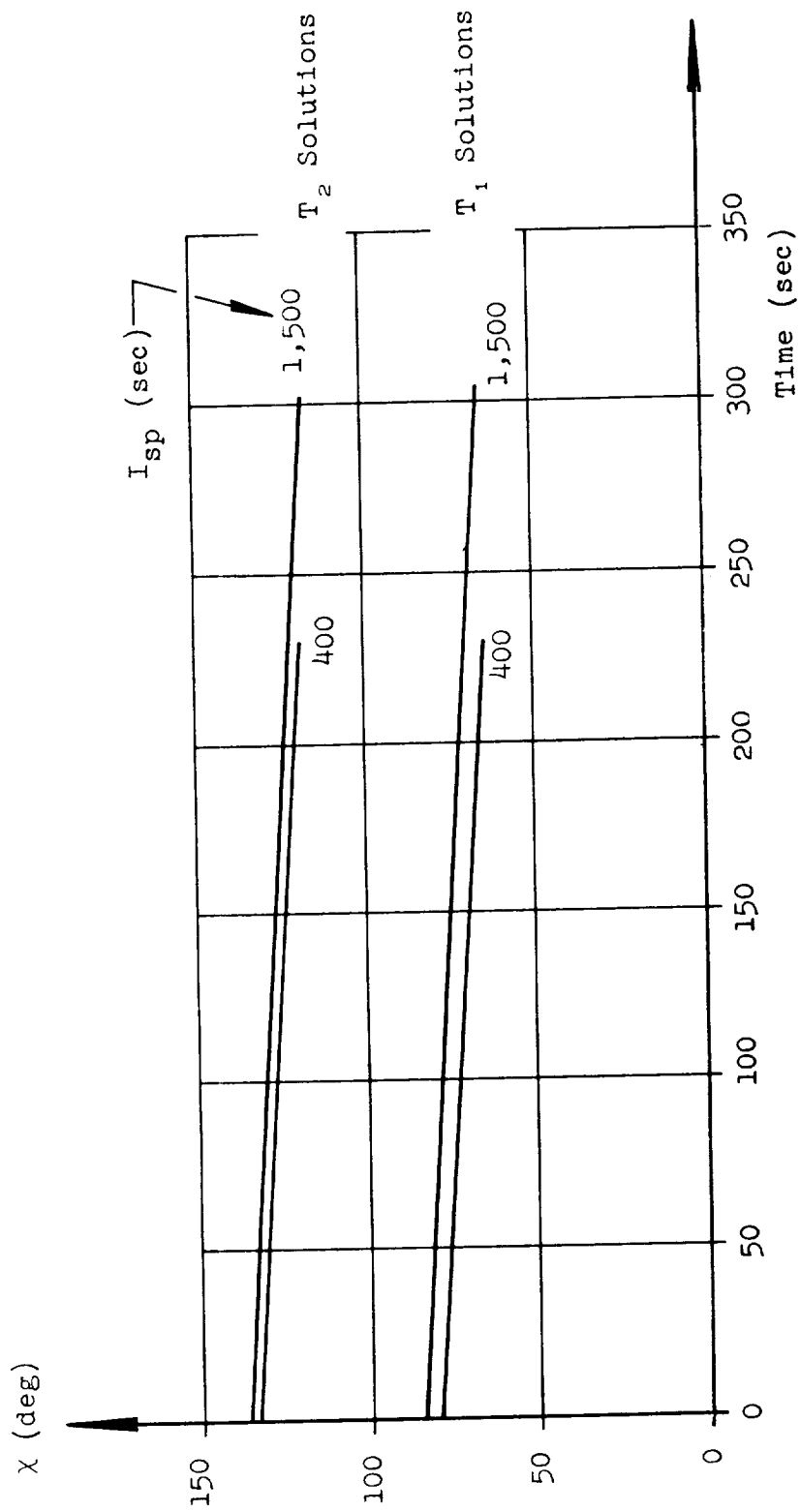


FIG. 57. OPTIMUM CONTROL HISTORIES FOR PARAMETERS OF I_{sp}

FOR $F/W_0 = 1$; $y_0 = 300$ km

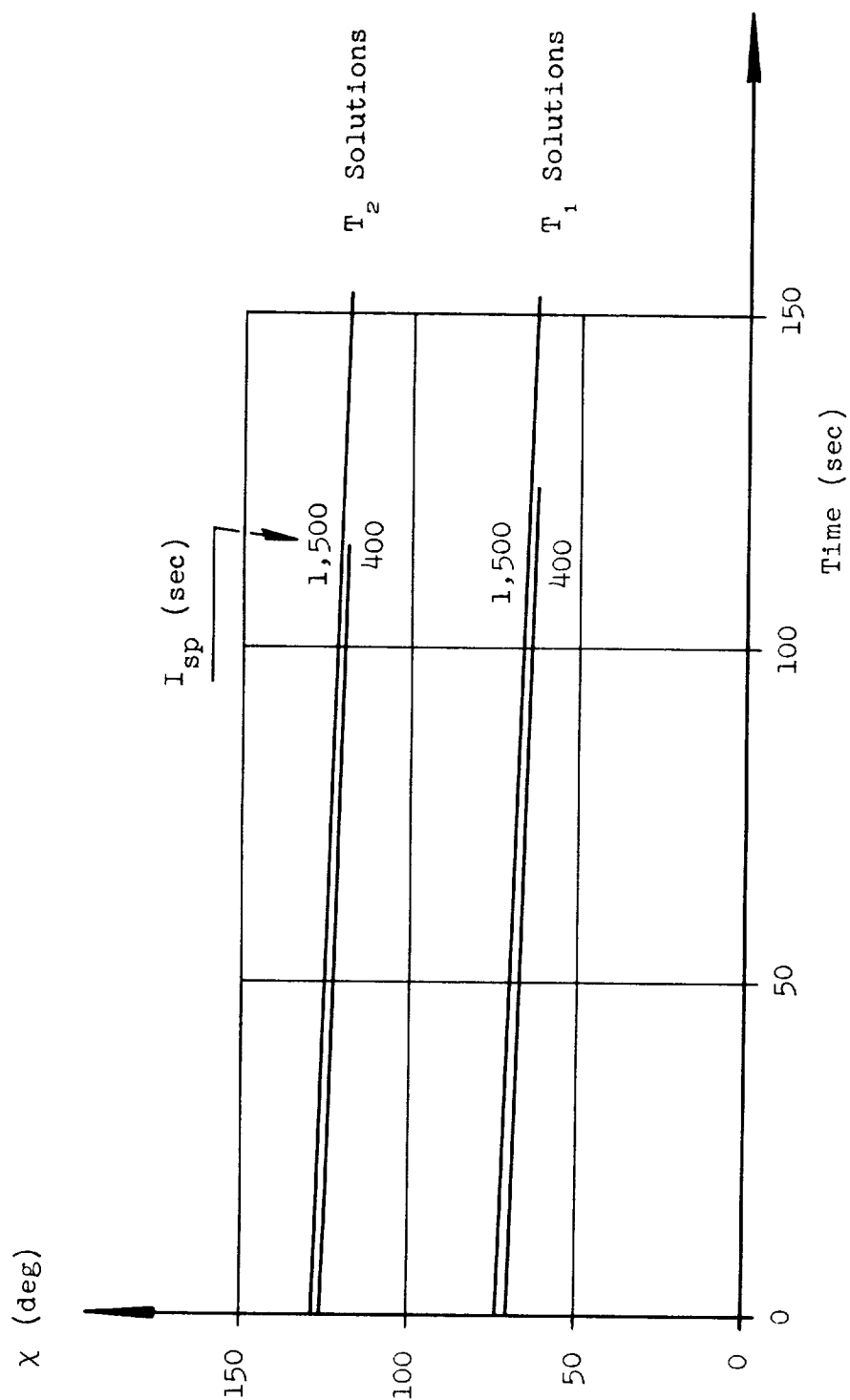


FIG. 58. OPTIMUM CONTROL HISTORIES FOR PARAMETERS OF I_{sp}

FOR $F/W_0 = 2$; $y_0 = 300$ km

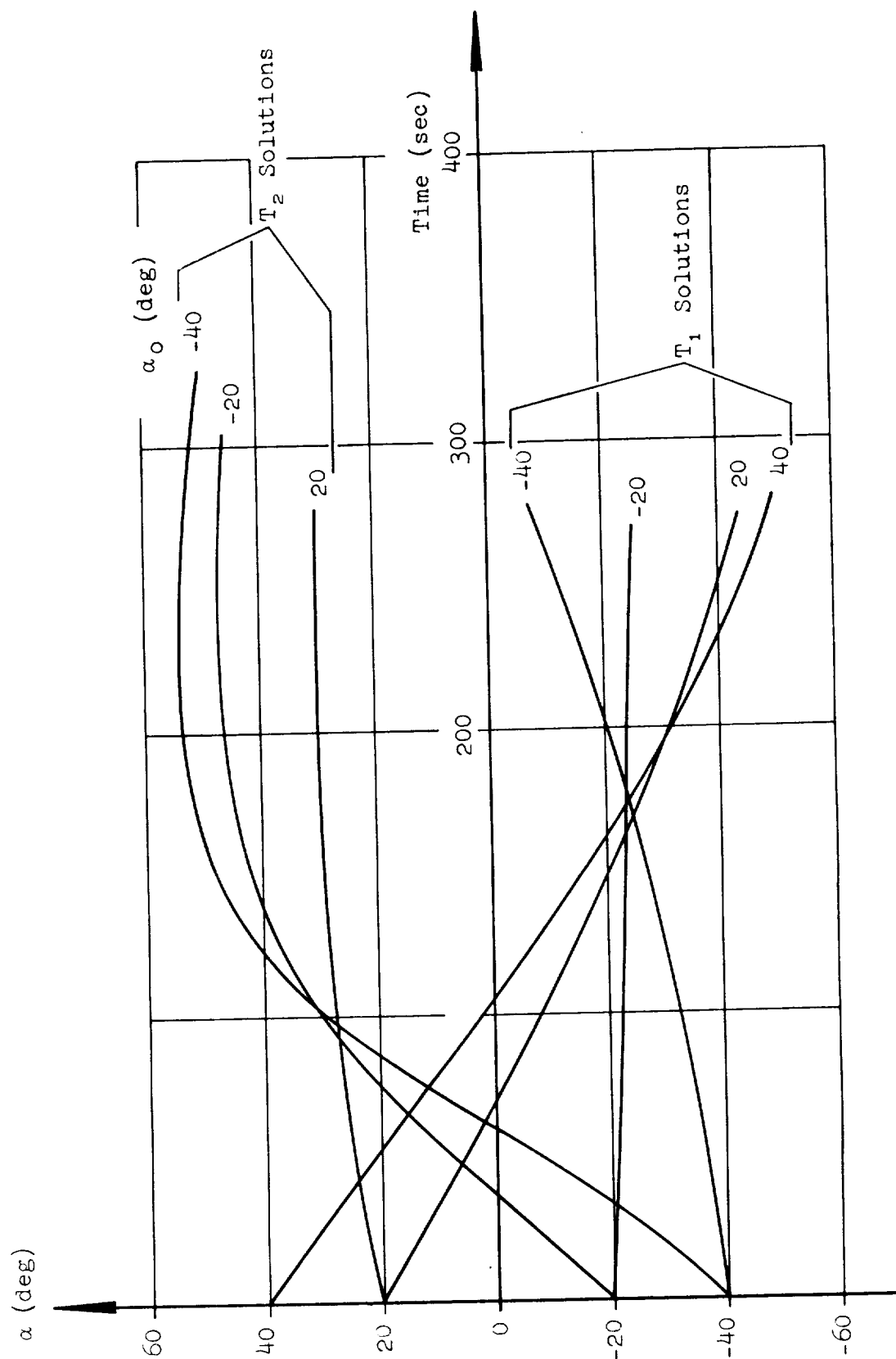


FIG. 59. NON-OPTIMUM ANGLE OF ATTACK HISTORIES
FOR PARAMETERS OF α_o
FOR $F/w_o = 1$; $I_{sp} = 700$ sec; $y_o = 300$ km

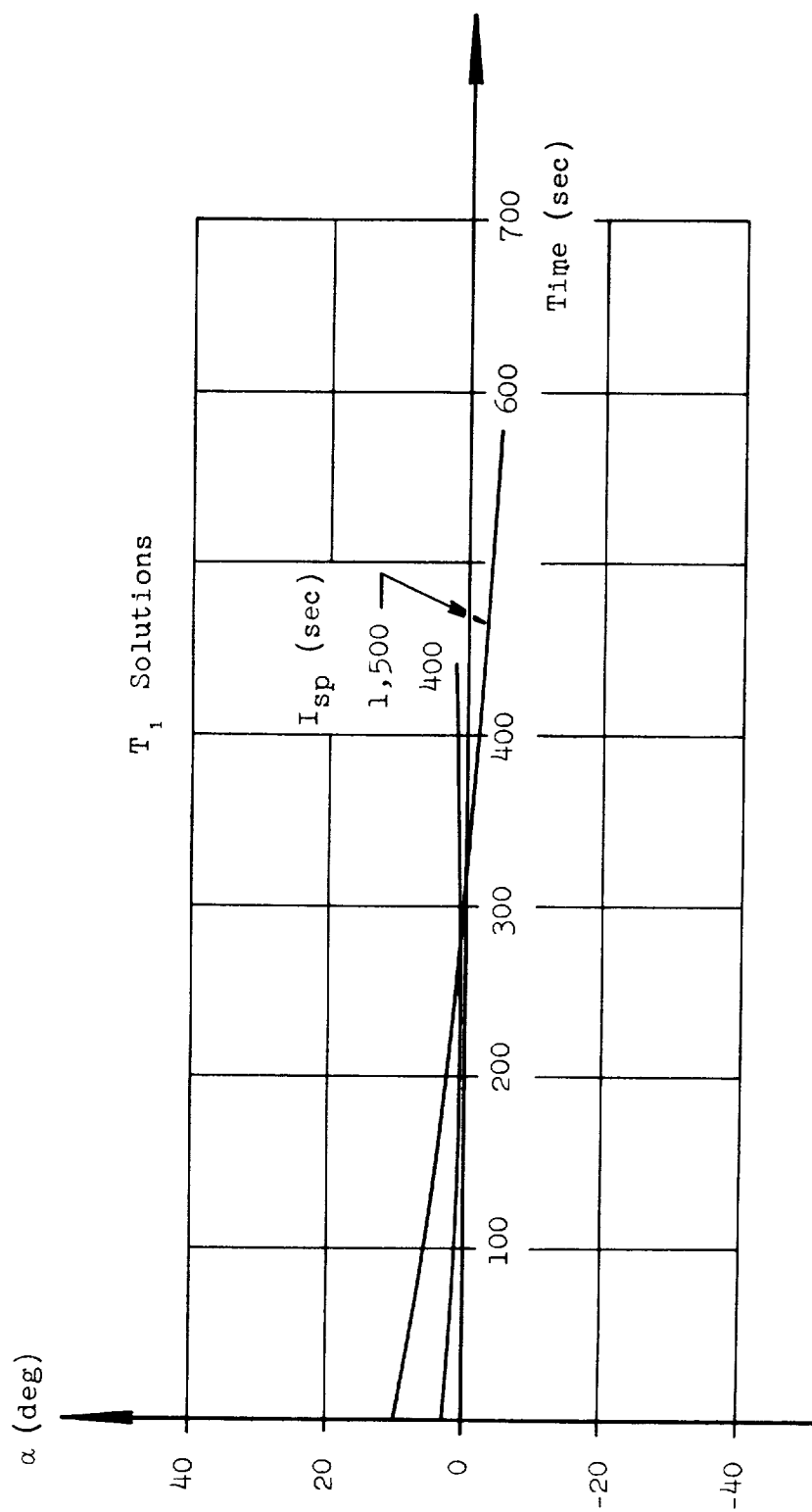


FIG. 60. OPTIMUM ANGLE OF ATTACK HISTORIES FOR PARAMETERS OF I_{sp}

FOR $F/W_0 = .5$; $y_0 = 100$ km

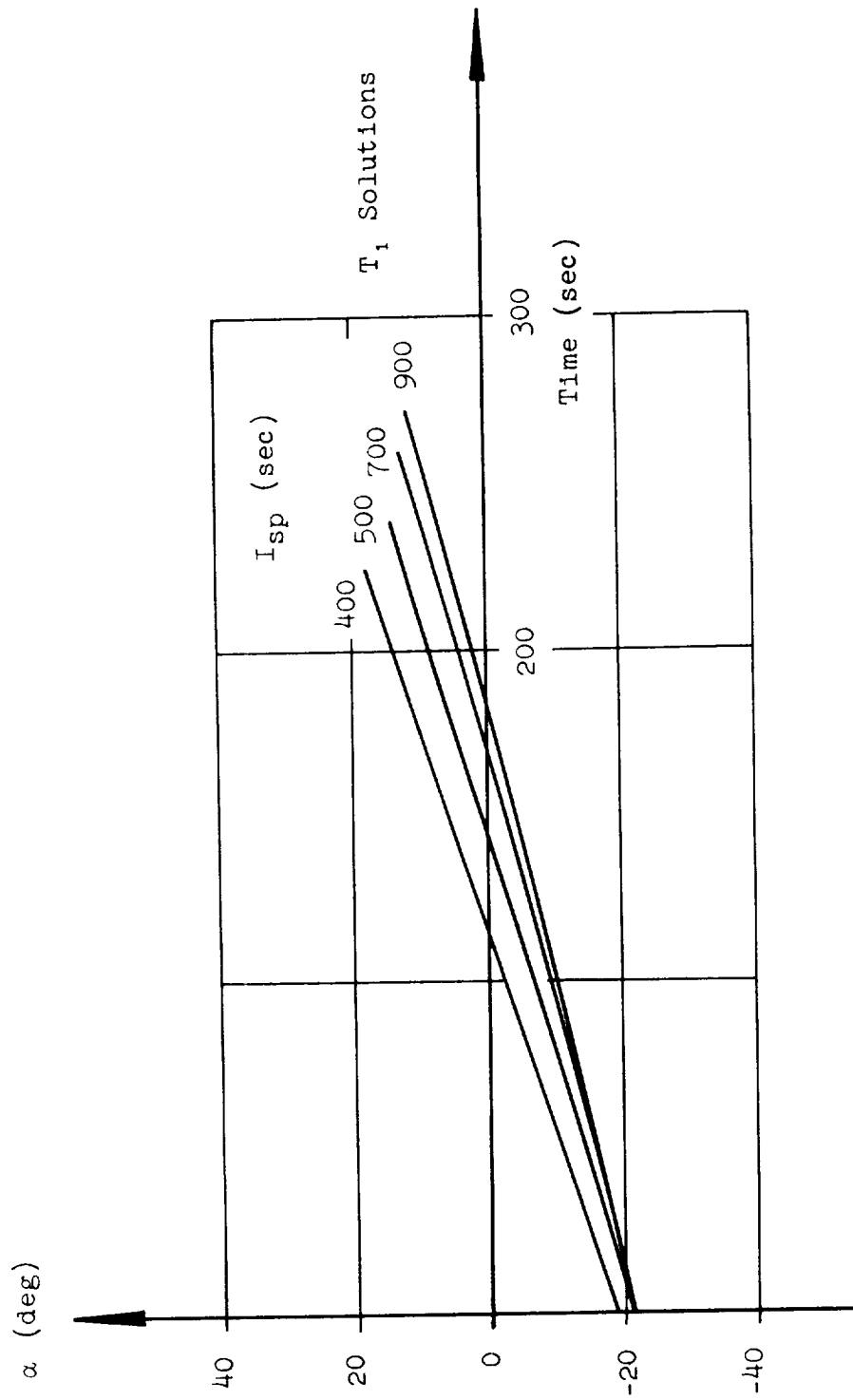


FIG. 61. OPTIMUM ANGLE OF ATTACK HISTORIES FOR PARAMETERS OF I_{sp}

FOR $F/w_0 = 1$; $y_0 = 100$ km

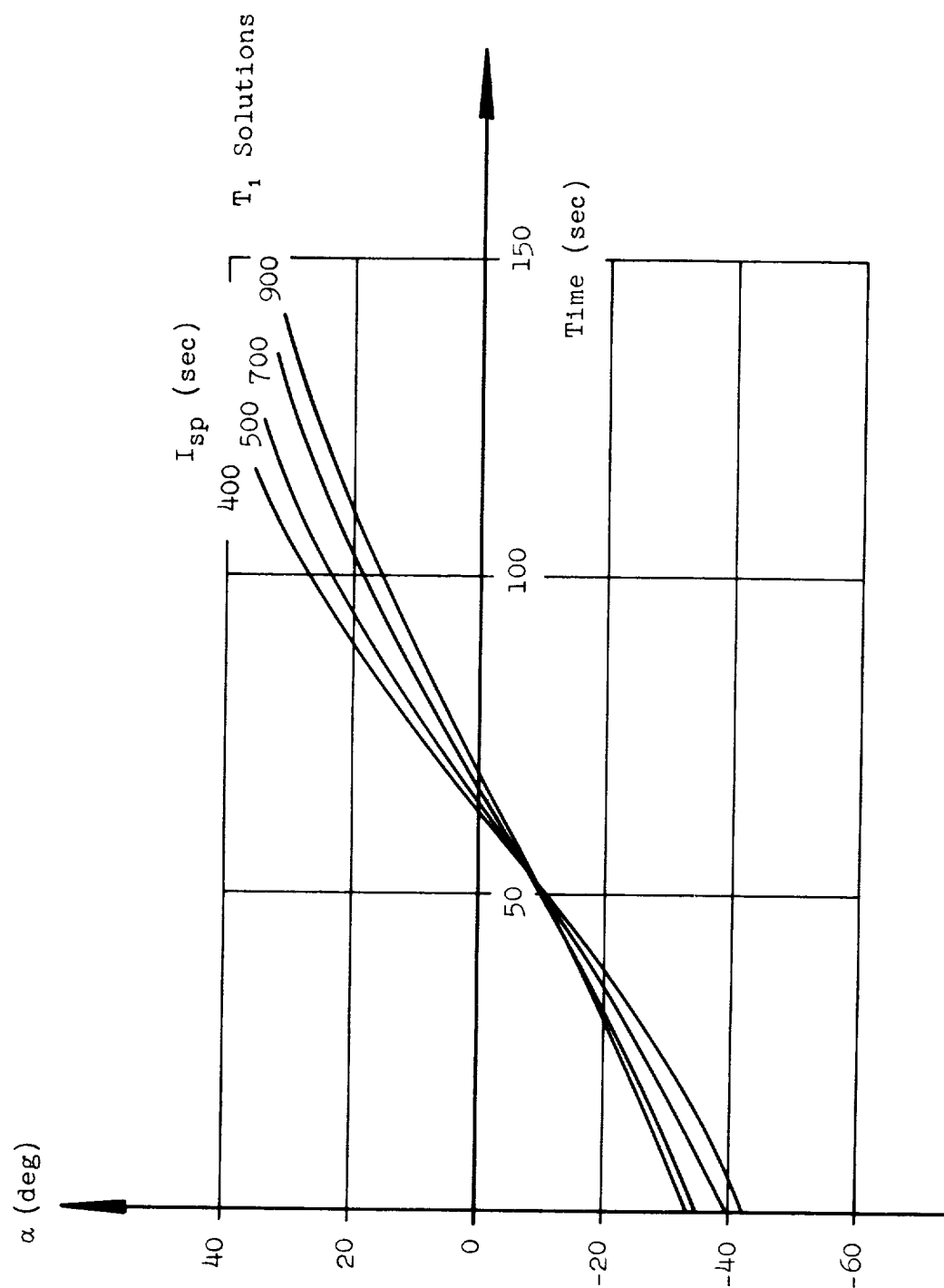


FIG. 62. OPTIMUM ANGLE OF ATTACK HISTORIES FOR PARAMETERS OF I_{sp}

FOR $F/w_0 = 2$; $y_0 = 100$ km

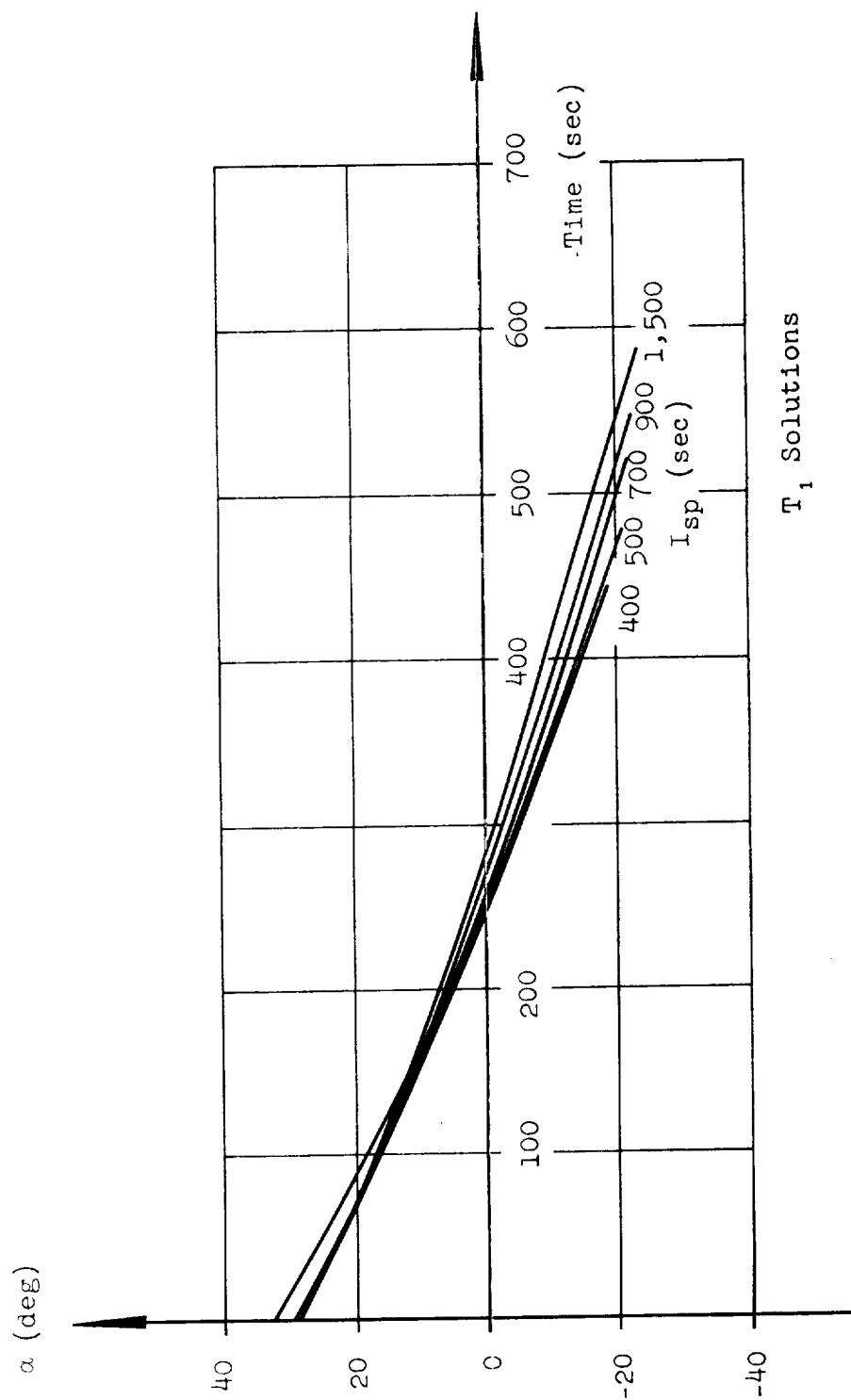


FIG. 63. OPTIMUM ANGLE OF ATTACK HISTORIES FOR PARAMETERS OF I_{sp}

FOR $F/W_0 = .5$; $y_0 = 200$ km

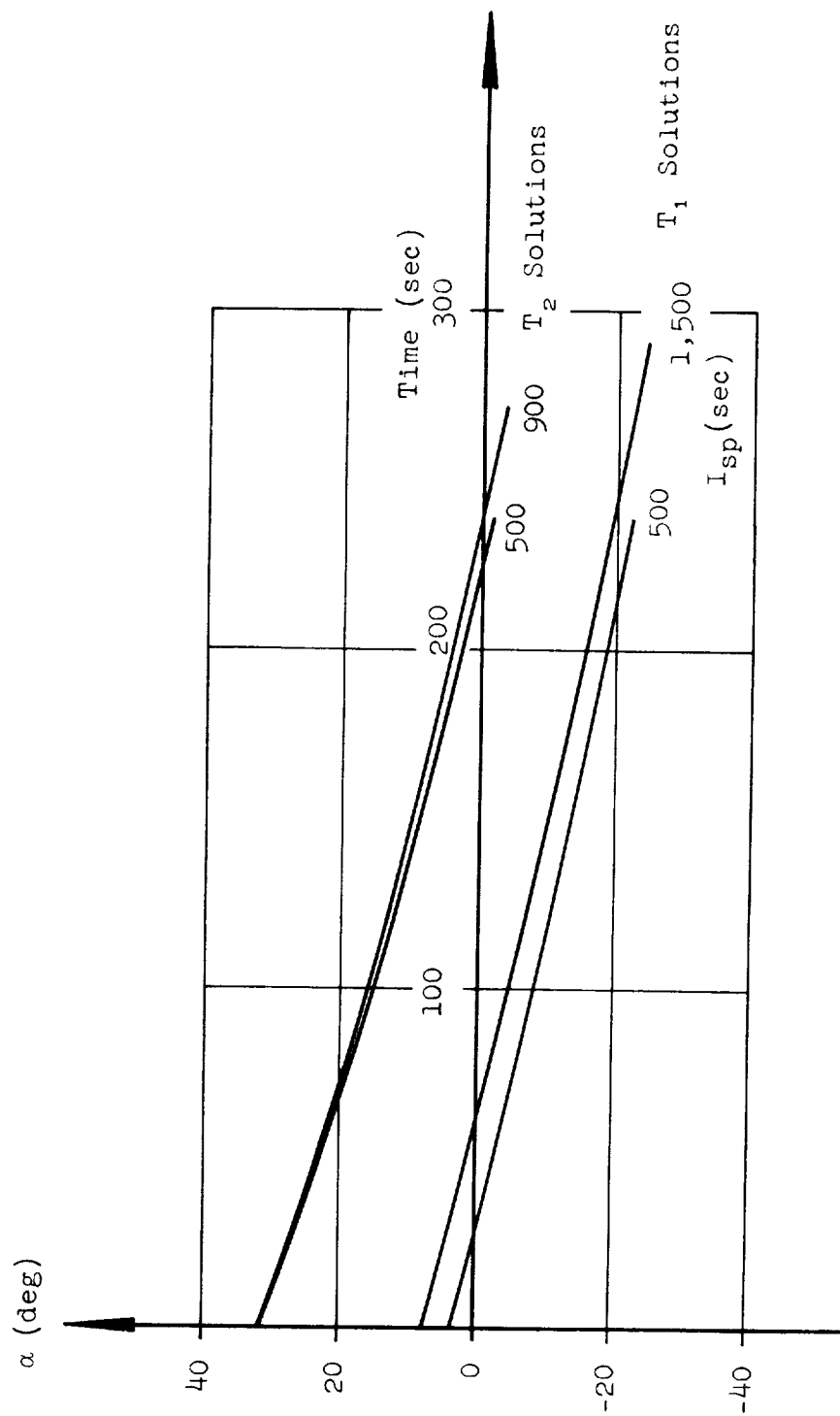


FIG. 64. OPTIMUM ANGLE OF ATTACK HISTORIES FOR PARAMETERS OF I_{sp}

FOR $F/w_0 = 1$; $y_0 = 200$ km

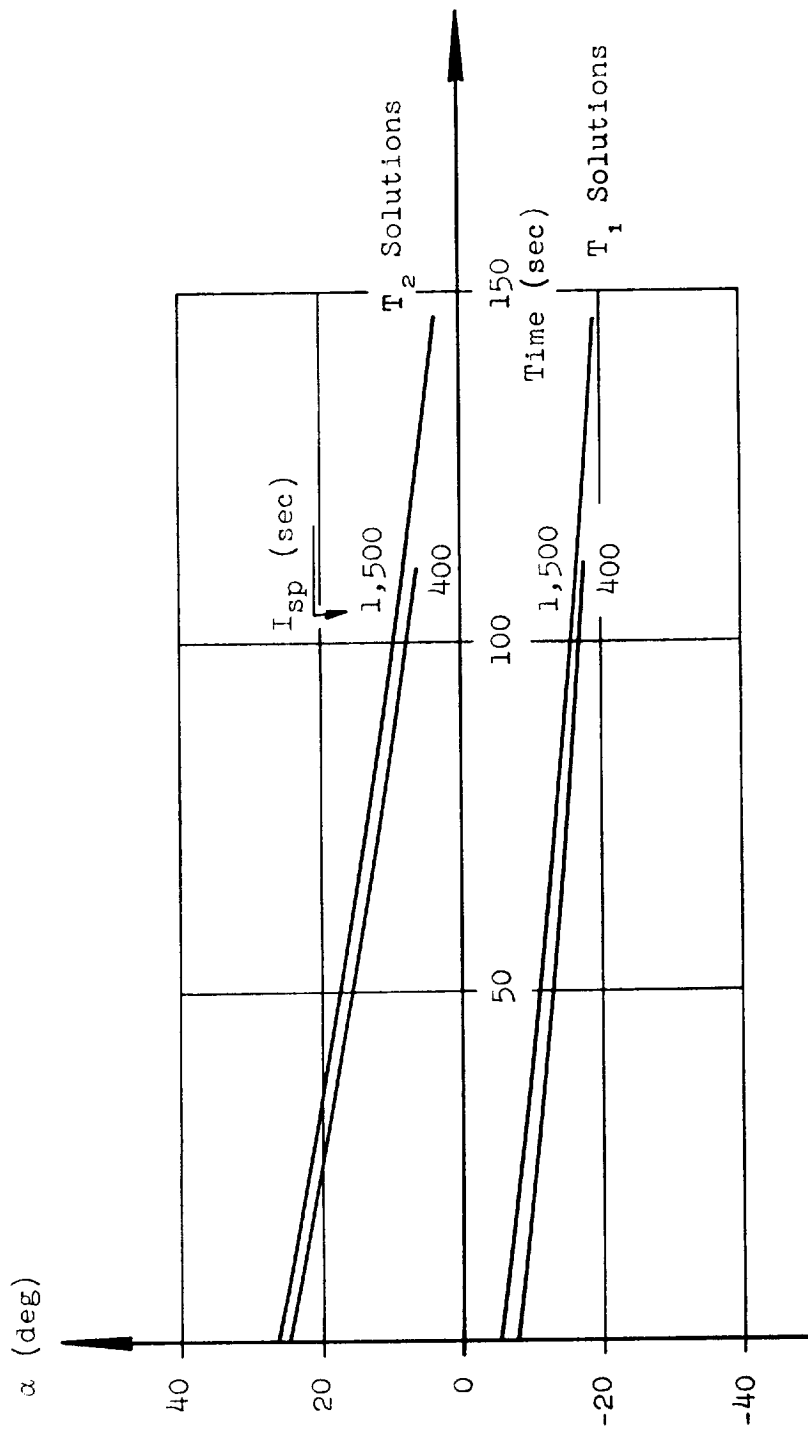


FIG. 65. OPTIMUM ANGLE OF ATTACK HISTORIES FOR PARAMETERS OF I_{sp}

FOR $F/W_0 = 2$; $Y_0 = 200$ km

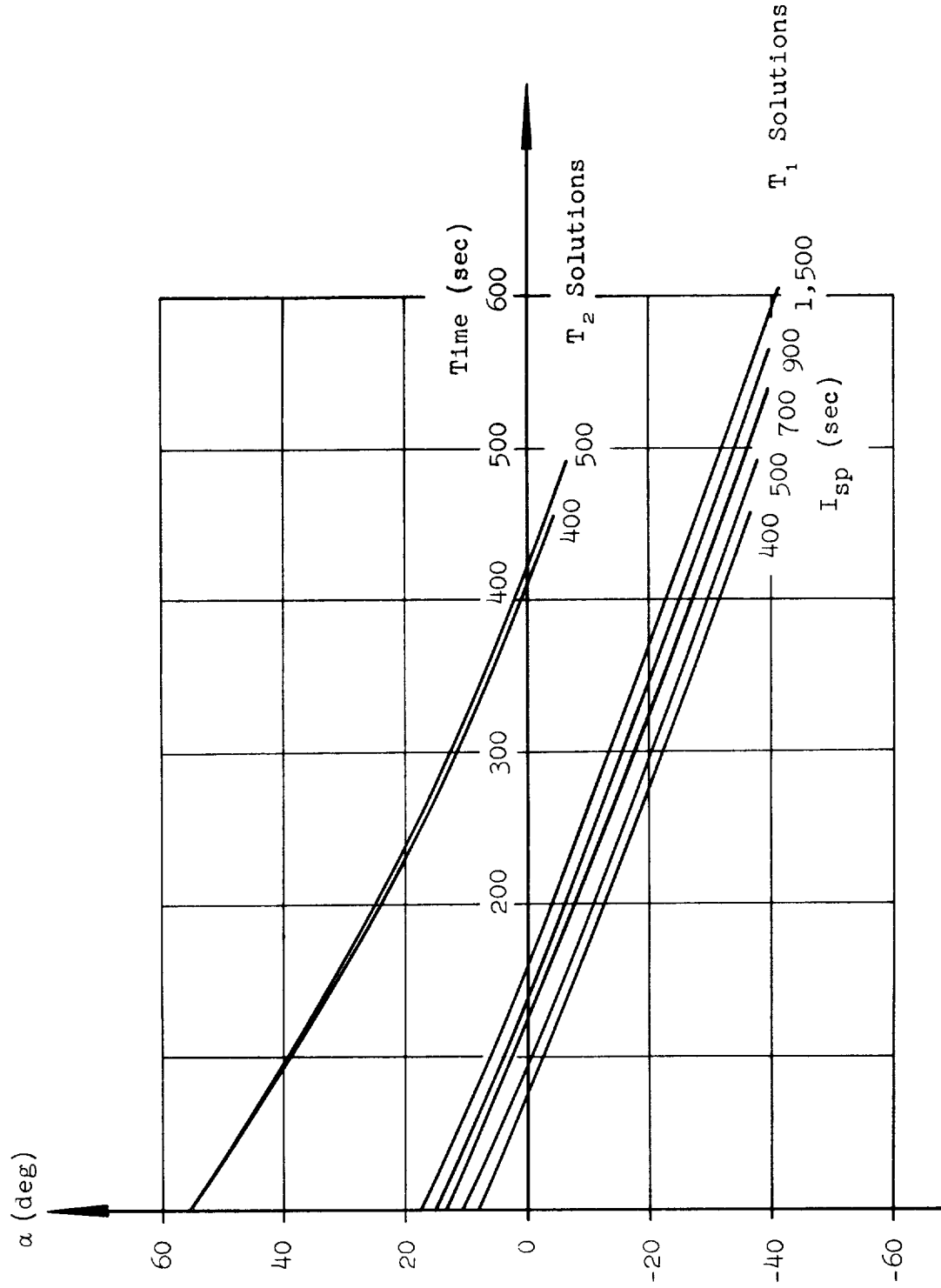


FIG. 66. OPTIMUM ANGLE OF ATTACK HISTORIES FOR PARAMETERS OF I_{sp}

FOR $F/W_0 = .5$; $y_0 = 300$ km

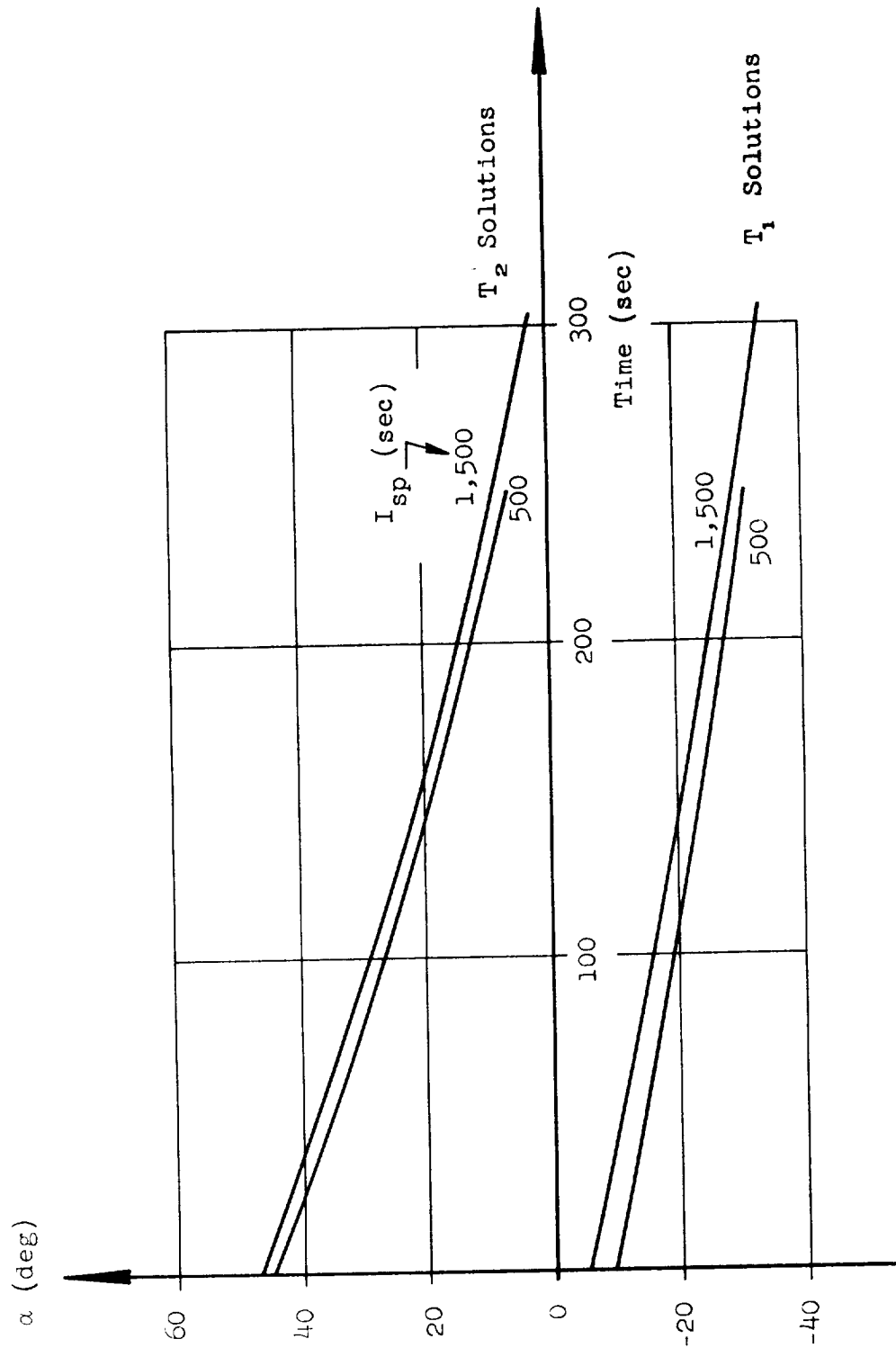


FIG. 67. OPTIMUM ANGLE OF ATTACK HISTORIES FOR PARAMETERS OF I_{sp}

FOR $F/W_0 = 1$; $y_0 = 300$ km

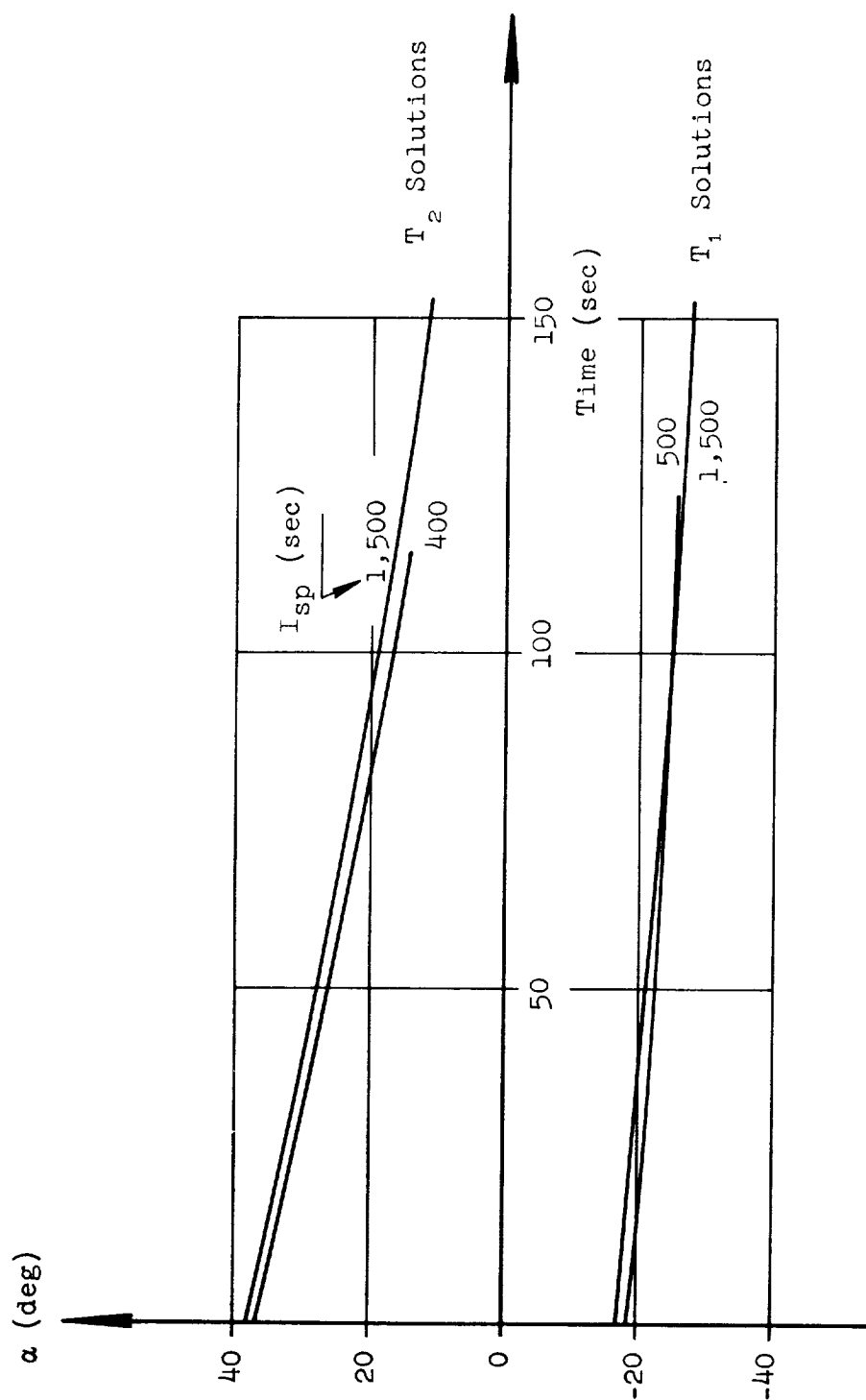


FIG. 68. OPTIMUM ANGLE OF ATTACK HISTORIES FOR PARAMETERS OF I_{sp}

FOR $F/W_0 = 2$; $y_0 = 300$ km

APPROVAL

A SURVEY OF THE INFLUENCE OF VARIATIONS
IN STAGE, CHARACTERISTICS ON OPTIMIZED TRAJECTORY SHAPINGPART II: TRANSFER FROM CIRCULAR ORBITS
INTO A SPACE FIXED ELLIPSE


By


Gary McDaniel

The information in this report has been reviewed for security classification. Review of any information concerning Department of Defense or Atomic Energy Commission programs has been made by the MSFC Security Classification Officer. This report, in its entirety, has been determined to be Unclassified.

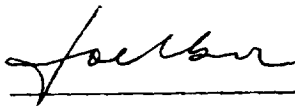
ORIGINATOR

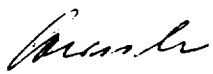
APPROVAL


GARY MCDANIEL
Aerospace Engineer
Space Projects Section II


JOHN B. WINCH, Chief
Space Projects Section II

APPROVAL


R. F. HOELKER, Chief
Future Projects Branch


E. D. GEISSLER, Director
Aeroballistics Division

DISTRIBUTION

INTERNAL

M-DIR
 M-DEP-R&D
 M-RP, Dr. Johnson

M-FPO, Mr. Koelle
 Dr. Ruppe

M-COMP, Dr. Arenstorff
 Mr. Davidson

M-P&VE, Dr. Krause
 Mr. Neighbors
 Mr. Galzerano
 Mr. Burns
 Mr. Swanson

M-ASTR, Mr. Richard
 Mr. Moore
 Mr. Hosenthien
 Mr. Blackstone
 Mr. Scofield
 Mr. Brooks
 Mr. Woods
 Mr. Digesu
 Mr. Thornton
 Mrs. Neighbors

M-MS-IP
 M-MS-IPL (8)
 M-PAT
 M-HME-P
 M-MS-H

Scientific and Technical Information
 Facility

ATTN: NASA Representative (S-AK/RKT) (2)
 P. O. Box 5700
 Bethesda, Maryland

M-AERO, Dr. Geissler
 Mr. Horn
 Mr. Hart
 Mrs. Chandler
 Mr. Callaway
 Mr. Thomae
 Mr. Scott
 Mr. Stone
 Mr. Baker
 Mr. Golmon
 Dr. Speer
 Mr. Lindberg
 Mr. Kurtz
 Mr. Vaughan
 Mr. Jean
 Mr. Thionnet
 Mr. McNair
 Mr. Teague
 Mr. McQueen
 Mr. deFries
 Mr. Bombara
 Dr. Hoelker
 Mr. Miner
 Mr. Schmieder
 Mr. Silber
 Mr. Dearman
 Mr. Braud
 Mr. Lisle
 Mr. Schwaniger
 Mr. Tucker
 Mr. Winch
 Mr. Cremin
 Mr. Goldsby
 Mr. McDaniel (20)

AUG 27 1963